MASTER IN CHEMISTRY RESEARCH FOCUS

Synthesis of sterically hindered phosphatriptycenes and computational investigation of their properties in the context of frustrated lewis pair chemistry

Mahaut, Damien

Award date:
2019

Awarding institution:
University of Namur

Université de Namur

Faculté des Sciences

SYNTHESIS OF STERICALLY HINDERED PHOSPHATRIPTYCENES AND COMPUTATIONAL INVESTIGATION OF THEIR PROPERTIES IN THE CONTEXT OF FRUSTRATED LEWIS PAIR CHEMISTRY

Mémoire présenté pour l'obtention

du grade académique de Master Chimie « Chimie du Vivant et des Nanomatériaux » : Finalité Approfondie

Damien MAHAUT

Janvier 2019

UNIVERSITE DE NAMUR

Faculté des Sciences

Secrétariat du Département de Chimie
Rue de Bruxelles 61 – 5000 NAMUR
Téléphone : +32(0)81 72.54.44 – Téléfax : +32(0)81 72.54.40
E-mail : enseignement.chimie@unamur.be - www.unamur.be/sciences

Synthèse de phosphatriptycènes encombrés et évaluation par études computationnelles de leurs propriétés pour la préparation de paires de Lewis frustrées

MAHAUT Damien

Résumé

Les paires de Lewis frustrées (**FLP**s) consistent en des acides et bases de Lewis encombrés qui ne peuvent pas former d'adduits de Lewis à cause de répulsions stériques. Ces systèmes bifonctionnels servent de catalyseurs d'hydrogénation sans métaux de transition et peuvent activer des petites molécules telles que le CO_2, NO_2, etc.

La synthèse de nouvelles bases de Lewis encombrées est cruciale pour le développement de nouvelles **FLP**s. Dans ce mémoire, le 9-phosphatriptycène et ses dérivés ont été avancés comme candidats prometteurs. Ce sont des structures rigides, robustes, avec de nombreuses positions fonctionnalisables et des propriétés stéréoélectroniques particulières. Plus précisément, nous avons proposé la synthèse de 9-phosphatriptycènes *ortho*-substitués pour augmenter l'encombrement stérique autour du de l'atome de phosphore.

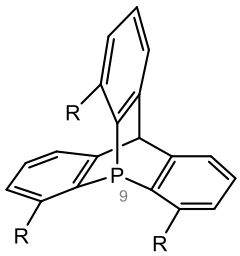

9-phosphatriptycène

Une nouvelle synthèse du 9-phosphatriptycène a été développée et adaptée à la synthèse de ses dérivés *ortho*-chlorés (R = Cl, H). Ces-derniers peuvent être convertis en de nombreux autres composés, aux potentielles applications variées telles que de la catalyse asymétrique. De plus, utilisant la théorie de la fonctionnelle de la densité, une étude computationnelle de l'association des composés d'intérêt avec un acide de Lewis boré a été réalisée, évaluant aux niveaux thermodynamique, structural et stéréoélectronique la formation de nouvelles **FLP**s.

Mémoire de Master en sciences chimiques à finalité approfondie

Janvier 2019

Promoteurs : Pr. Guillaume BERIONNI et Pr. Benoît CHAMPAGNE

UNIVERSITY OF NAMUR

Faculté des Sciences

Secrétariat du Département de Chimie
Rue de Bruxelles 61 – 5000 NAMUR
Phone number : +32(0)81 72.54.44 – Fax number : +32(0)81 72.54.40
E-mail : enseignement.chimie@unamur.be - www.unamur.be/sciences

Synthesis of sterically hindered phosphatriptycenes and computational investigation of their properties in the context of frustrated Lewis pair chemistry

MAHAUT Damien

Abstract

Frustrated Lewis Pairs (**FLP**s) consist in sterically hindered Lewis acid and base that cannot form a Lewis adduct because of steric repulsions. These bifunctional systems have been extensively used as transition metal-free catalysts for hydrogenation reactions and small molecules activation (CO_2, NO_2, …).

The synthesis of new sterically hindered Lewis bases is crucial for the development of new types of **FLP** catalysts. In this Master thesis, 9-phosphatriptycene derivatives are put forward as promising candidates for this purpose. They are rigid, robust structures with many functionalizable positions and singular stereoelectronic properties. More specifically, we proposed the synthesis of 9-phosphatriptycene substituted in *ortho*-position relative to the phosphorus in order to increase its steric hindrance.

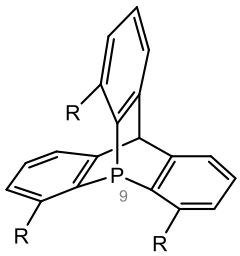

9-phosphatriptycene

A novel synthesis of the unsubstituted 9-phosphatriptycene was developed and adapted to the synthesis of chlorosubstituted derivatives (R = Cl, H). The latter can be converted in a number of compounds with various applications, including potential asymmetric catalysis. In addition, a density functional theory investigation of the association of the studied compounds with a prototypical boron Lewis acid $B(C_6F_5)_3$ and an analysis of their thermodynamic, structural, and stereoelectronic properties has been undertaken in view of the rational development of a novel type of **FLP**s.

Master thesis in chemistry, research focus

Janvier 2019

Promotors: Pr. Guillaume BERIONNI et Pr. Benoît CHAMPAGNE

Je tiens à remercier mes deux promoteurs, les professeurs Guillaume Berionni et Benoît Champagne, pour m'avoir accueilli dans leur laboratoire respectif pour la réalisation de ce mémoire. Je les remercie pour leur constante motivation, leur écoute, disponibilité et expertise tout au long de ces 10 mois de mémoire. Merci également pour le temps qu'ils ont consacré aux corrections et relectures de ce travail, essentiels à sa bonne réalisation.

Merci également à Aurélien Chardon (« Philiiippe ! ») pour ses grandes connaissances en chimie organique, toujours disponible pour aider ou répondre à nos questions, et à Lei Hu pour sa bonne humeur inébranlable, sa générosité et son « triptycen'T » qu'on ne parvient pas à enlever.

Je remercie également l'ensemble du laboratoire RCO pour la bonne ambiance dans notre petit groupe. Merci aussi aux membres du LCT qui m'ont chaleureusement accueilli une semaine sur quatre, et plus particulièrement à Pierre Beaujean, pour sa disponibilité en toutes circonstances.

Un grand merci à Arnaud Osi et Xavier Antognini Silva pour ces super moments passés ensemble pendant le mémoire, les fous rires mais aussi les pétages de plomb quand les réactions et les colonnes plantaient. Merci pour leur solidarité et soutien, quand le projet ne va pas, c'est toujours plus sympa de savoir qu'il ne pas chez les autres non plus (Osi, je ne t'inclus pas ici).

Enfin, je remercie profondément ma famille, qui m'a toujours soutenu et a cru en moi pendant mon cursus et bien au-delà. Merci aussi à Amélie, qui est avec moi au quotidien et trouve l'énergie pour me motiver dans les moments difficiles.

Table of content

PART I - Introduction

1. General introduction

The pioneer work of Gilbert N. Lewis on acids and bases in 1923 led to the development of one of the most important and unifying theories of reactivity in modern chemistry [1]. Lewis defined acids and bases as, respectively, electron-pair acceptors and donors. According to him, both would react to form covalently bonded adducts, effecting a mutual stabilisation (i.e. quenching) of the two compounds, as shown with the example of the reaction of trimethylphosphine with borane (Scheme 1)[2, 3].

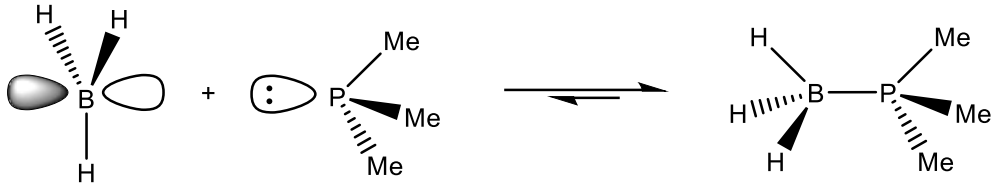

Scheme 1 - Reaction of a Lewis acid (borane) and a Lewis base (trimethylphosphine), both unstable in air, to form a Lewis adduct, stable in air and water. The lone pair of electrons of the phosphorus atom overlaps the empty p orbital of the boron atom to form a covalent bond.

Phosphines (PR_3) constitute an important class of Lewis bases which display a high propensity to form bonds with a wide variety of electrophiles, or to oxidize into phosphine oxides, owing to the lone pair of electrons of the P atom. The oxidation of phosphines is the driving force of several important organic reactions such as the Mitsunobu, the Apple or the Staudinger reactions[4].

The phosphorus being below the nitrogen in the periodic table, there is a strong similarity between the reactivity of amines (NR_3) and phosphines as their valence configuration is the same. Phosphines are generally weaker Brønsted bases, due to their high polarizability and low electronegativity, and are more nucleophilic than amines for similar substituents[5]. Tertiary phosphines PR_3 and amines NR_3 are pyramidal, but the latter will easily undergo inversion ("flipping") at room temperature whereas the former retain their configuration even above room temperature[6]. P-chirogenic phosphines (phosphines with the chiral centre on the phosphorus) are thus configurationally stable.

The stereoelectronic properties of phosphines can be readily modulated by varying the nature of the groups linked to the phosphorus atom (alkyl, aryl, halogen, …). These modulable properties make them particularly useful as ligands in organometallic chemistry, which has ever been their main field of applications (see section 3)[7]. In recent years, the use of phosphines as organocatalysts (i.e. where the phosphine itself acts as catalyst) has received increasing interest from organic chemists, as discussed in section 4[2, 8].

2. Measurements of the stereoelectronic properties of phosphines

The quantification of the stereoelectronic properties of phosphines is necessary to rationalize and predict their reactivity. Chemists have thus endeavoured to develop new measurements of these properties. Most notably, Chadwick A. Tolman studied both electronic and steric factors of ligands in organometallic chemistry and defined in 1970 the phosphine cone angle[9], still in use today to describe steric effects of phosphine ligands. From a zerovalent nickel atom at 2.28 Å of the phosphorus atom of the ligand, he constructed a cone that comprises the entirety of the ligand (Figure 1). To quote, the measurement corresponds to "*the apex angle of a cone, centered on the metal, just large enough to enclose the van der Waals radii of the outermost atoms of the ligand*"[9].

The cone angle is a direct measure of the steric effect of the ligand: the larger the angle value, the bulkier the ligand. In parallel to the cone angle, Tolman also developed a measure of the electronic parameter of phosphine ligands: in a mixed ligands nickel complex $NiL(CO)_3$, he measured the influence of the phosphine ligand L on the infrared stretching frequency of the carbonyl ligands[10]. The C-O stretching frequency decreases with stronger ligands (Figure 1). Other strategies to assess the stereoelectronic parameter of phosphine ligands include ^{31}P NMR measurements of the $^{1}J_{P\text{-}C}$ and $^{1}J_{P\text{-}Se}$ coupling constants of the corresponding methylated phosphine and phosphine selenide, respectively[11].

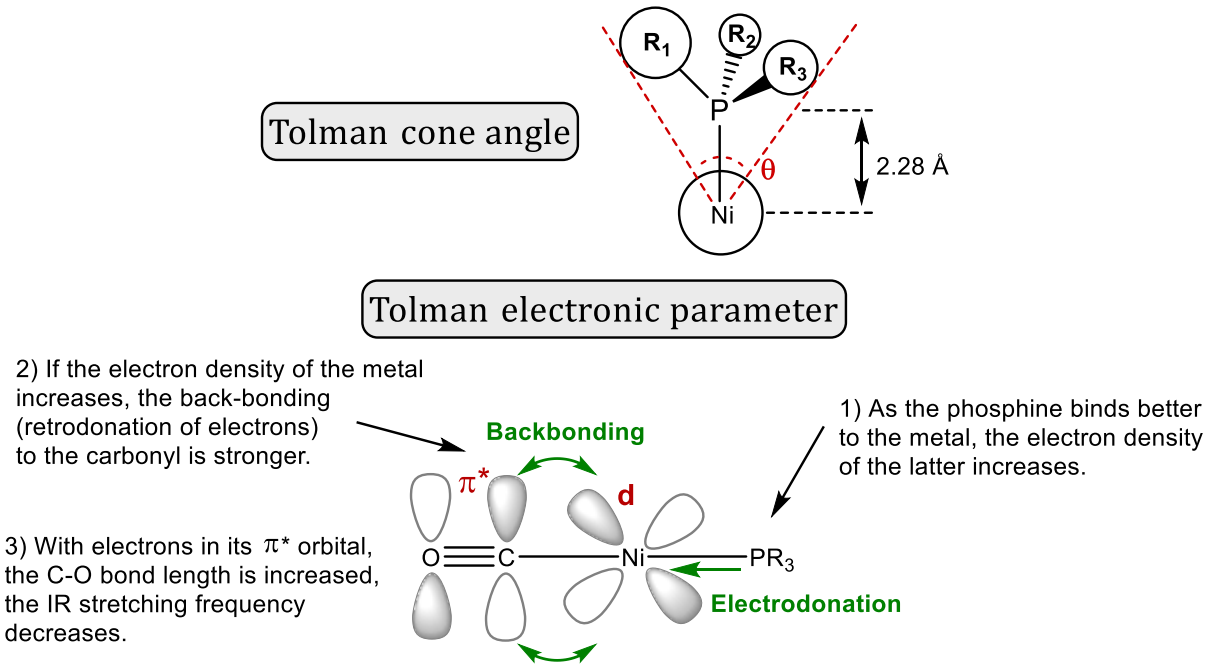

Figure 1 - Cone angle θ as defined by C. A. Tolman. [9] and principle of the measure of the Tolman electronic parameter.

To evaluate the reactivities of phosphines commonly used as organocatalysts, several Lewis basicity scales have been developed for comparing the affinity of a multitude of Lewis bases to a selected reference Lewis acid. Several scales are based on quantum chemical calculations such as the methyl cation affinity (MCA)[12] and the halenium (F^+, Cl^+, Br^+, I^+) affinity (*HalA*) scales[13]. Experimental Lewis basicity scales are based on equilibrium constants of association of Lewis bases with reference Lewis acids such as benzhydryl cations (Ar_2CH^+) for the Mayr scale[14] or BF_3 for the BF_3 affinity scale (BF_3A). The former scale links for instance the equilibrium constant to a Lewis acidity (*LA*) and a basicity (*LB*) parameter. With known *LA* parameters for the reference, one can determine the *LB* parameter with a simple mathematical relation (Figure 2).

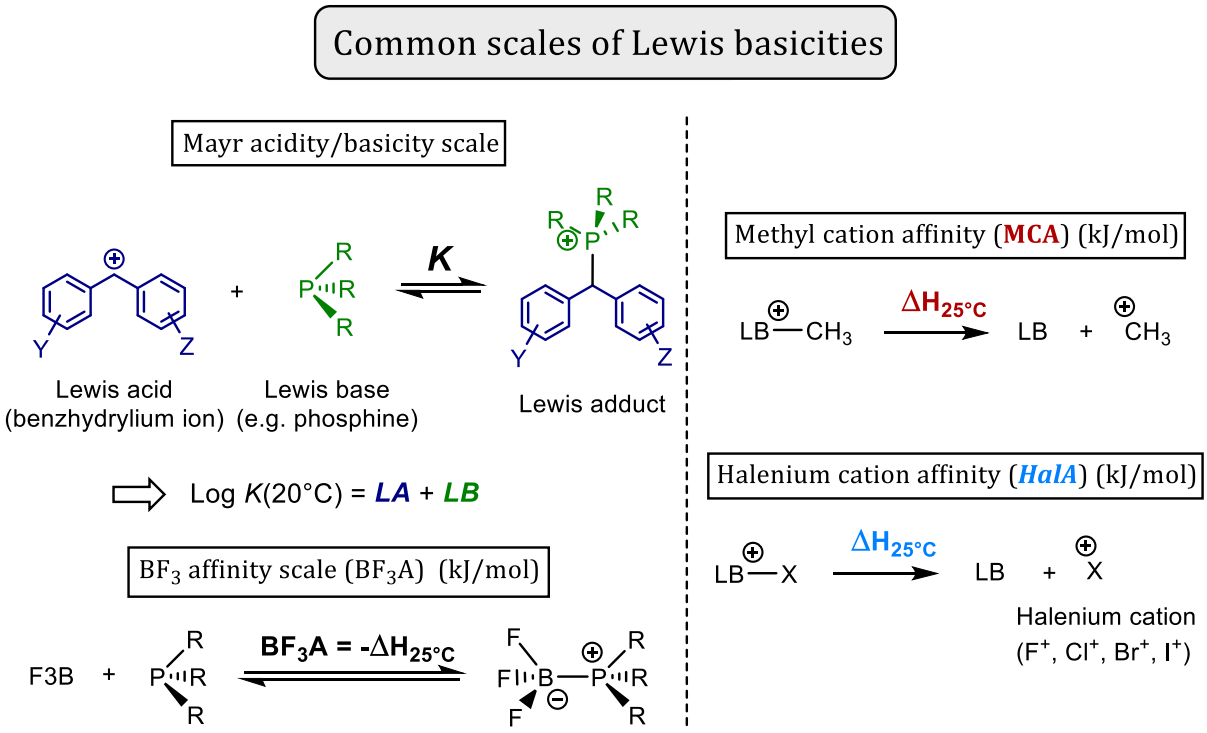

Figure 2 – Common Lewis basicity scales.[15]

3. Phosphines in transition-metal catalysis

As mentioned earlier, phosphines are widely used as ligands in organometallic catalysis owing to their strong coordinating properties towards transition metals. The orbitals of the phosphorus atom are well adapted for an efficient binding with metals through two distinct modes: σ-donation and retrodonation (or back-bonding). The latter is due to the overlap between the partially filled d orbitals of the metal and the antibonding orbitals of the P-R bonds (σ*)[16] (Figure 3).

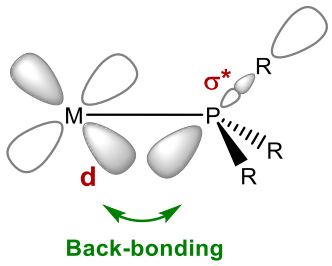

Figure 3 - Overlap between partially filled d orbital of the metal and σ orbital of the P-R bond.*

Ligands that accept back-bonding such as phosphines are called π-acceptors or π-acids. This property, among other factors, distinguishes phosphines in terms of ligand ability from amines (NR_3), which are not π-acidic.

The functional groups around the phosphorus tune the stereoelectronic properties of the phosphine and subsequently its bonding with metals. For examples, electrowithdrawing groups such as fluorine atoms will enhance the π-acidity of the phosphine[16] or sterically demanding groups like *i*-propyl substituents will limit the number of ligands bonded to the metal and allow for the formation of "sterically stabilised" species[17].

A large number of major organic reactions are catalyzed by transition metal complexes with phosphine ligands. Notably, a wide range of coupling reactions such as the Suzuki-Miyaura, the Hiyama-Denmark and the Negishi couplings[4]. The Buchwald-Hartwig coupling uses a palladium complex with a phosphine ligand such as triphenylphosphine or tris(*o*-tolyl)phosphine to carry out a C-N bond formation between an aryl halide and an amine to form a tertiary aryl amine (Scheme 2)[18, 19].

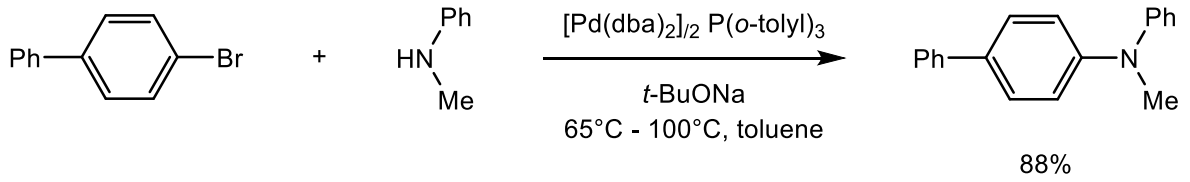

Scheme 2 - Example of a Buchwald-Hartwig C-N coupling reaction.[18]

Recent improvements of these reactions by Buchwald led to the development of a new class of phosphines (Figure 4a) which are bulky, electron-rich monodentate ligands with high activity in C-N[18, 20], C-O[21] and C-C coupling reactions (Scheme 3)[22, 23]. Phosphine ligands also possess a wide application in asymmetric catalysis. Since the pioneer work of H. Kagan on the asymmetric hydrogenation of ethylene derivatives using chiral diphosphines[24], they have become ligands of choice in enantioselective transition-metal catalyzed reactions[25]. One such ligand is the bidentate BINAP ligand (Figure 4b)[26].

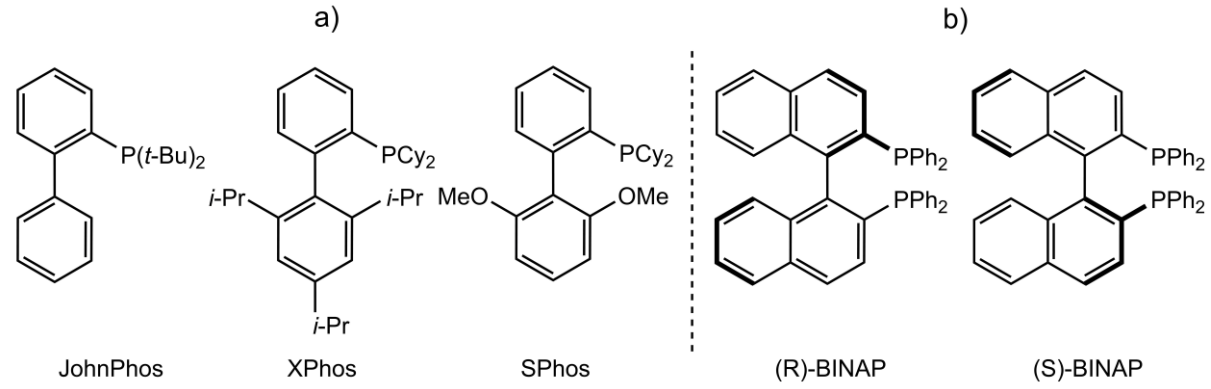

Figure 4 - a) Examples of Buchwald's dialkylbiarylphosphine ligands (JohnPhos, XPhos, SPhos)[23]. b) (S)- or (R)-BINAP (2,2′-bis(diphenylphosphino)-1,1′-binaphthyl) ligand, the limited rotation around the bond between the naphthyl groups induces an axial chirality in the molecule (i.e. a locked spatial arrangement without chiral centre that is non-superposable to its mirror image).

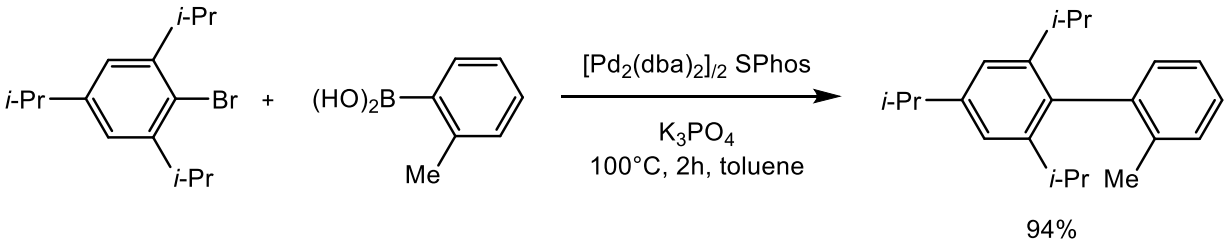

Scheme 3 - Example of a palladium-catalyzed Suzuki-Miyaura cross-coupling reaction with the SPhos ligand.

To further demonstrate the importance of phosphines in organometallic chemistry, a few examples of transition-metal catalysts with phosphine ligands can be put forward (Table 1).

Table 1 - Examples of famous transition-metal complexes with phosphine ligands and some of their applications.

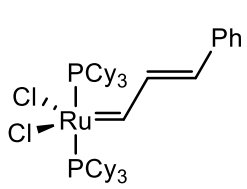 (Grubbs' Catalyst)	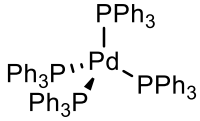	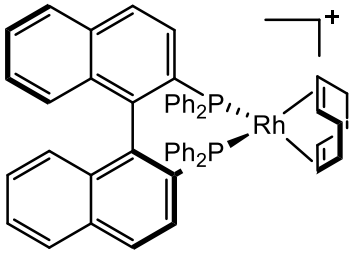	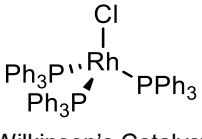 (Wilkinson's Catalyst)
Ring-closing and olefins metathesis[27]	Widely used in cross-coupling reactions[28]	Industrial synthesis of (-)-menthol[29]	Industrial hydrogenations of olefins[30]

4. Phosphines as organocatalysts

4.1 The Morita-Baylis-Hillman and other phosphine-catalyzed reactions

Phosphines are also involved as catalysts in many transition-metal free organic reactions. In most cases, they do Michael-type additions to many types of C-C multiple bonds electrophiles such as alkenes and alkynes (through a n → π* HOMO-LUMO overlap). During the last few years, the use of phosphines as organocatalysts has grown exponentially, both in "classical" and asymmetric catalysis, as illustrated below[31, 32].

The Morita-Baylis-Hillman (MBH) reaction consists in a Lewis base-catalyzed C-C bond formation between the α-position of an electrodeficient alkene and an aldehyde (Scheme 4).

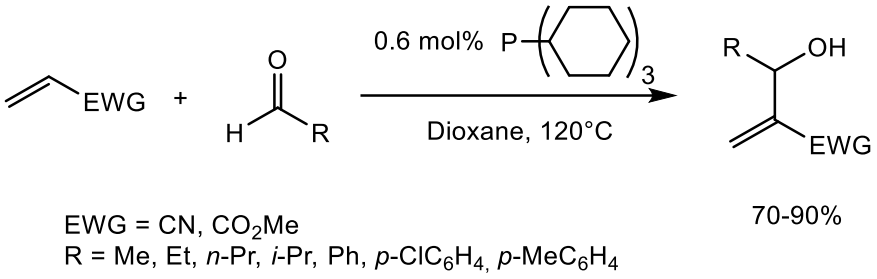

Scheme 4 - Morita-Baylis-Hillman reaction as discovered by K. Morita in 1968[33]. EWG = electrowithdrawing group.

This reaction was first described by Morita in 1968 with a phosphine catalyst [33] and later, in 1972, by Baylis and Hillman with an amine catalyst[34]. The mechanism of this reaction is a Michael-type addition-elimination sequence (Scheme 5) [35].

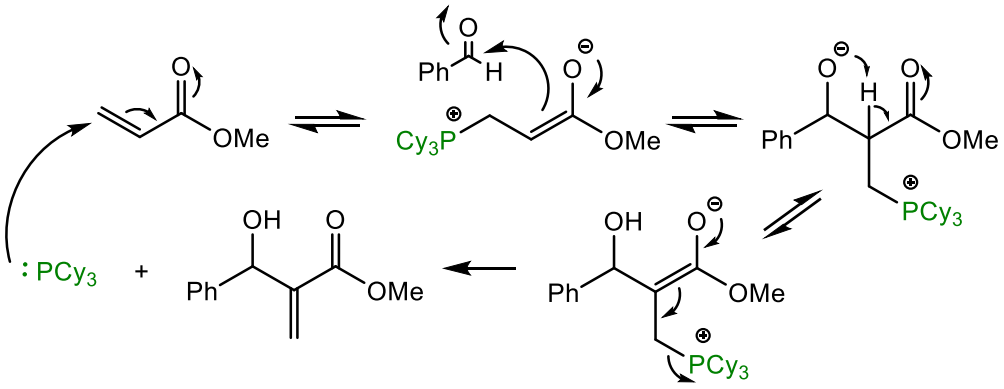

Scheme 5 - Mechanism of the MBH reaction[35].

The main drawback of this reaction was the high dependence of the yields and conversions on the substrate[8]. At first, this limited the applications in complex syntheses but new developments after the 90's, in particular the design of better catalysts, overcame these problems until the MBH became a prominent method for the synthesis of new C-C bonds[35]. Tertiary amines are more

often used as catalysts because of their low costs and less toxic character although phosphines usually perform better and in easier conditions[8].

The asymmetric variant of the MBH reactions has been extensively developed in the recent years[36]. Notably, multifunctional chiral phosphine catalysts based on the BINOL scaffold have been developed to increase the stability of the reaction intermediates as well as enantio- or diastereoselectively form the desired product (Figure 5)[37].

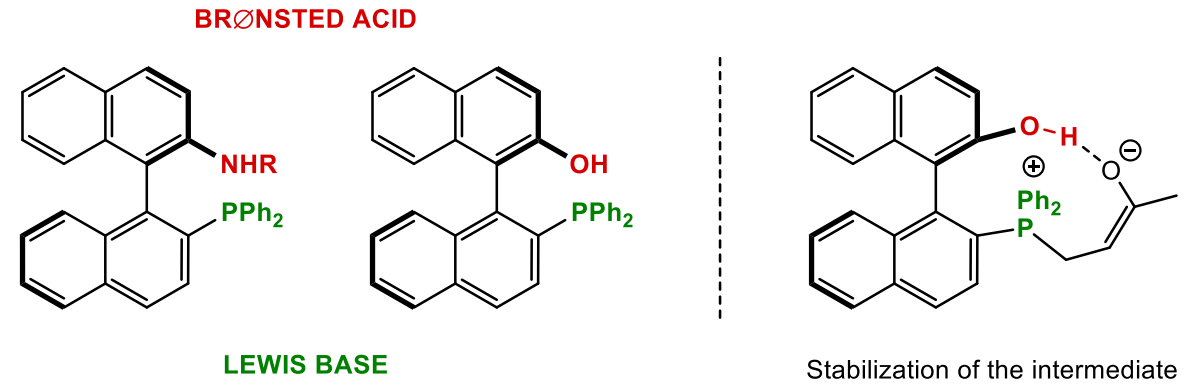

Figure 5 - New chiral multifunctional catalysts for MBH reaction (left) and stabilising effect of intramolecular hydrogen bond in the reaction intermediate (right). A hydrogen bond donor in proximity to the Lewis base is necessary to stabilise the reaction intermediate[37].

P-chiral phosphines also serve as catalysts for asymmetric acylation reactions and give moderate to good enantiomeric excess[31].

The utility of chiral phosphines in asymmetric organocatalysis (either P-chiral phosphines or phosphines in a chiral structure) has dramatically increased in the last decade. New chiral phosphines have been developed to maximize the nucleophilicity of the catalyst in a chiral scaffold (Scheme 6)[32], but their applications will not be detailed as it is beyond the scope of this work.

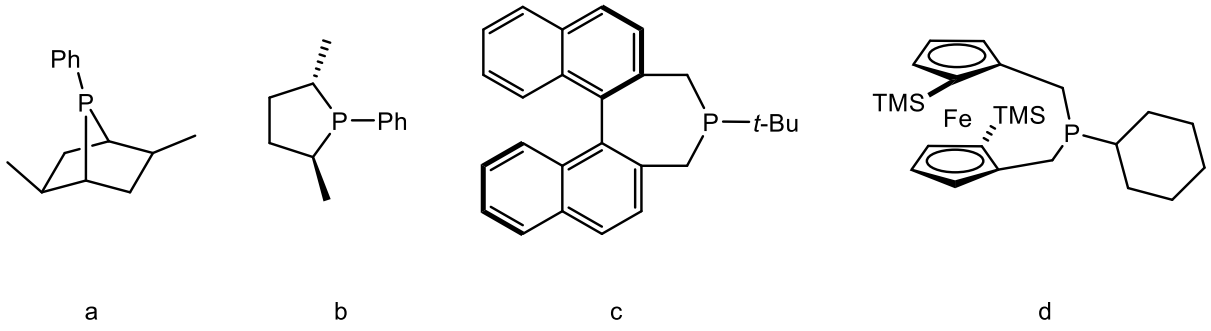

Scheme 6 - Examples of chiral phosphines, bearing a bridged skeleton (a), cyclic (b), with a biaryl scaffold (c) and based on ferrocene (d)[32].

4.2 Frustrated Lewis pair catalysis

4.2.1 From the discovery of frustrated Lewis pairs to hydrogenation catalysis

Frustrated Lewis pairs provide new prospects in phosphine organocatalysis. As mentioned in Section 1, according to the G. N. Lewis theory[1], a Lewis base (e.g. PR_3) will combine with a Lewis acid (e.g. BH_3) to form a covalent adduct ($R_3P{\rightarrow}BH_3$). However, the subtle effect of steric hindrance on their association was investigated later[38]. With bulky substituents R around the coordinating atom (*tert*-butyl, mesityl and adamantyl groups), the formation of a donor-acceptor bond between the acid and the base cannot proceed[38]. This led to the introduction of the concept of "frustrated Lewis pairs" (FLPs) by D. W. Stephan in 2008[39]. Stephan defined FLPs as sterically hindered Lewis acids and bases which cannot form the corresponding adduct because of steric repulsions (Figure 6). These systems display completely new catalytic properties since both Lewis acid and base are now able to act synergistically on a reagent of small size in a "third component" type reaction[39].

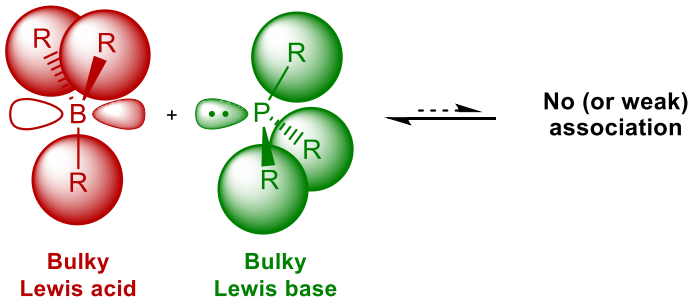

Figure 6 - Stephan's definition of frustrated Lewis pairs.

The first example of small molecule activation by FLP is of huge interest since it is the heterolytic cleavage of H_2 by an intramolecular phosphinoborane compound (Figure 7a)[40] Simple phosphine/borane combination also cleaves dihydrogen (Figure 7b)[41], though intramolecular FLPs usually perform better because of a reduced entropy of activation. Such systems and other later-developed FLPs have now been extensively used for transition-metal free hydrogenations of unsaturated compounds, notably imines (Figure 7c), alkenes, aromatics and aldehydes[42, 43].

Understanding the reactivity of frustrated Lewis pairs and the mechanism of hydrogen activation is still a challenge. Many research groups have undertaken computational studies to give insight into the complex reactivity of FLPs[44, 45, 46, 47]. Notably, the group of Pápai and co-workers has reported a quantum chemistry study of the activation of dihydrogen by a FLP of tris(*tert*-butyl)phosphine (P*t*-Bu_3) and tris(pentafluorophenyl)borane ($B(C_6F_5)_3$) (Figure 7b)[48].

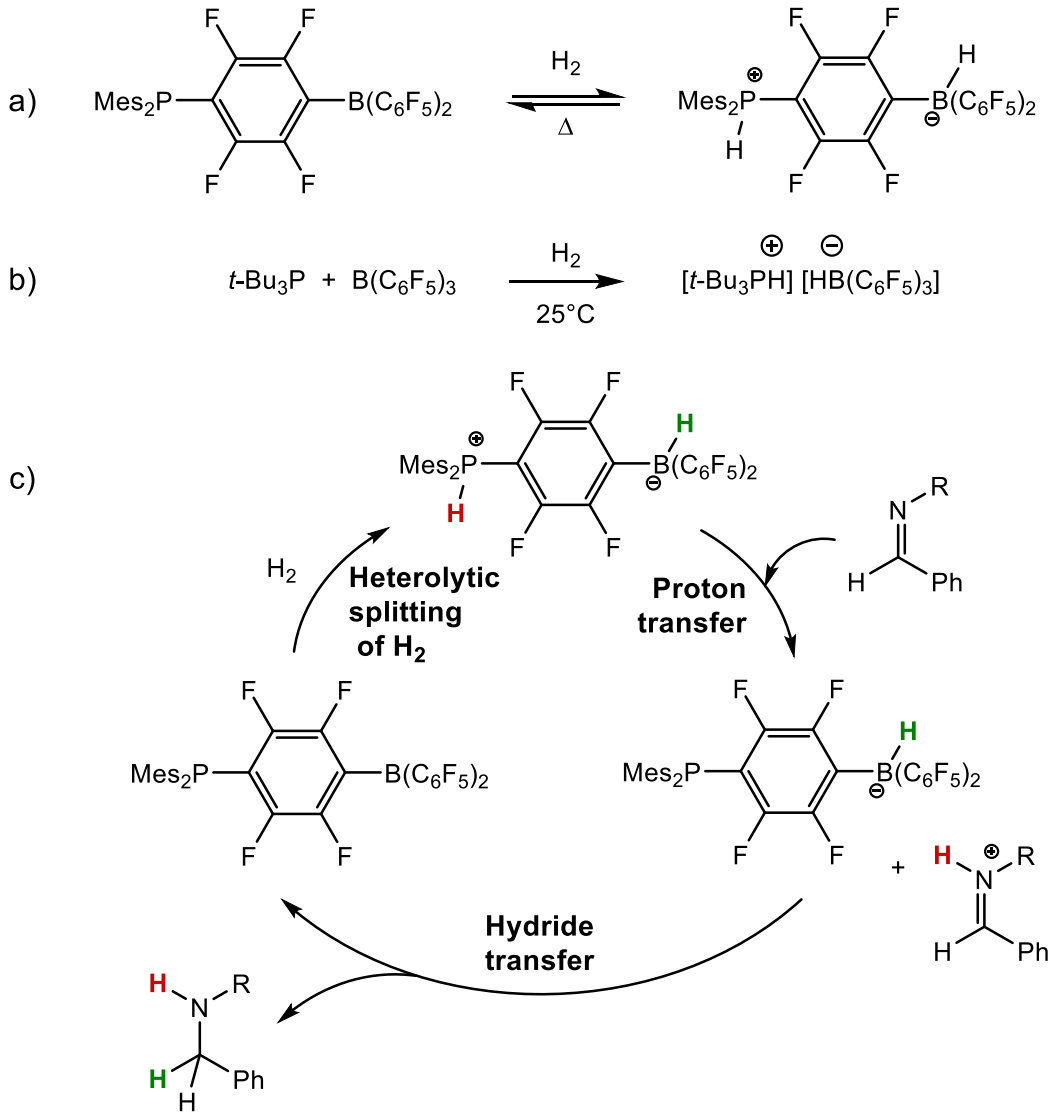

Figure 7 - a) First reversible heterolytic cleavage of H_2 by a FLP; b) Hydrogen splitting by a borane/phosphine system; c) Catalytic cycle of the reduction of an imine by a FLP.

They pointed out that the splitting of the hydrogen molecule is neither due to a preliminary borane-H_2 or phosphine-H_2 complexation but to a concerted mechanism: a simultaneous breaking of the H-H bond and formations of P-H and B-H covalent bonds. The Lewis acid and the Lewis base associate through weak interactions, without direct P-B charge transfer (mainly dispersion interactions and C-H···F hydrogen bonds), to form a cavity in which can easily be inserted H_2 (Figure 8). The H-H bond heterolytic cleavage happens subsequently through a transition state stabilised by the same weak intermolecular interactions between the phosphine and the borane to form the product, itself further stabilised by a P-H···H-B hydrogen bond. In view of all these results, they could explain why this reaction happened quantitatively and under very mild conditions. The understanding of these reaction mechanisms, of the interactions between all involved compounds through computational studies is a key step in predicting the properties of FLPs and designing new ones.

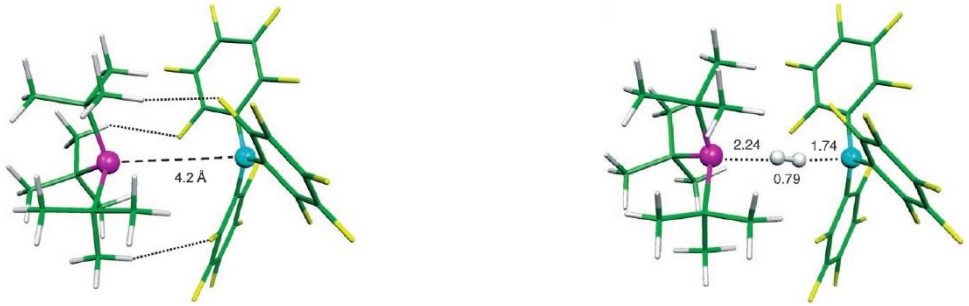

Figure 8 - Structure of the t-Bu$_3$P···B(C$_6$F$_5$)$_3$ complex (a) with C-H···F hydrogen bonds ($d_{H\text{-}F}$ <2.4 Å) dotted and transition-state of the hydrogen cleavage (b) with distances given in Å. Structures calculated at the SCS-MP2/cc-pVTZ level of theory extracted from reference [48]. LEGEND: Purple = Phosphorus; White = Hydrogen; Yellow = Fluorine; Green = Carbon; Blue = Boron.

4.2.2 Small molecules activation

A number of small molecules can be captured and activated by FLPs, such as CO, CO_2, SO_2 and N_2O (Figure 9)[43]. Most of these reactions are requiring a stoichiometric amount of phosphine borane and no catalytic system has yet been developed that converts CO_2 (nor any other abovementioned molecule) without consuming irreversibly the FLP.

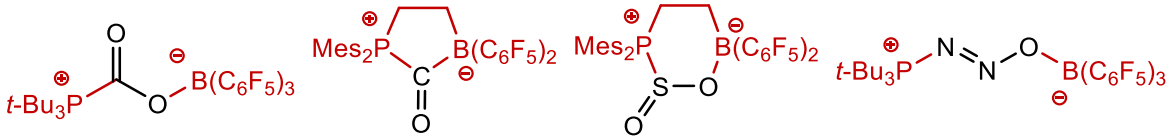

Figure 9 - CO_2, CO, SO_2 and N_2O molecules captured by FPLs (red)[43].

A compound of great interest that cannot yet be activated by FLPs is methane (CH_4). Methane is one the major gases responsible for global warming and its conversion into useful products such as methanol would be most profitable. However, no FLP has been able to successfully activate methane to this day. Several theoretical studies tried to address this problem by understanding the reasons behind this difficulty. Wang *et al.*[46] first compared hydrogen and methane activation and concluded that FLPs were less reactive with methane mainly because of a high entropic penalty in the transition-state as an inversion of the central carbon occurs (Figure 10). Erker *et al.*[49] demonstrated through indirect syntheses of the possible products of methane C-H activation that these were actually very stable, even when heated. This further indicated a very high kinetic barrier of the reaction. Finally, Rincon and co-workers[50] calculated that the high activation barrier is not only due to the distortion of the methane to reach the transition-state but also to a large distortion of the Lewis acid to better interact with the methane. Furthermore, they concluded that alane Lewis acids such as tris(pentafluorophenyl)alane (Al(C$_6$F$_5$)$_3$), instead of the classical boranes, are the most promising candidates for methane activation as they considerably reduce the activation barrier.

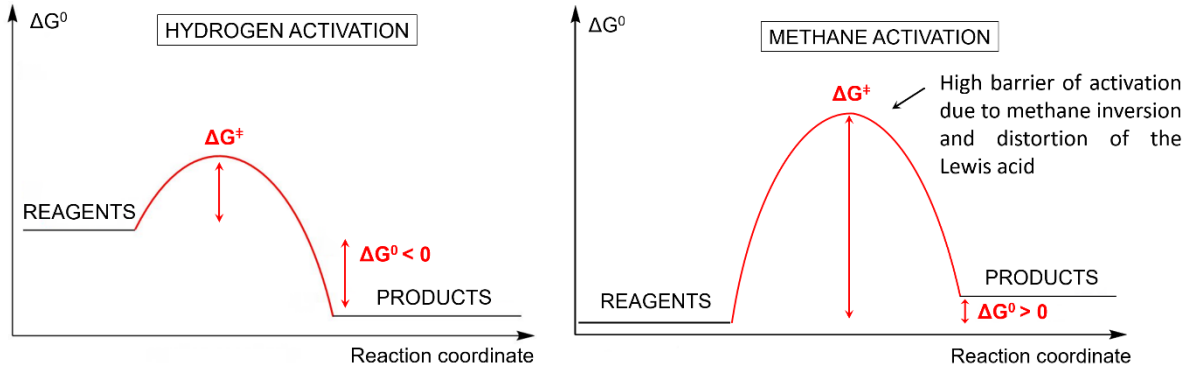

Figure 10 - Qualitative comparison of the energy profiles of the reactions of hydrogen and methane activation.

The current available methods for catalytically activating methane are catalyzed by transition metals. Periana *et al.*[51] developed the first catalytic conversion of methane into a methanol derivative using a Pt (II) complex. More recently, the groups of Sanford[52] and Mindiola and co-workers[53] developed catalytic C-H borylations of methane using Ir, Rh and Ru complexes (Scheme 7).

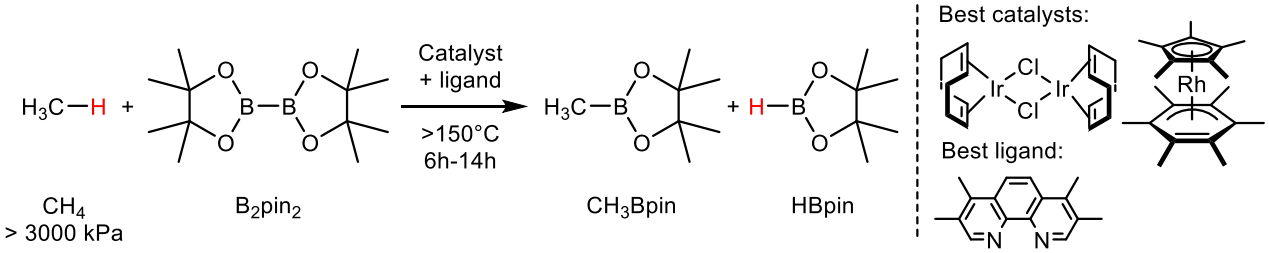

Scheme 7 - Transition-metal catalyzed selective monoborylation of methane[52].

4.2.3 Development of new bulky Lewis bases

Substantial advances in the area of frustrated Lewis pair catalysis are reliant on the design and synthesis of new bulky Lewis bases. In the past years, a wide series of bulky Lewis bases, phosphines and amines, have been developed[54, 55, 56] (Figure 11). However, ring-strained phosphines remain largely understudied, though their structural and electronic properties are unique, as discussed in the next section.

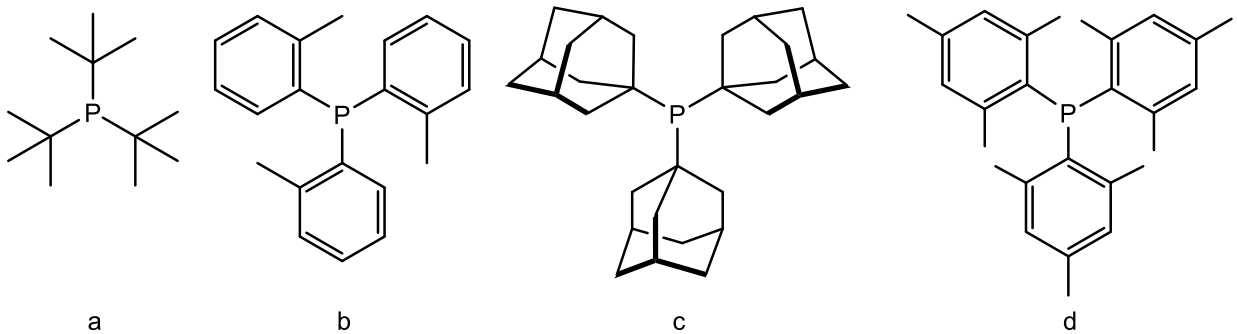

Figure 11 - Examples of sterically hindered phosphines: tris(tert-butyl)phosphine (a), tris (o-tolyl)phosphine (b), tris(1-adamantyl)phosphine (c), tris(mesityl)phosphine (d).

5. Phosphatriptycene

A nearly unexplored and yet promising class of phosphines are 9-phosphatriptycene derivatives. The 9-phosphatriptycene (henceforth simply called "phosphatriptycene") is a strongly pyramidalized ring strained phosphine with its phosphorus fixed in the 9-position of the tricyclic bridgehead of the [2.2.2]-bicyclooctane inner motif. The phosphatriptycene was first synthesised by Bickelhaupt in 1974 with 35% yield (Scheme 8)[57].

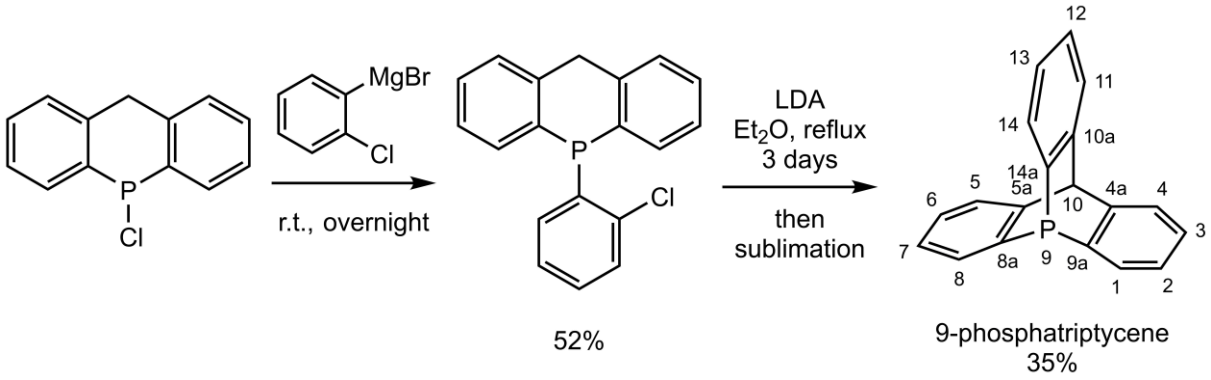

Scheme 8 - Bickelhaupt's synthesis of 9-phosphatriptycene. The atomic numbering used is introduced by Chen and Ma in reference [58].

In the past fifteen years, several new developments and syntheses were made on the phosphatriptycene and its derivatives. A new synthetic pathway was designed by the group of Kawashima in 2003[59] that uses phosphatriptycene oxides intermediates to access methoxy substituted phosphatriptycenes (Figure 12a). Other oxide derivatives were later described by the same group[60]. Tsuji *et al.*[61] reported the synthesis of new 9-phospha-10-silatriptycenes (Figure 12b) and derivatives as well as a study of their structure and properties. In order to have a better solubility in common organic solvents, the group of Mazaki[62] introduced methyl groups on phosphorus- and antimony-based diheteratriptycenes. These methyl groups were added on the 2, 3, 6, 7, 12 and 13-positions (Figure 12c).

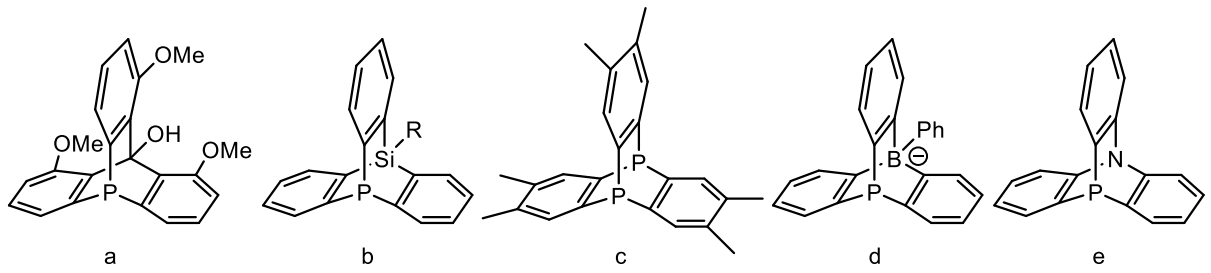

Figure 12 - Phosphatriptycene derivatives: Kawashima's phosphatriptycene derivative (a)[59], Tsuji's 9-phospha-10-silatriptycene (b)[61], Mazaki's methylated 9,10-diphosphatriptycene (c)[62], Sawamura's 9-phospha-10-boratriptycene derivative (d)[63] and Shionoya's 9-phospha-10-azatriptycene (e)[64].

A significantly greater challenge, however, is to add substituents in positions 1, 8 and 14 (i.e. in *ortho* position relative to the phosphorus), and no example of triptycenes with this interesting substitution pattern has been reported so far.

To this day, the applications of phosphatriptycenes are limited to being used as ligands in organometallic chemistry. These strong π-acids and rather weak σ-donors have been shown to be effective ligands in palladium-catalyzed reactions, Stille coupling and Heck reactions[65]. Recently, the group of Sawamura reported the synthesis of a 9-phospha-10-boratriptycene (Figure 12c), used as ligand in a Pd-catalyzed Suzuki-Miyaura cross-coupling[63]. In heterogeneous catalysis, a silica-supported phosphatriptycene has also displayed strong ligand properties in Pd-catalyzed Suzuki-Miyaura cross-couplings[66] and Rh-catalyzed selective C-H borylations[67]. Shionoya *et al.*[64] described the synthesis of azaphosphatriptycene (Figure 12e) as a rotor in a palladium-centred molecular gear.

The phosphatriptycene has never been tested as a Lewis base in FLPs or in any other types of organocatalysis. It possesses however interesting properties. The scaffold is very robust and can be heated to very high temperatures without degradation. *Ortho*-substituents in the unique structure of the triptycene would be fixed in a rigid position, pointing forward. This could be very useful in a number of applications (Figure 13). The stereoelectronic properties of the phosphatriptycene could be modulated by adding alkyl groups to increase steric hindrance around the phosphorus (and, to a smaller extent, increase the electrodonating character of the phosphorus). Also, a Lewis acidic site could be grafted on that position, thus forming an intramolecular FLP. Finally, addition of a protic group such as an amine or an alcohol to the phosphatriptycene scaffold would produce a bifunctional catalyst for MBH reactions, as it fulfills the criteria described in Figure 5. With three distinct substituents in the aryl groups, the phosphatriptycene would become P-chiral, with the major advantage that it cannot undergo inversion, even under high heating (which was the limiting factor of classical chiral phosphines), thereby opening a great potential for asymmetric catalysis.

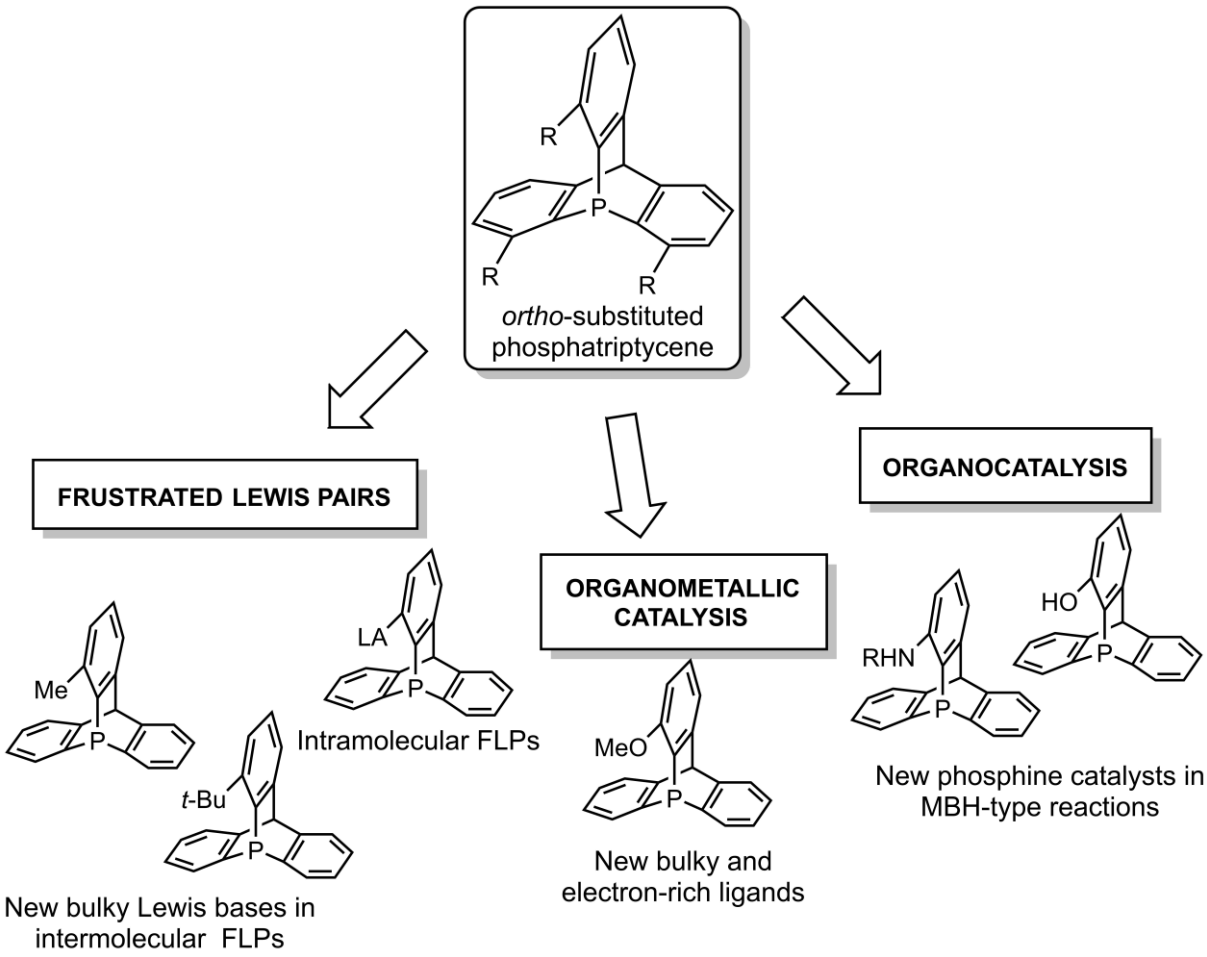

Figure 13 - Possible applications of the ortho-substituted phosphatriptycene. LA = Lewis acid.

PART II - Research objectives

Since their discovery by D. Stephan a little more than ten years ago[40], FLPs have prompted considerable interest and have undoubtedly become a major field of transition-metal free catalysis. In this context, our group endeavours to synthesize novel types of Lewis acids and bases, mainly boranes and phosphines, aiming to develop new FLPs, both inter- and intramolecular[68].

As shown in the previous section, the phosphatriptycene and its derivatives have only received limited attention since the first synthesis of phosphatriptycene in 1974. It is surprising given its unique scaffold and properties. Furthermore, phosphatriptycenes have never been involved in any FLP process. This work aims to pursue the investigation of this peculiar compound and its derivatives and probe its capacity in frustrated Lewis pair catalysis.

As the phosphatriptycene has a tedious and unpractical synthesis[57], the first objective of this work is to develop and optimize a new synthetic method. In addition, the second goal is to access the *ortho*-substituted phosphatriptycene, either the mono, bis or trisubstituted compound. These substitution patterns are the most challenging and have not been previously reported. This will considerably increase the steric hindrance around the phosphorus atom, especially when methyl or tert-butyl substituents will be employed. The target compounds of this master thesis are thus the methyl substituted phosphatriptycenes, compounds **1a**-**d**. The *tert*-butyl groups being even more challenging to add due to their steric hindrance, the synthesis of *tert*-butyl substituted phosphatriptycenes will not be addressed in the present work.

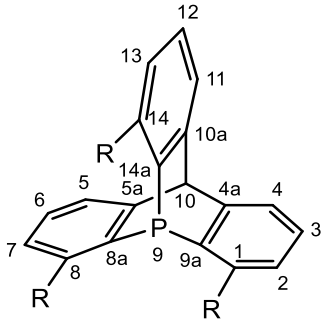

1a – $R^{1,8,14}$ = H
1b – R^{1} = Me, $R^{8,14}$ = H
1c – R^{1} = Me, R^{8} = Me, R^{14} = H
1d – R^{1} = Me, R^{8} = Me, R^{14} = Me

*Figure 14 - Structures of the novel phosphatriptycenes studied in this work **1a-d**.*

Our proposed retrosynthetic strategy to synthesize phosphatriptycenes is shown in Scheme 9. This strategy consists in the synthesis of a tribrominated phosphine precursor that undergoes a lithium-halogen exchange, then cyclizes on phenylchloroformate to give a 9-phospha-10-hydroxytriptycene that is further reduced into the target phosphatriptycene (Scheme 9).

X-Ray analyses of several isolated products have been carried out and will be further discussed.

In parallel to the experimental work, a Density Functional Theory study of the association of the studied compounds with a Lewis acid and an analysis of their thermodynamic, structural, and stereoelectronic properties has been undertaken in view of the development of a novel type of FLPs.

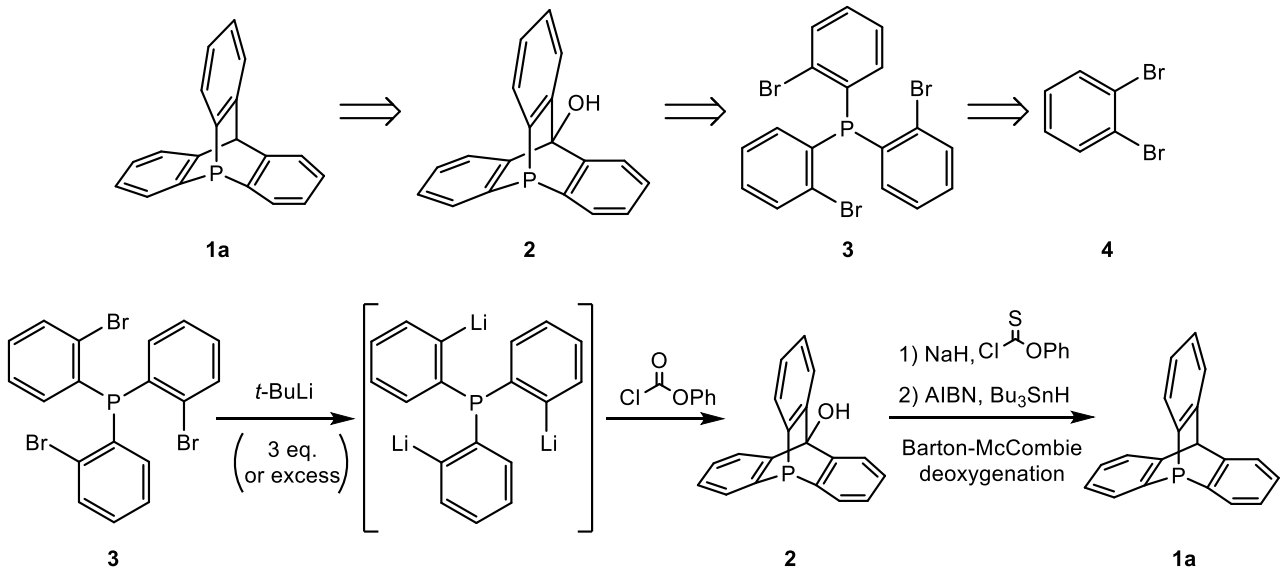

*Scheme 9 - Retrosynthetic (up) and synthetic (down) approach to form phosphatriptycene **1a**.*

PART III - Experimental results and discussion

1. Synthesis of phosphatriptycene

1.1 Phosphine precursor synthesis

The proposed synthesis of phosphatriptycene **1a** starts from the tris(2-bromophenyl)phosphine precursor **3**, itself prepared from 1,2-dibromobenzene **4** in 50% yield (Scheme 10)[61]. The brominated triphenylphosphine **3** is air-stable and is not oxidized even after months-long periods open to air.

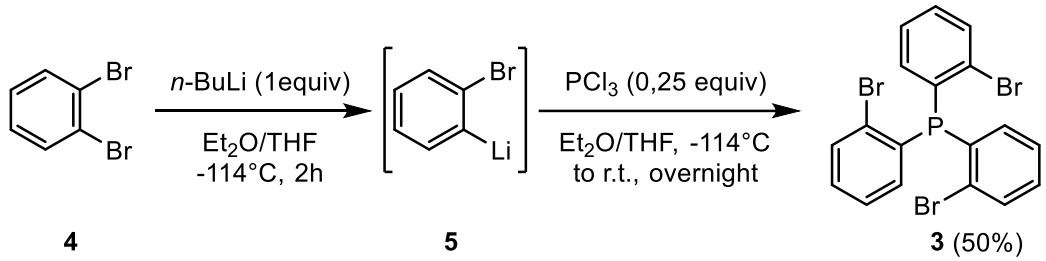

*Scheme 10 - Synthesis of tris(2-bromophenyl)phosphine **3**.*

The first step of this reaction is a Br/Li exchange to form the *o*-bromophenyllithium intermediate **5** which then performs a three-fold nucleophilic attack on PCl_3. This reaction was first described by Tsuji *et al.* in the synthesis of 9-phospha-10-silatriptycene (*Part I*, section 5)[61]. The very low temperature of -114°C (using an ethanol/$N_{2(l)}$ cooling bath) is necessary to avoid the formation of benzyne **6** from compound **5** (through LiBr elimination[69]) which would result in polymerization and side-reactions to give undesired by-products such as biphenylene **7** and triphenylene **8** (Scheme 11). The same reaction performed at a higher temperature (-94°C, using an acetone/$N_{2(l)}$ cooling bath) only gave benzyne degradation products. Careful reaction temperature control is thus a crucial parameter to have reasonable yields of **3**. Furthermore, the dihalogenobenzene used also has a significant impact on benzyne formation: *o*-iodophenyllithium **9** derived from 1,2-diiodobenzene **10** is unstable, even at -114°C, and only benzyne degradation products are observed with this reagent (Scheme 11). The leaving group ability of the halogen determines the relative stability of the corresponding *o*-halogenophenyllithium (from less stable to more stable: $I^- < Br^- < Cl^- < F^-$)[69].

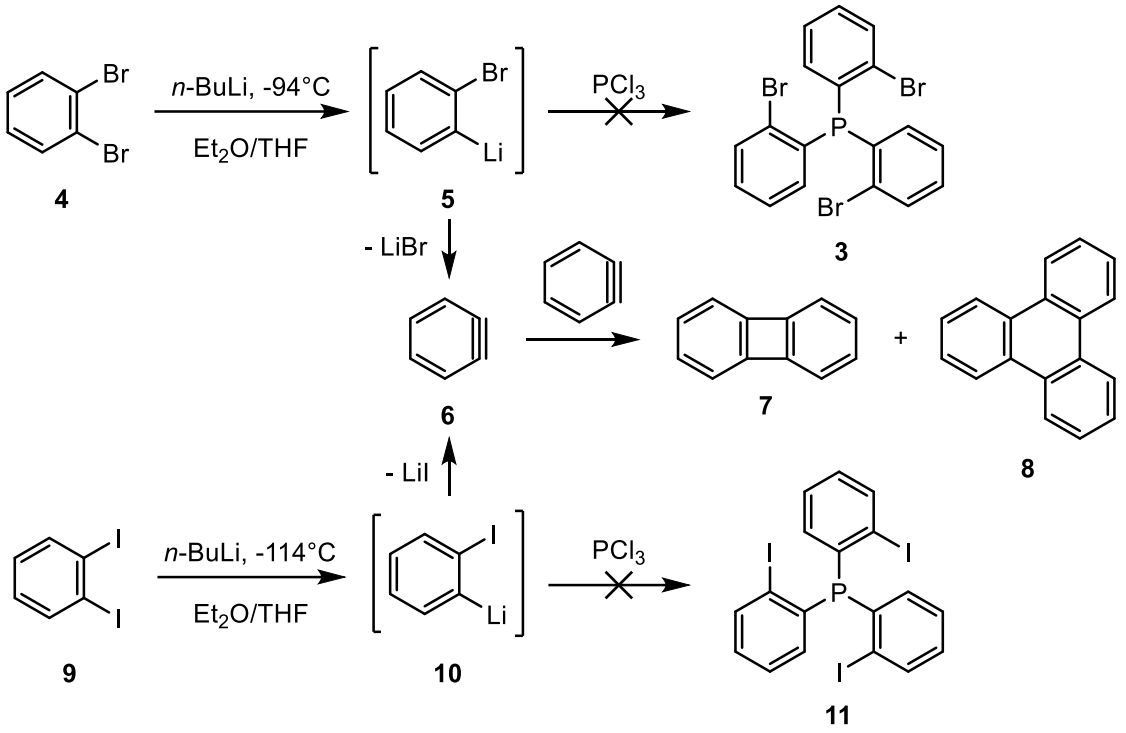

*Scheme 11 - Attempted syntheses of phosphine precursors and formation of possible undesired by-products biphenylene **7** and triphenylene **8**.*

A more efficient and practical synthesis of **3** has also been reported using the organomagnesium reagent **13** instead of the lithium reagent **5** as a nucleophile. By applying these conditions[63], we synthesised **3** in 81% yield starting from 1,2-iodobromobenzene **12** via a magnesium-bromine exchange using *i*-PrMgCl and subsequently adding PCl_3 in the presence of a catalytic amount of copper (I) iodide (CuI) (Scheme 12). The presence of CuI is really crucial since no product was formed without this copper salt.

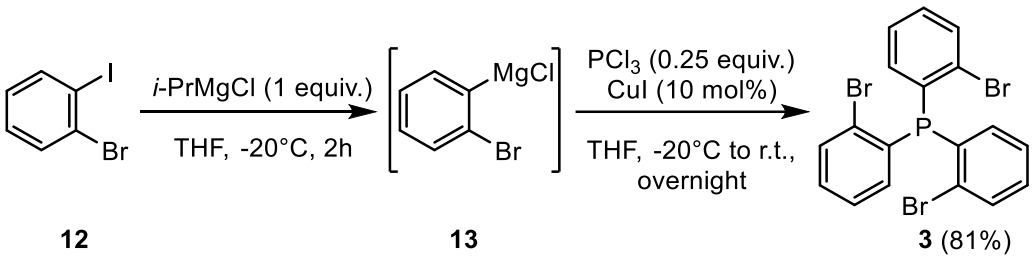

*Scheme 12 - Copper (I) catalyzed synthesis of tris(2-bomophenyl)phosphine **3**.*

The reaction can be performed at -40°C and -20°C because the intermediate is much more stable towards MgBrCl elimination and benzyne formation than its lithium counterpart. From a mechanistic point of view, it is believed that the reaction proceeds through the formation of an organocopper intermediate **14** resulting from Mg/Cu exchange with intermediate **13** (Scheme 13). After addition on the phosphine, CuCl is generated and, in the presence of MgICl, a salt metathesis reaction occurs to regenerate the CuI catalyst while $MgCl_2$ precipitates.

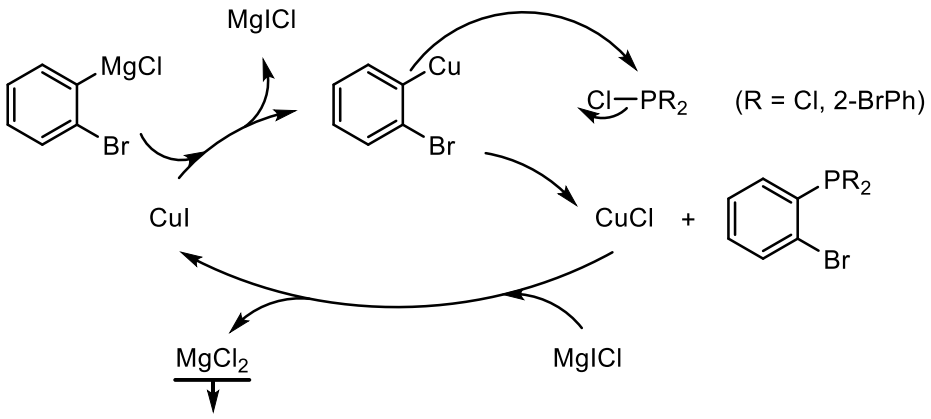

Scheme 13 - Proposed catalytic cycle of CuI in the addition reaction.

In order to assess its reactivity and eventually develop the syntheses of new tertiary phosphines (see section 2.1.2), we endeavoured to isolate the Ar_2P-Cl reaction intermediate **15** (Scheme 14).

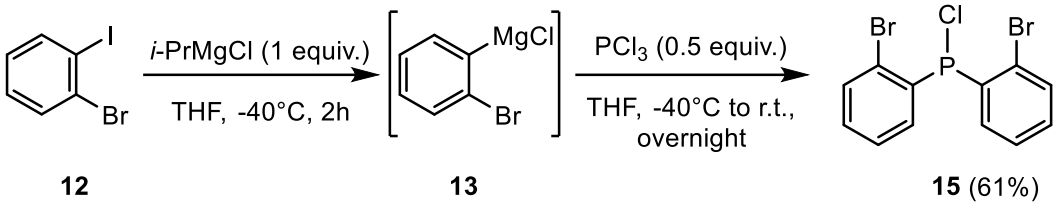

*Scheme 14 - Formation of intermediate **15** from 1,2-iodobromobenzene **12**.*

Diarylchlorophosphines Ar_2P-Cl are known to be reactive towards nucleophiles and are generally sensitive to water, easily oxidized and must be manipulated under inert atmosphere[70]. Unexpectedly, compound **15** is air-stable and the reaction workup has been performed in open air conditions as well as the following manipulations: weighting, filtration, crystallisation, storing, … It is stored in argon-flushed flasks without apparent degradation for several weeks. This unusual stability can be rationalised by the presence of the large bromine atoms in ortho-position which protect the P-Cl bond from oxidation and hydrolysis. The formation of phosphine **3** directly from **15** has been carried out successfully (Scheme 15).

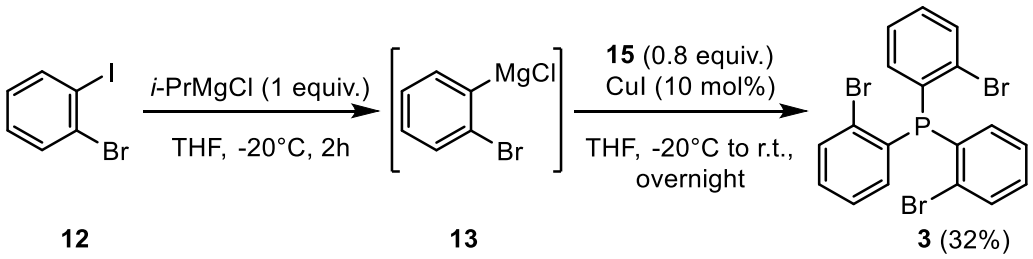

*Scheme 15 - Formation of phosphine **3** using the diarylchlorophosphine **15**. This reaction was only done once, and the unexpected low yield is due to partial loss of product by accident during the treatment.*

This observation enables us to better understand the kinetics of the reactions described in Scheme 10 or Scheme 12. The rate-determining step of these reactions is the third addition of intermediate **5** and **13** on the diarylchlorophosphine **15** formed in-situ. As a key to success, the organometallic

reagent must be reactive enough at a low temperature in order to avoid degradation into benzyne. In the present situation, the lithium compound **5** at -114°C exhibits enough nucleophilicity to overcome the steric barrier of the rate-determining step and form phosphine **3** while a CuI catalyst is needed for the magnesium compound **13** at -20°C.

1.2 Cyclization reaction

The 9-phospha-10-hydroxytriptycene **2** is obtained by the triple Br/Li exchange of the phosphine precursors **3** and their cyclization reaction on phenyl chloroformate (Table 2). The optimal amount of *t*-BuLi has been found to be about 3.5 equivalents. *Tert*-butyllithium is widely used in halogen-lithium exchange reactions as it gives fast and clean exchanges over a broad range of temperatures[71]. Two equivalents are almost systematically used, the first one to perform the Br/Li exchange and the second to eliminate the subsequently formed *t*-BuBr (Scheme 16).

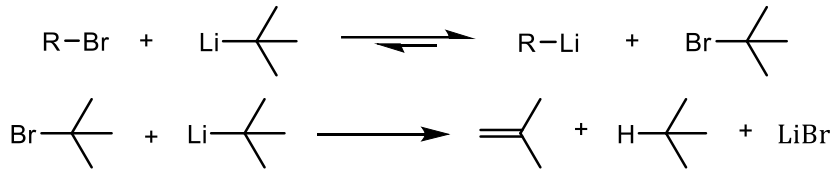

Scheme 16 - Lithium-bromine exchange with t-BuLi and elimination of the formed t-BuBr. Scheme reproduced from reference [72].

Six equivalents of *t*-BuLi (i.e. twice the number of bromine atoms on compound **3**) were thus expected to give the best yields for our reaction but, unexpectedly, it was observed that the best yields were obtained with only three (Table 2). A similar observation (best results with 1.0 equivalent) was reported by Waldmann *et al.*[72] in lithium exchanges of aryl bromides at -53°C in diethyl ether.

*Table 2 - Synthesis of 9-phospha-10-hydroxytriptycene (**2**) from tris(2-bromophenyl)phosphine (**3**) and yields of the reaction for several numbers of equivalents of t-BuLi.*

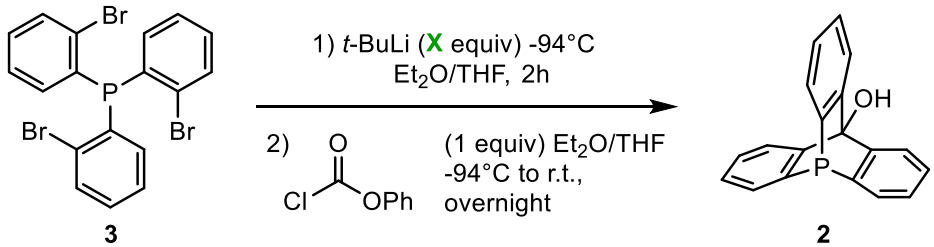

3 **2**

Equivalents of *t*-BuLi (**X**)	Isolated yield of **2** (%)
6.0	44 (over 2.0 g)
4.0	62 (over 1.1 g), 57 over (0.5 g)
3.0	59 (over 2.1 g), 79 (over 0.5 g)
2.0	25 (over 2.0 g), 34 (over 0.5 g)

More surprisingly, we discovered that with two equivalents of *t*-BuLi on compound **3**, a mixture of 9-phospha-10-hydroxytriptycene **2** and of **16** with a ratio of approximately 1:1 is obtained, although **17** was expected (Figure 15).

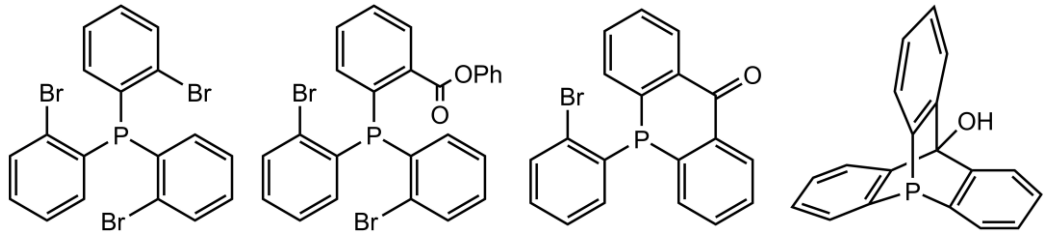

3 **16** **17** **2**

*Figure 15 - Products of the first (**16**), second (**17**) and third (**2**) addition of the mono-, bis- and tris-lithiophosphines derived from **3** on phenyl chloroformate.*

A plausible explanation to explain this result (Scheme 17) is that upon addition of 2 equivalents of *t*-BuLi, the bis-lithio compound **18** is obtained. When phenyl chloroformate is added, a first attack by compound **18** takes place, immediately followed by the second addition because of close proximity between the reactants, giving product **17**. A Br/Li exchange happens next between **17** and **18**. The subsequent non-reversible intramolecular cyclization to form 9-phosphatriptycene **2** displaces the equilibrium towards the products. As an end result, for each phosphatriptycene formed, a monoaddition product **16** is formed with the same proportion.

A worthy investigation that has not been attempted in this master thesis is the use of *n*-butyllithium for the lithium-bromine exchange of compound **3**. Indeed, if most cyclization reactions of triptycene derivatives described in the literature are performed with *t*-BuLi[61, 64, 62], Agou et al. reported the lithiation reaction of arylbis(2-bromophenyl)phosphines with *n*-BuLi[73]. This would provide a safer and cheaper cyclization reaction of compound **3**.

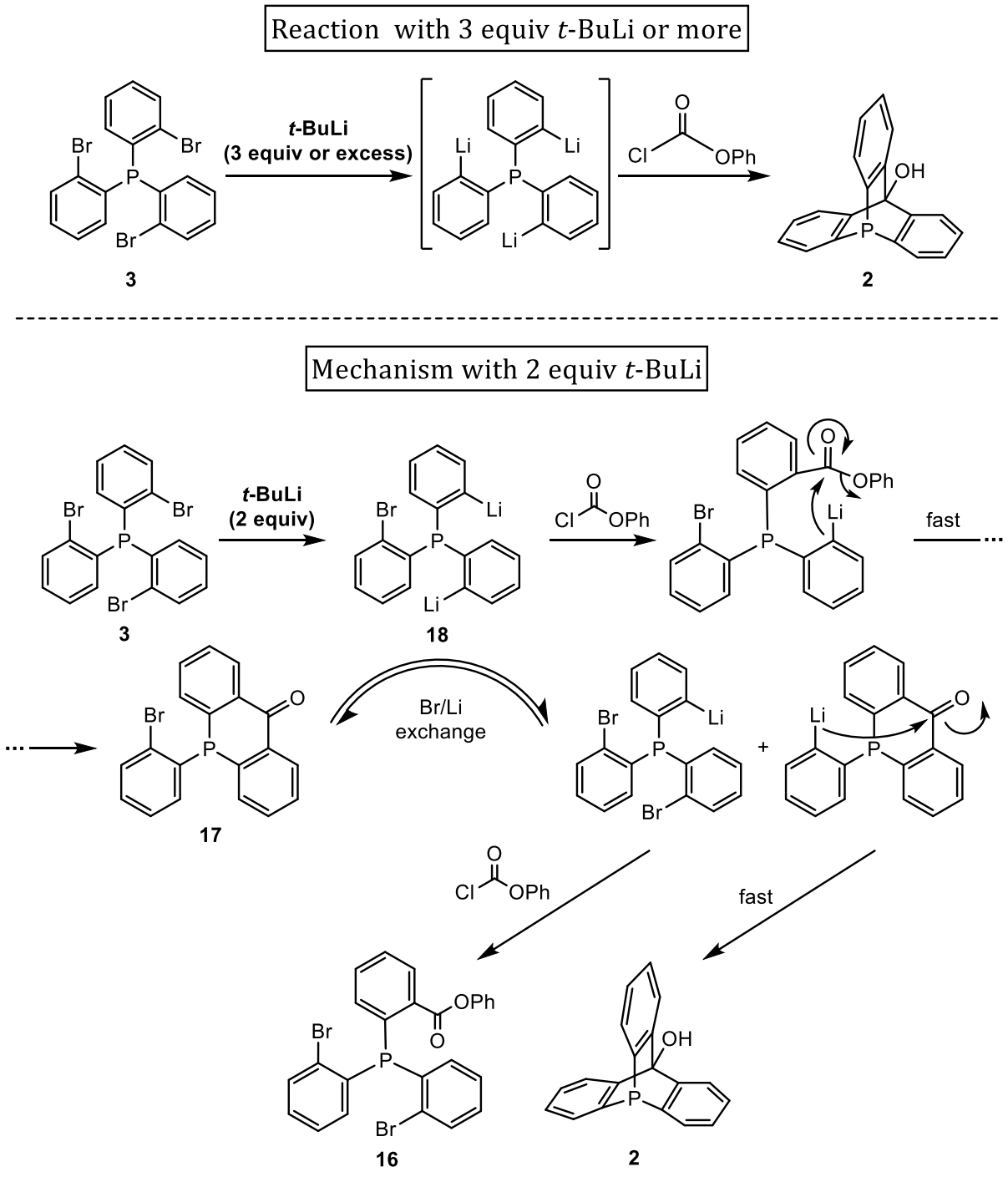

*Scheme 17 - Proposed mechanism of the cyclization reaction with three or more equivalent of t-BuLi and with two equivalents of t-BuLi. The quick formation of **2** displaces the Li/Br exchange equilibrium of **17** towards formation of the products.*

1.3 Alcohol reduction and formation of phosphatriptycene

Due to the rigid character of the triptycene scaffold, no classical alcohol reduction under Lewis or Brønsted acidic conditions could be achieved. The OH group attached to a non-planar bridgehead carbon is not ionized under acidic conditions because the formation of a non-planar carbocation is thermodynamically very unfavourable. S_N1 reactions to generate a carbocation C-9 are thus non-feasible in our case. S_N2 reactions cannot proceed either because the opposite side of the carbon is not accessible to a nucleophile. Reactions of compound **2** with triethylsilane under Lewis (BF_3-OEt_2) and Brønsted (TFA) acidic conditions were attempted but the phosphatriptycene **1a** was not detected even after 7 days of reaction.

Another method to reduce alcohols is the Barton-McCombie deoxygenation (Scheme 18). This reaction proceeds through a radical process, which is not limited by the issues mentioned above, and was tested for 9-phospha-10-hydroxytriptycene **2**.

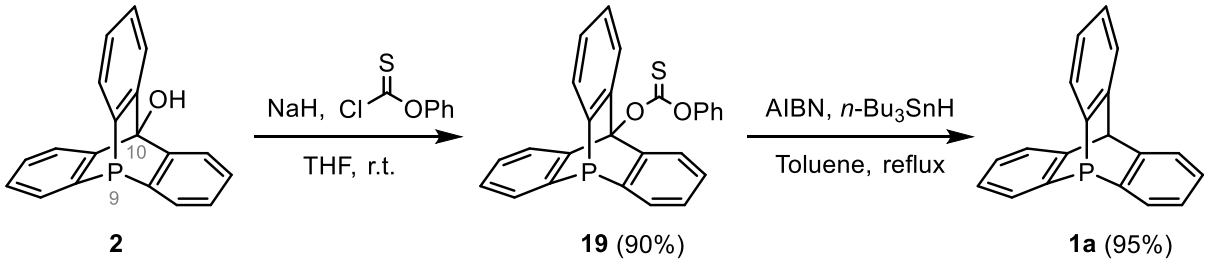

2 **19** (90%) **1a** (95%)

Scheme 18 - Barton-McCombie deoxygenation (performed by Lei HU). AIBN = Azobisisobutyronitrile.

The overall yield of the reduction is 86% over two steps. A novel synthesis of the phosphatriptycene **1a** was thus successfully developed, starting form 1,2-iodobromobenzene **12** in four steps (phosphine precursor synthesis, cyclization reaction and two steps of Barton-McCombie deoxygenation) in an overall yield of 55%. Alternative reagents for Barton-McCombie reaction were tested: $(TMS)_3SiH$ was used instead of the *n*-Bu_3SnH in the presence of AIBN and gave phosphatriptycene **1a** in 71% yield. The yield of the reaction is reduced but it has the advantage to avoid using toxic tin reagents and by-products.

1.4 Alternative strategy for the synthesis of phosphatriptycene

Sections 1.1 to 1.3 describe the synthesis of phosphatriptycene in an approach that starts from a phosphorus-centred precursor that cyclizes on a carbon electrophile (phenyl chloroformate) to form the triptycene scaffold. However, an alternative synthetic route exists with the exact opposite approach: from a carbon-centred precursor that cyclizes on a phosphorus electrophile to give phosphatriptycene **1a**. The proposed strategy relies on a tris(2-halogenophenyl)methane

20 precursor that undergoes triple Br/Li exchange with *t*-BuLi and then performs cyclization with PCl_3. Compound **20** would be synthesised from reaction of 1,2-dibromobenzene on phenyl chloroformate and reduction of the subsequently formed alcohol in strongly acidic conditions (Scheme 19). This method has the major advantage of avoiding removal of the alcohol on the terminal bridgehead carbon of the triptycene. On a triphenylmethanol derivative, a S_N1 mechanism can take place, meaning that Lewis or Brønsted acids are sufficient to perform the reduction. However, we have not been able to synthesize compound **20** despite several attempts. This is probably due to the steric hindrance around the ketone group of **20A.** Since the reaction is carried out at -110°C to avoid benzyne formation, the lithium compound formed from reacting **4** with *n*-BuLi cannot perform the attack on the ketone group on the third step.

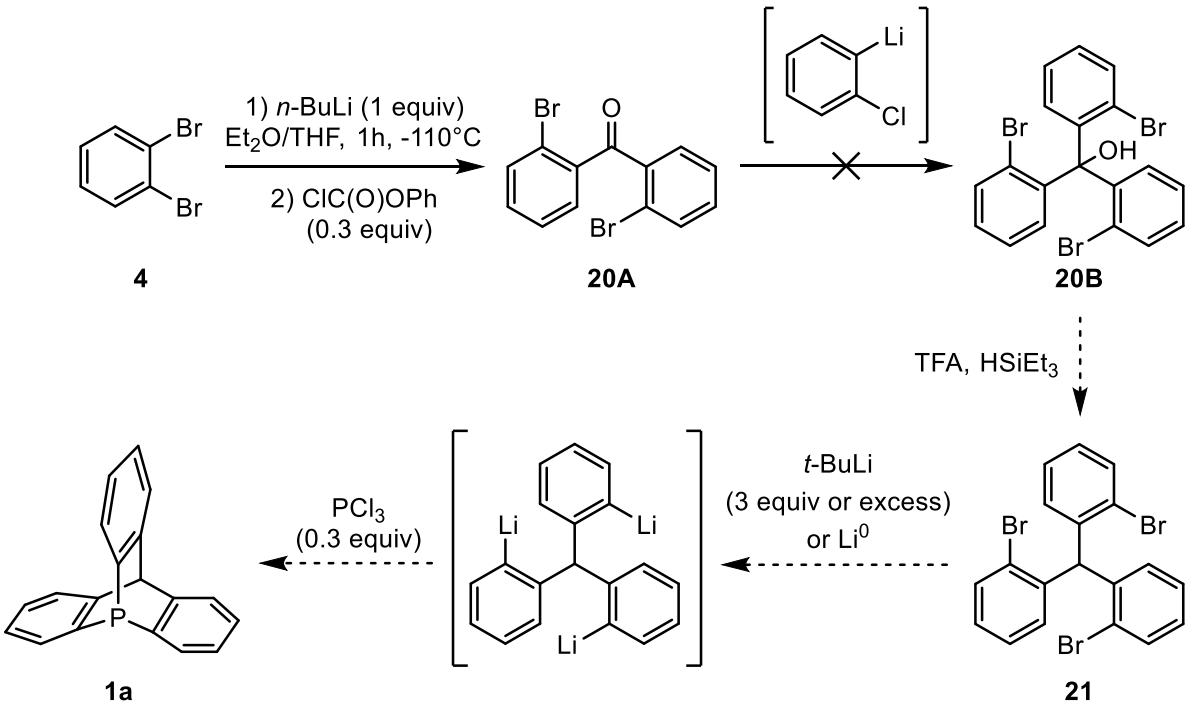

Scheme 19 - Synthesis of phosphatriptycene from a triphenylmethane precursor.

Finally, by reacting bis(2-bromophenyl)(2-iodophenyl)methane **22,** analogue of tris(2-bromophenyl)methane **21**, with *t*-BuLi and PCl_3, phosphatriptycene was afforded in 62% yield. Compound **22** has a four steps synthesis from diphenyl(2-iodophenyl)methane (global yield of 39%)[74] and was improved by Arnaud OSI in the context of his master thesis. This strategy represents a completely new synthetic route to phosphatriptycene, however less practical, with an overall yield of 24% and two more steps than the phosphine precursor pathway.

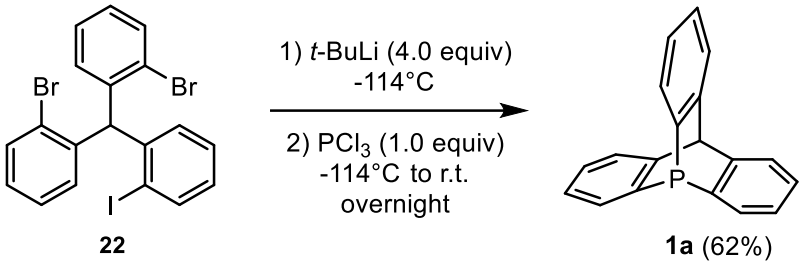

*Scheme 20 - Synthesis of phosphatriptycene **1a** from bis(2-bromophenyl)(2-iodophenyl)methane **22**. Reaction performed by Lei HU.*

A significant challenge would be to obtain substituted derivatives from **22** to access substituted phosphatriptycenes. Another approach is to start from substituted phosphines as described in the next part.

2. Accessing *ortho*-substitution on phosphatriptycene

2.1 Phosphine precursors syntheses

2.1.1 Precursor to trisubstituted phosphatriptycene

Not any phosphatriptycene substituted at the *ortho*-position have been synthesised so far. The simplest strategy to access *ortho*-methylated phosphatriptycenes is to start from the previously developed synthesis and adapt it by adding methyl groups on the starting material. First, we will endeavour to prepare trimethylphosphatriptycene **1d**, the synthesis of mono- and dimethyl phosphatriptycene will be discussed later. The following retrosynthesis is planned (Scheme 21).

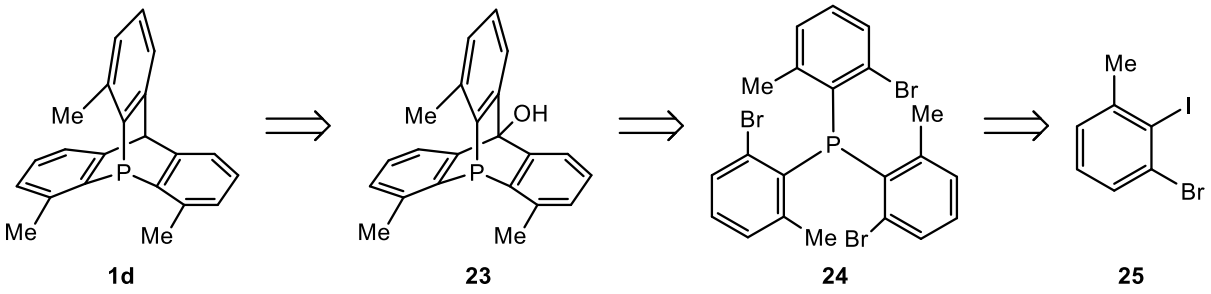

*Scheme 21 - Retrosynthesis of methyl-substituted phosphatriptycene **1d**.*

As in the case of the unsubstituted phosphatriptycene **1a**, the first step will be the synthesis of the tris(*o*-bromo-methyl)phosphine precursor **24** from the 1-bromo-2-iodo-3-methylbenzene **25** starting material. This tris-substituted benzene was readily prepared from commercially available 2-bromo-6-methylaniline **26** in 93% yield using a Sandmeyer reaction (Scheme 22)[75].

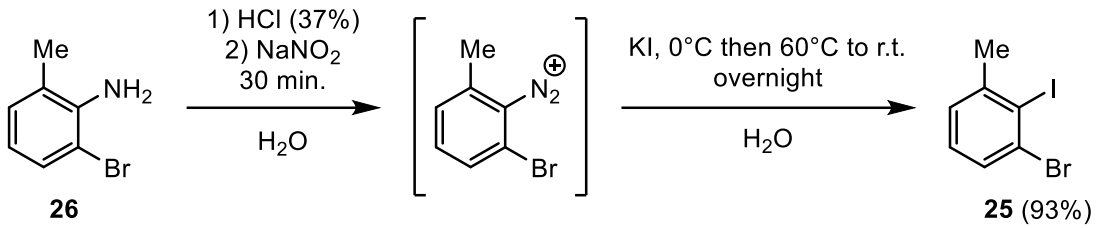

*Scheme 22 - Sandmeyer reaction to form 1-bromo-2-iodo-3-methylbenzene (**25**) from 2-bromo-6-methylaniline (**26**).*

An I/Li exchange was performed on starting material **25** using *n*-BuLi before adding PCl_3 to form phosphine **24** (Scheme 23). As the rate of lithium/iodine exchange is significantly higher that of Br/Li one, there should be a selective metalation on the position of the iodine atom.

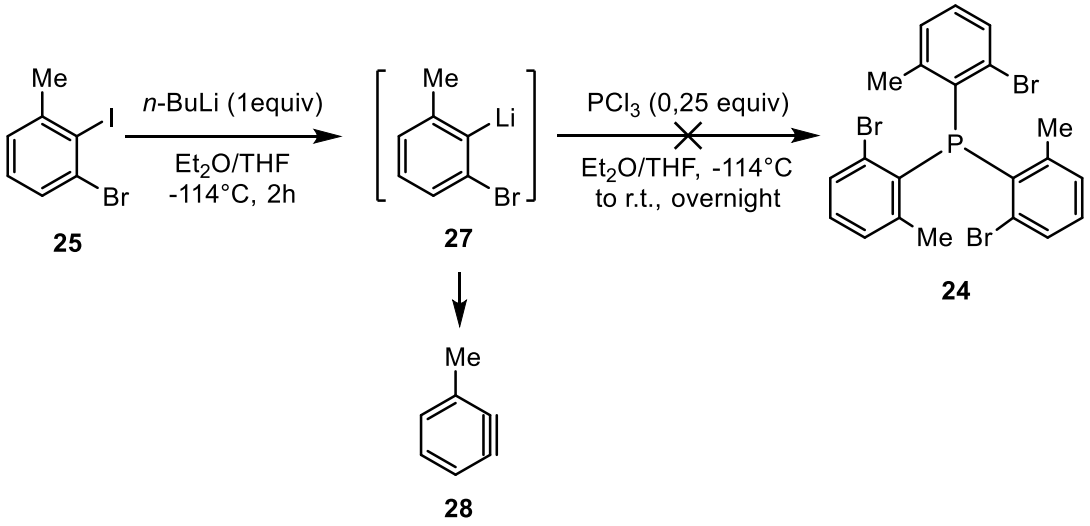

*Scheme 23 - Attempted synthesis of phosphine precursor **24** using an organolithium intermediate.*

Unfortunately, only benzyne degradation product was observed after the reaction. This result is not surprising considering the electronic and steric effect of the methyl group on its neighbouring lithiated carbon. The electrodonating character of the methyl group destabilises the negative charge on the carbon and its bigger size "pushes" the vicinal lithium towards the bromine atom and accelerates formation of benzyne (Scheme 24).

- **Electronic destabilization**: with an inductive donor effect of the methyl group, the negative charge is destabilised, hence more reactive.
- **Steric destabilization**: due to its size, the methyl group pushes the lithium towards the bromine atom, accelerating the formation of benzyne.

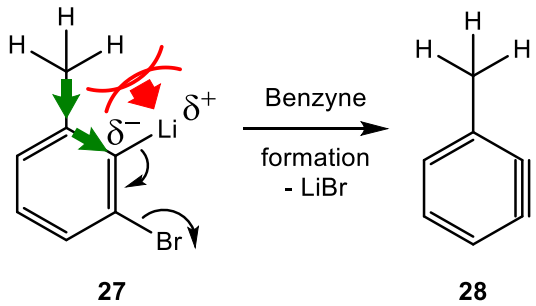

Scheme 24 – Destabilisation induced by the ortho-methyl group leading to benzyne formation.

We decided to use the organomagnesium reagent *i*-PrMgCl instead of *n*-BuLi. *Ortho*-halogeno aryl magnesium species are less prone to form benzyne than organolithium compounds. The copper-

catalysed method used for the synthesis of phosphine **3** was unsuccessful for obtaining **24** (Scheme 35) either at -40°C or at -20°C. An alternative test was then performed using TMEDA (N,N,N',N'-tetramethylethylenediamine) in stoichiometric quantity instead of the CuI catalyst as this method is also described in the literature for phosphine synthesis. This second test also failed.

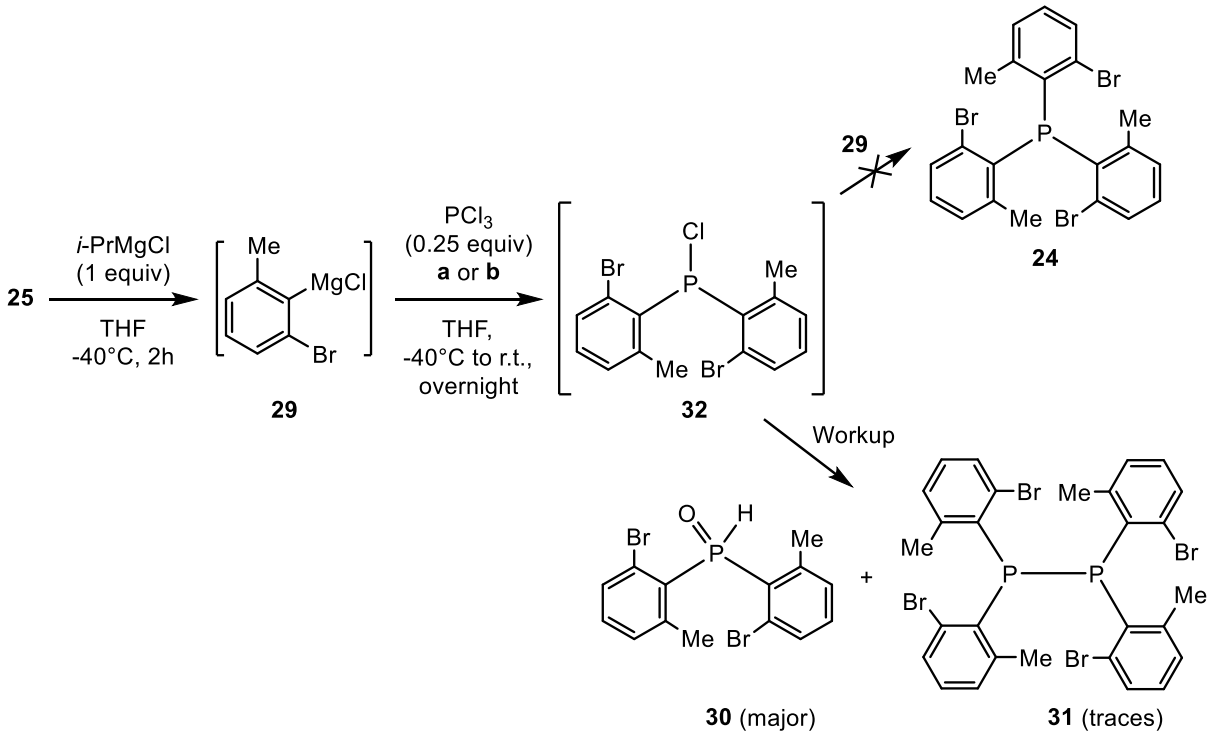

*Scheme 25 - Attempted synthesis of phosphine precursor **24** using a Grignard intermediate. Conditions: **a** = CuI (10 mol%); **b** = TMEDA (1 equiv).*

In both cases, the major products were the phosphine oxide **30** and a diphosphine **31,** thus unambiguously proving that diarylchlorophosphine **32** was formed in situ. Quenching of the reaction hydrolyses the P-Cl bond, forming the corresponding diarylphosphinous acid **33**, and further tautomerization forms the observed product **30** (Scheme 26A)[76]. The other by-product **31** is probably resulting from a radical dimerization of chlorophosphine **32** after homolytic cleavage of the P-Cl bond possibly induced by ambient light and heat (Scheme 26B)[77].

The phosphorus in the diarylchlorophosphine **32** is sterically hindered because of the two bulky substituents (Br and CH_3) in *ortho* position. Intermediate **29** is bulky as well and the reactivity of the Grignard reagent is simply not sufficient to overcome this steric barrier.

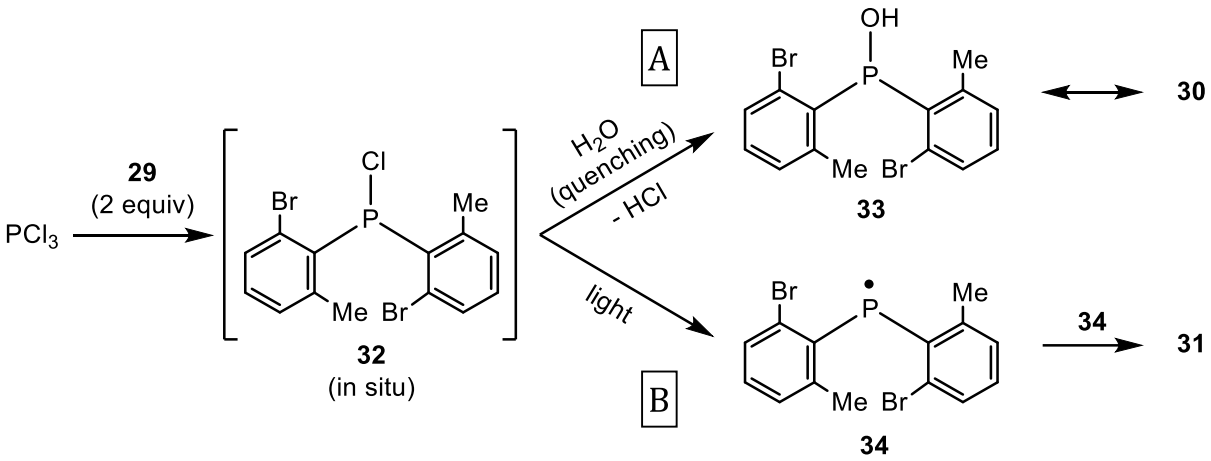

*Scheme 26 - Formation of the observed products of the reaction shown in Scheme 25 from decomposition of diarylchlorophosphine **32**.*

In contrast to the common harsh experimental conditions required to obtain the highly hindered tris(mesityl)phosphine (reflux of THF, long reaction time), heating the reaction mixture cannot be a viable alternative for our case because the degradation by MgBrCl elimination from the *ortho*-halogenomagnesium benzene will be very fast.

If the Grignard reagent is not reactive enough at -40°C and the lithium intermediate **27** is not stable at -114°C, a dead-end seems to be reached with this method and new strategies must be envisioned to access trisubstituted phosphatriptycene. Some of these strategies will be discussed in the perspectives of this work (see Part V, section 2) but in view of these reported unsuccessful attempts, we decided to focus on the synthesis of the less hindered mono-and disubstituted phosphatriptycene.

2.1.2 Precursors for mono- and disubstituted phosphatriptycenes

Adding one or two substituents on the phosphine precursor should be easier because it would create less steric hindrance around the phosphorus atom. The first strategy that was investigated is a direct application of a synthesis of unsymmetrical tertiary phosphine oxides reported by Hosoya *et al.*[78] (Scheme 27). This method consists in a sequential substitution of a phosphine oxide **36** with Grignard reagents. The phosphine oxide is substituted with *para*-tolylsulfanyl groups (-S-*p*-Tol) that will act as leaving groups. It is a stepwise process: after each substitution, the resulting phosphine oxide is isolated before another substitution takes place with another Grignard reagent. In three steps, an unsymmetrical phosphine oxide (i.e. with three different substituents) can be synthesised.

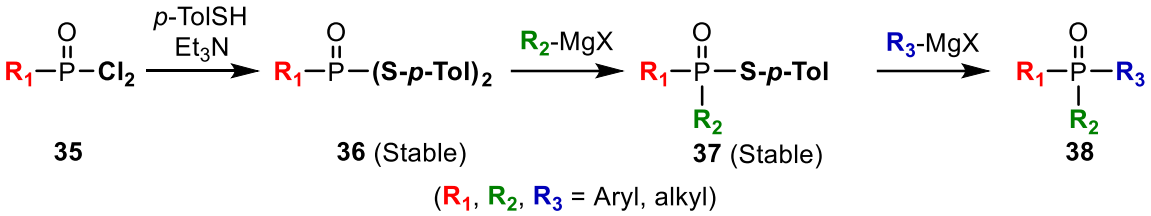

Scheme 27 - Hosoya's method for unsymmetrical phosphine oxides synthesis. Scheme reproduced from reference [78].

This method is viable because the leaving group ability of the *p*-tolylsulfanyl substituent is inferior to that of the chlorine atom (present in the usual phosphine oxide precursor $O{=}PCl_3$) but its reactivity is sufficient to act as leaving group upon attack of a Grignard reagent. Due to its chemical stability, each intermediate can, in principle, be isolated and purified before undergoing a new addition. The synthesis of the unsymmetrical phosphine oxide is followed by reduction to the corresponding phosphine using $HSiCl_3/Et_3N$.

For the present work, only two distinct substitutions have to occur in the syntheses of the mono- (**40**) and dimethylated (**41**) phosphine precursors (Scheme 28).

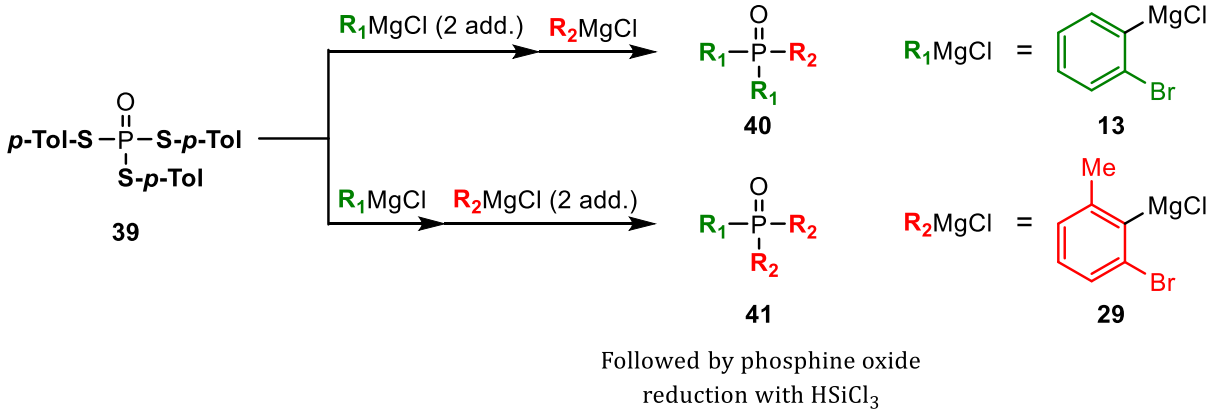

*Scheme 28 - Synthesis of mono- and dimethylated phosphine precursors **39** and **40** using Hosoya's method for unsymmetrical phosphine oxides. (add. = additions)*

The phosphine oxide precursor **39** was synthesised from trichlorophosphine oxide **42** in 65% yield (Scheme 29).

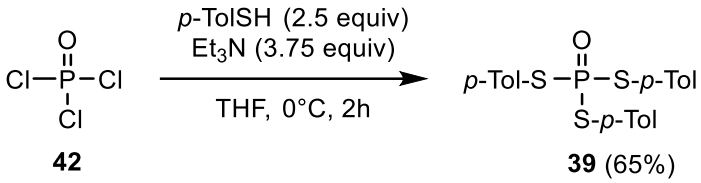

*Scheme 29 - Synthesis of phosphine oxide precursor **39**.*

The synthesis of compound **40** will be attempted before the one of **41** because **40** contains only one methyl group and should be easier to form. According to Hosoya's paper, the bulkiest group should be inserted first on the phosphine oxide. In this case, it means the methylated Grignard

reagent **29**. The first step has been attempted (Scheme 30) but the expected product was just detected, the starting material remained mostly unreactive.

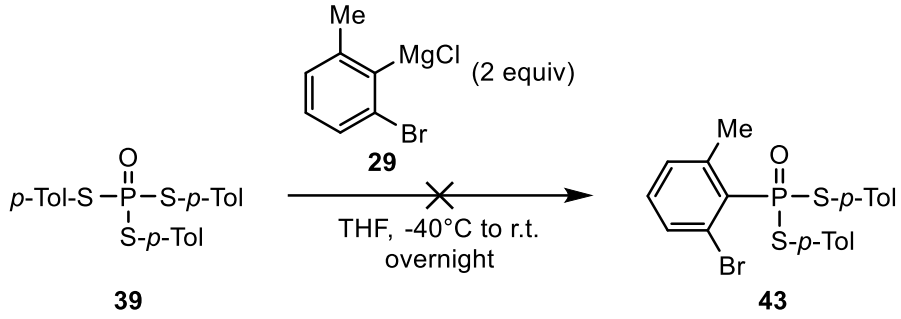

*Scheme 30 - Attempted first addition of Grignard reagent on phosphine oxide precursor **39**. The reaction only gave the starting material.*

In view of this result, we understood that the Grignard reagent **29** was too bulky to add on compound **39**. To evaluate the feasibility of the method, the use of the Grignard reagent **13** was tested (Scheme 31). This compound does not possess methyl groups and should be easier to add on phosphine oxide **39**. The resulting tris(2-bromophenyl)phosphine oxide **44** had already been synthesised by our group and its NMR chemical shifts were known. It is thus easy to detect its formation. The analysis of the reaction crude of **39** and an excess of **13** indicated that the reaction did not lead to the formation of the expected phosphine oxide. We therefore concluded that the method was not adapted to the synthesis of bulky phosphine oxides and this strategy was abandoned.

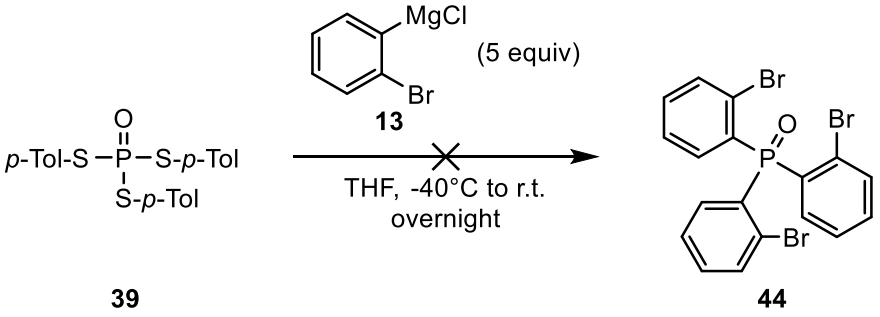

*Scheme 31 - Attempted synthesis of tris(2-bromophenyl)phosphine oxide **44** with an excess of o-bromophenylmagnesium chloride **13**.*

Once again, the organomagnesium reagent appears to be insufficiently reactive to overcome the steric barriers of addition to bulky electrophiles. As stated earlier, organolithium compounds are more reactive than their magnesium analogues and should prove a suitable alternative. However, this issue has already been raised in section 2.1.1 and it was shown that the lithium intermediate **27** of our starting material 1-bromo-2-iodo-3-methylbenzene **25** is not stable and leads to benzyne **28** formation (Scheme 32).

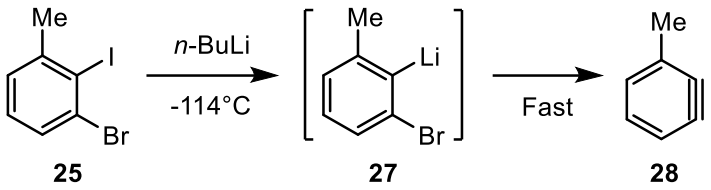

*Scheme 32 – Benzyne **28** formation from 2-bromo-6-methylphenyllithium **27**.*

Another starting material must then be considered that forms a stable lithium intermediate at low temperatures and can be used to access substituted phosphatriptycenes. The chosen compound that fulfills these criteria is 2-bromo-6-chloroiodobenzene **45**.

There are several advantages to use this starting material. The electrowithdrawing chloride substituent stabilises the negative charge on the carbon and is smaller in size than the methyl group. Furthermore, the corresponding chloro-substituted phosphatriptycene could be converted in methylphosphatriptycene **1b** or any other substituted phosphatriptycene through insertion of metallic magnesium and addition on the relevant electrophile (Scheme 33).

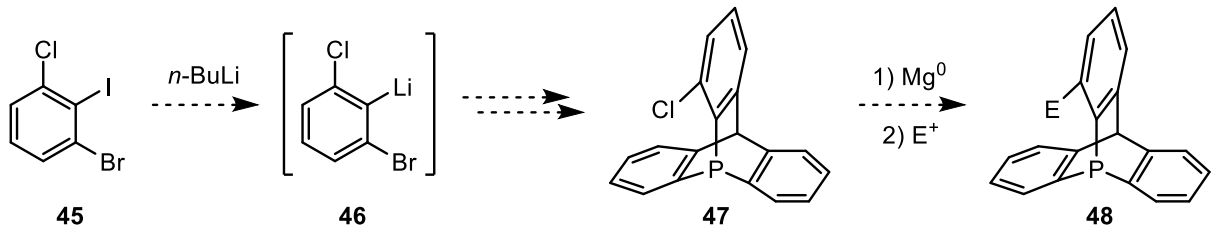

*Scheme 33 - Accessing ortho-substituted phosphatriptycene starting from 2-bromo-6-chloroiodobenzene **48**.*

We took advantage of the chemical stability of the diarylchlorophosphine **15** (presented in section 1.1) and, as a delighting result, phosphine precursor **49** was obtained in 55% yield (Scheme 34).

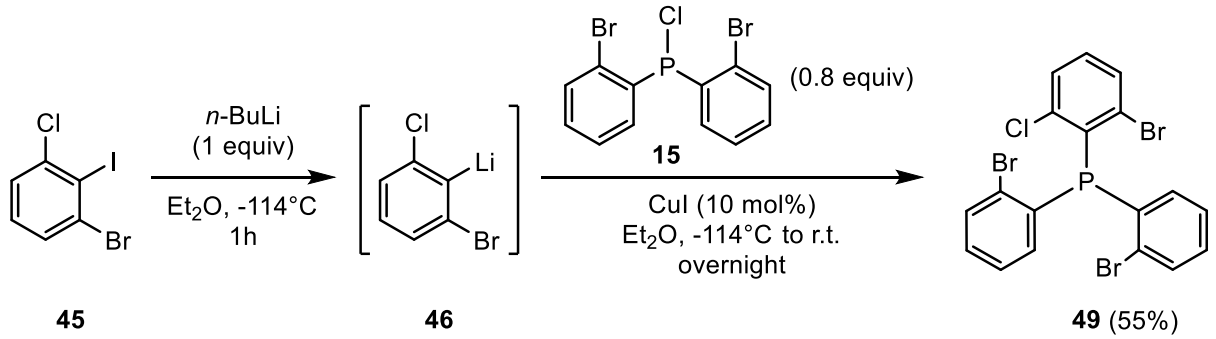

*Scheme 34 - Synthesis of chloro-substituted phosphine precursor **52.***

Having in hand the optimal conditions for the synthesis of **49**, the scope of the reaction was further examined in order to isolate new diarylchlorophosphines that will lead to the formation of other phosphine precursors similar to **49**. Two such diarylchlorophosphines were isolated, although the synthesis of the corresponding phosphine precursors **51** and **52** could not be attempted during this master thesis (Scheme 35).

Phosphine **49** is the first precursor to a monosubstituted phosphatriptycene such as **1b** that we have synthesised. The cyclization reaction relative to that compound is described in section 2.2. If the syntheses of phosphine precursors **51** and **52** are successful, they would give access to disubstituted phosphatriptycenes, having either two chlorine atoms or two methyl groups in *ortho*-position, leading to compound **1c**. However, we still lack a synthesis of a trimethylated precursor of phosphatriptycene **1d**. To this end, the alternative synthesis proposed in section 1.4 for the unsubstituted phosphatriptycene **1a** could be adapted to form the trimethylated phosphatriptycene (see section 2.3).

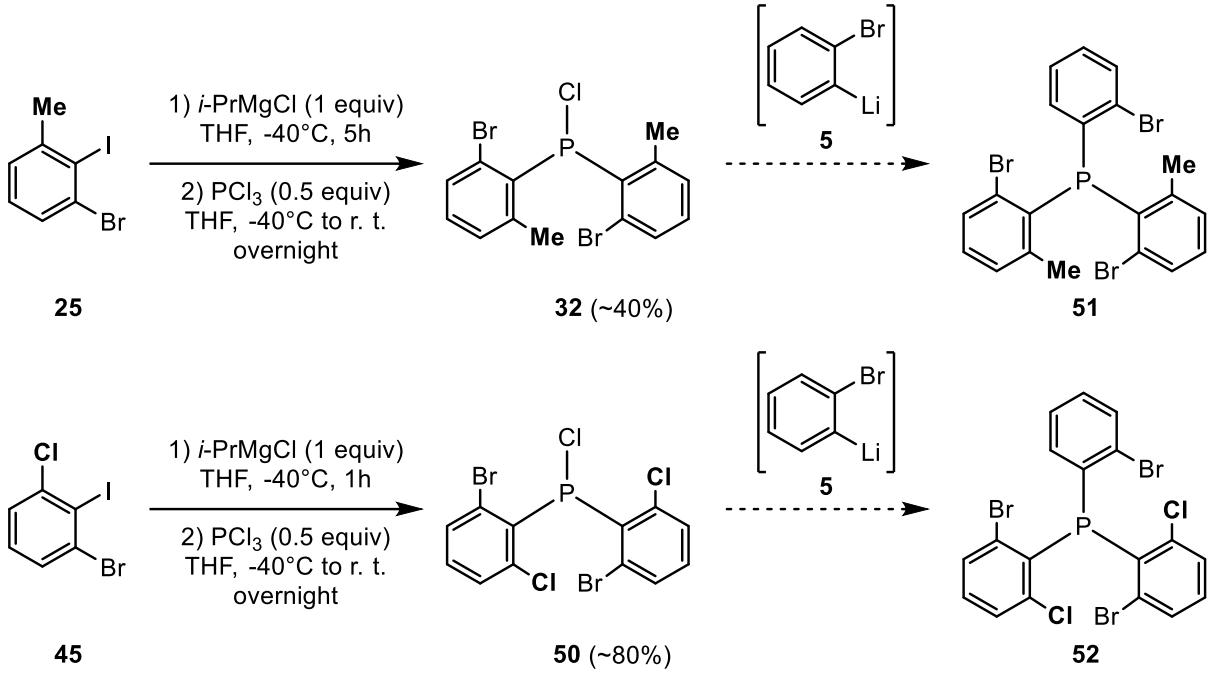

*Scheme 35 - Synthesis of diarylchlorophosphines **32** and **50** and potential formation of phosphine precursors **51** and **52** derivated from **32** and **50** respectively. Approximate yields are indicated as these compounds could not be isolated with high purity. The syntheses of **51** and **52** were not attempted during this master thesis due to lack of time.*

2.2 Cyclization reaction

The next step towards an *ortho*-substituted phosphatriptycene is the cyclization reaction of the phosphine precursor **49** on phenyl chloroformate (Table 3). When the optimal conditions employed previously for the unsubstituted phosphatriptycene synthesis were used, the reaction from **49** gave a mixture of up to 5 products amongst which the desired triptycene **53** was detected by ^{31}P NMR.

*Table 3 - Synthesis of 1-chloro-9-phospha-10-hydroxytriptycene (**53**) from tris(2-bromophenyl)phosphine (**3**) and yields of the reaction for several numbers of equivalents of t-BuLi.*

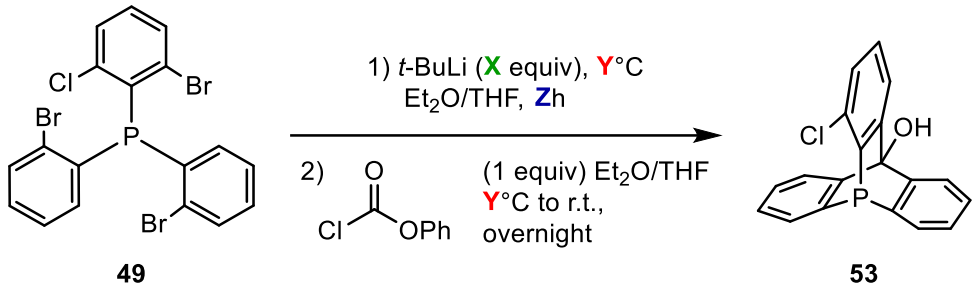

49 **53**

Equivalents of *t*-BuLi (**X**)	Temperature (**Y**)	Reaction time (**Z**)	Isolated yield of **53**
3.0	-94°C	2h	None (detected by NMR)
3.5	-114°C	3h	None (detected by NMR)
5.5	-130°C	4h	14%

We suspected that an intramolecular side reaction could occur between the aryl chloride and the aryllithium (Scheme 36).

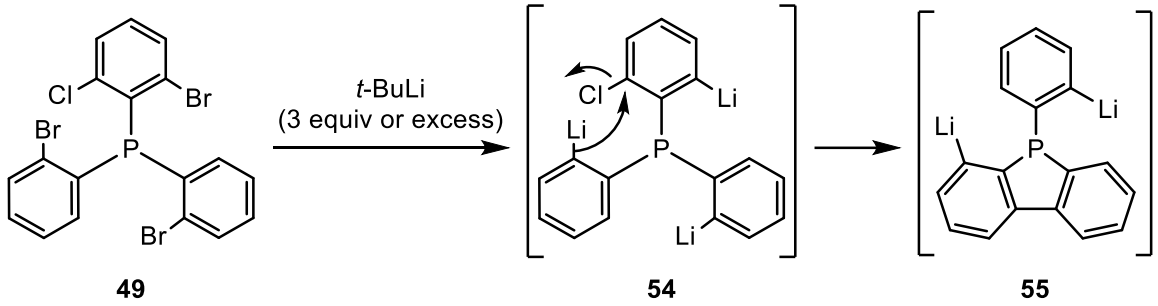

49 **54** **55**

*Scheme 36 - Possible formation of a reaction intermediate **55** that could leads to a variety of undesired products from side reactions. The intramolecular reaction of **54** would proceed through a S_NAr mechanism.*

This intermolecular S_NAr process should be favoured entropically and the C-Cl and the C-Li bonds are ideally located in close special proximity in compound **54**.

Two tests at lower temperature and with higher excess of *t*-BuLi were performed to eventually slow-down the intramolecular reaction. The reaction time was not however kept constant because we believed that the Br/Li exchange will be also slower, and a thorough screening of the reaction conditions was not carried out (Table 3). As the chloro-substituted phosphatriptycene derivative **53** was isolated in 14% yield under these non-optimised conditions, we are confident that further methodological optimisation will allow us to increase the yield significantly.

2.3 Alternative synthesis of trimethylated phosphatriptycene

In a similar approach to the one presented in section 1.4, trimethyl-phosphatriptycene **1d** could be synthesised through a triphenylmethane precursor **58** (Scheme 37). The starting material is 3-bromo-2-chlorotoluene **56**. In this situation, the methyl groups do not significantly increase the steric hindrance on the central carbon of compound **58**. A similar reactivity to the synthesis described in section 1.4 is expected. This reaction was attempted only once and product **57** could not be isolated. New conditions and purifications must be tested.

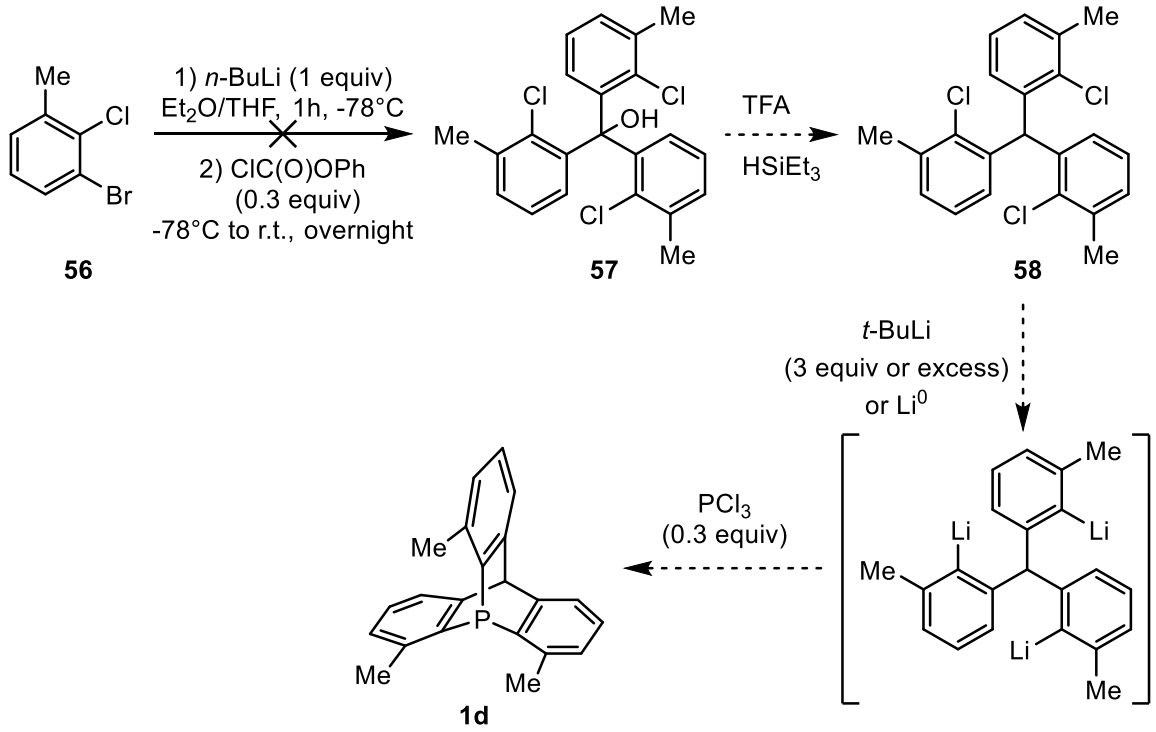

*Scheme 37 - Proposed alternative synthesis of trimethylated phosphatriptycene **1d** through a triphenylmethane precursor.*

3. Crystallographic analysis

Several X-ray structures were collected during this work. In order to analyse them, two geometric parameters must first be defined. In the triptycene scaffold, the d_{ter} parameter represents the distance in Å between the phosphorus atom and the terminal bridging atom of the triptycene. The Pyr parameter is a measure in Å of the pyramidalisation of the phosphorus atom. It is the distance between the phosphorus atom and the plane formed by its three adjacent atoms divided by the mean P-C bond length (Figure 16). A higher Pyr value means the phosphorus has a stronger pyramidal character while a lower value means the phosphorus is less pyramidal.

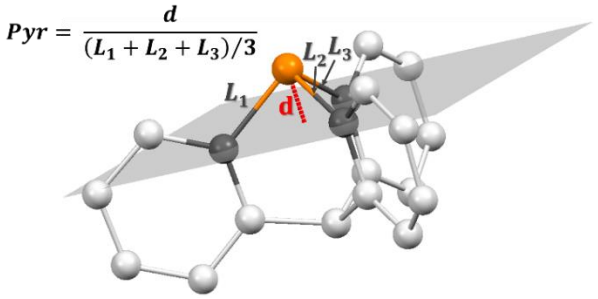

Figure 16 - Measure of the Pyr parameter in the case of phosphatriptycene.

The X-Ray structures are shown in Figure 17. Their geometric parameters are given in Table 4. These structures consist in three "classical" phosphines and three phosphatriptycene derivatives.

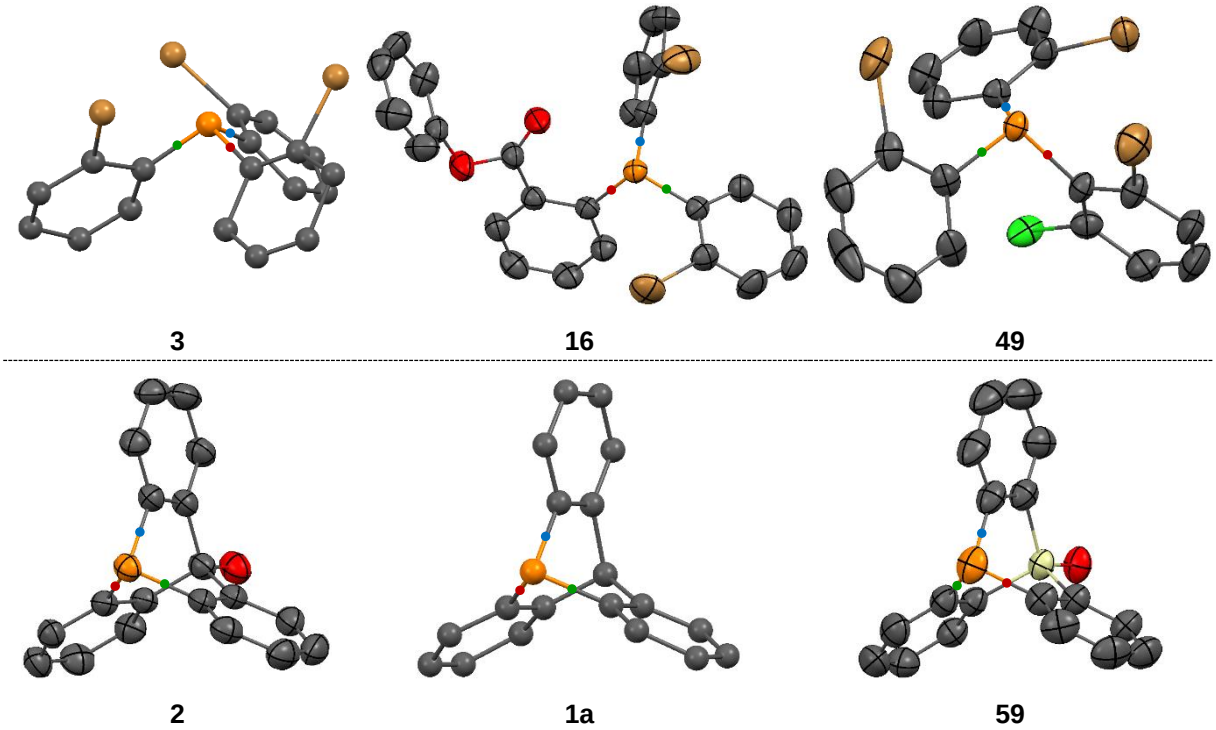

*Figure 17 - Molecular structures of compounds **3**, **16**, **49** (classical phosphines), **2**, **1a** and **59** (phosphatriptycene derivatives). Thermal ellipsoids are set at 50% probability. Hydrogen atoms are omitted for clarity. The coloured dots refer to the bond lengths indicated in Table 4. Compound **59** was synthesised by Lei Hu in the context of his Ph.D and is shown for comparison purpose.*

*Table 4 - Distances in Å in compounds **3**, **16**, **49**, **2**, **1a**, **59** and Pyr parameter. The coloured values correspond to the coloured bonds in Figure 17. *structure of lesser precision due to poor quality of the crystal; **structure extracted from the CCSD (Cambridge Crystallographic Structural Database).*

Compound	3*	16	49	2	1a**	59
L_1	1.79(5)	1.847(3)	1.874(9)	1.839(2)	1.8533	1.856(3)
L_2	1.82(7)	1.840(3)	1.85(1)	1.837(2)	1.8291	1.852(3)
L_3	1.79(6)	1.844(3)	1.81(1)	1.838(2)	1.8525	1.851(3)
Mean	1.80	1.844	1.84	1.838	1.8433	1.853
Pyr	0.458	0.455	0.432	0.530	0.566	0.482
d_{ter}	-	-	-	2.928(2)	2.9511	3.086(1)

The influence of steric hindrance on the geometry of phosphines can be studied in compounds **3**, **16** and **49**. A general tendency is that the phosphorus atom tends to adopt a less pyramidal geometry when it bears bulkier substituents because they push the rings apart to minimise steric interactions. This is observed with phosphine **49**, with a Pyr value of 0.432, lower than the 0.458 and 0.455 values of phosphines **3** and **16,** respectively. According to these values, **3** and **16** have roughly the same steric hindrance. Phosphines linked to a bulkier group seem to have a longer C-P bond length, once again due to steric hindrance, as seen for the $\mathbf{L_1}$ bond in compound **16** and **49**, slightly longer than the other P-C bonds.

The P-C bond lengths are not significantly modified when the P atom is distorted in a triptycene scaffold (**2**, **1a**, **59**). However, there is a significant increase of the Pyr parameter, indicating a very strong pyramidalisation of the phosphorus. The bigger size of the silicon atom in compound **59** explains the longer d_{ter} value. The C-Si bond length (1.861 Å) is significantly longer than the C-C bond (1.555 Å) and slightly longer than the P-C bond (1.851 Å). This means that in the rigid triptycene scaffold, the phenyl rings are drawn towards the phosphorus in compound **59** (explaining the lower Pyr parameter) while in the **1a** or **2** compounds, they are drawn towards the bridgehead carbon atom (Figure 18).

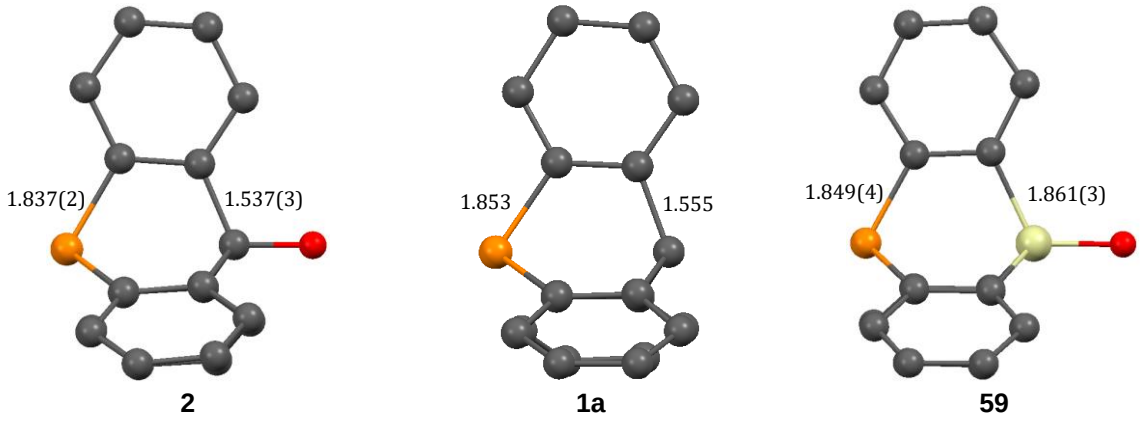

*Figure 18 - Side view of compounds **2**, **1a** and **59**, the P-C, C-C and C-Si bond lengths are indicated in Å.*

The geometry of the phosphorus atom in the triptycene scaffold has a strong effect on the electronic state of its lone pair. Because of the strong pyramidalisation of the phosphorus, the lone pair acquires a high s character and lower energy than the p orbital (Figure 19) and is thus considered weak σ-donor (because the overlap between s and p orbital is less efficient than p-p orbital overlap)[79]. As explained in *PART I*, section 5, this feature is very interesting since phosphatriptycenes can be used as effective ligands in Stille couplings or Heck reactions that require low σ-donating ligands.

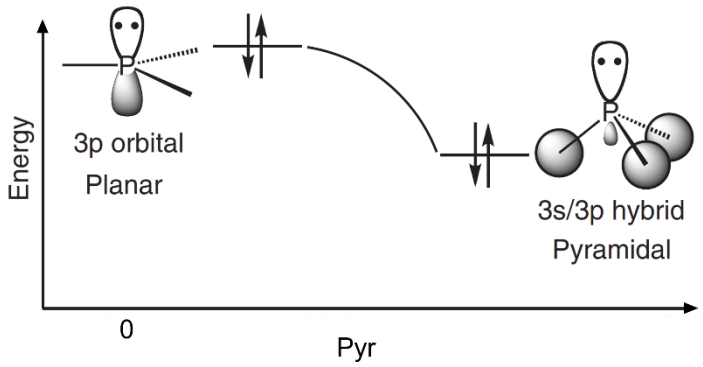

Figure 19 - Walsh diagram of phosphine adapted from reference[79].

A noteworthy observation is the supramolecular structure of 9-phospha-10-hydroxytriptycene **2**. It organizes itself in space through π-π stacking and P···H-O hydrogen bonds (Figure 20). If the former is common in aromatic compounds, examples of the latter are scarce in the literature (a search in the Cambridge Structural Database showed that only twelve compounds are known with this feature).

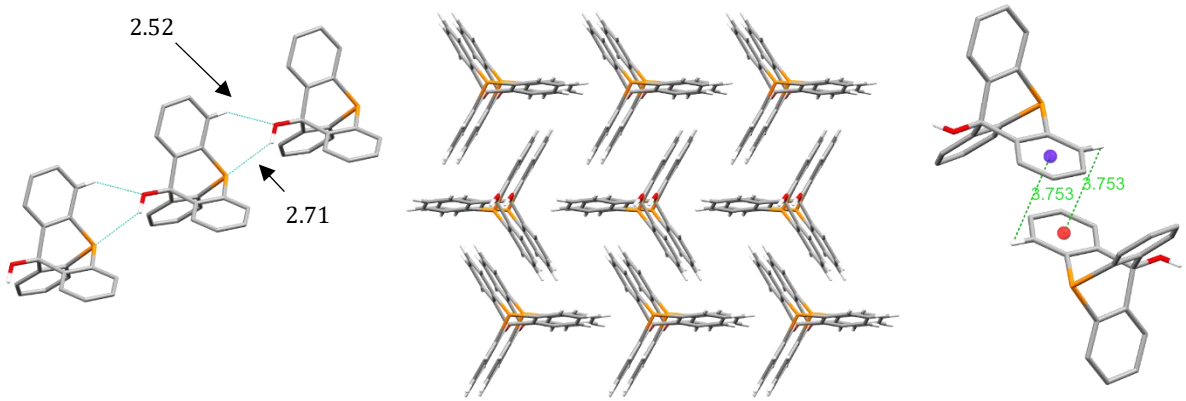

*Figure 20 - Supramolecular organisation of 9-phospha-10-hydroxytriptycene **2**. Distances indicated in Å.*

PART IV - Theoretical results and discussion

1. Studied reactions and calculation methods

The theoretical part of the master thesis consists in a *Density Functional Theory* (DFT) study of the association between several Lewis bases and a Lewis acid. The latter is a perfluorinated borane, tris(pentafluorophenyl)borane (**60**), while the formers are phosphatriptycene derivatives with ortho-substituents (Table 5). These include the methylated compounds that we aim at synthesizing (**1a**-**d**), as well as phosphatriptycenes substituted with *tert*-butyl groups (**1e**-**g**). The formation of Lewis adducts or of Frustrated Lewis Pairs is analysed through the thermodynamic state function of the reaction, the geometrical parameters of the equilibrium structures and ^{31}P as well as ^{11}B NMR analyses. Using the Gaussian16 package[80], geometry optimisations and vibrational frequency calculations were performed at the M06-2X/6-311G(d) level of theory and the NMR calculations at the B3LYP/6-311+G(2d,p) level of theory. The geometry optimisations were performed using a tight convergence threshold. For each compound, all vibrational frequencies are real, demonstrating that the structures are minima on the potential energy surface. A benchmark study on complexes between model Lewis acids and bases has compared DFT with high-level wavefunction methods [MP2 and CCSD(T)] and has established that M06-2X is the most suited exchange-correlation functional to describe these systems. Solvent (Dichloromethane, DCM) effects were modelled using the IEFPCM approach.

2. States of association between Lewis bases and acids

Several geometry optimisations of complexes **61a**-**g** led to the discovery that there are two distinct states of association between the Lewis acid **2** and the phosphatriptycene derivatives **1a**-**g**, both minima on the potential energy hypersurface**.** The first one corresponds to a Lewis adduct (*State 1*, **S1**) with a covalent bond between the boron and the phosphorus atoms and the second one to a state similar to Frustrated Lewis pairs (*State 2*, **S2**) where there seems to be no interaction between the boron and the phosphorus. An example is shown in Figure 21 with the two states of complex **61d** being pictured.

S1 compounds are characterised by shorter distances between the boron and the phosphorus atoms and more distortion in the two molecules in the complex compared to the isolated ones. The formation of these **S1** compounds is driven by the creation of a new bond (i.e. the adduct formation) between the boron and the phosphorus.

*Table 5 – Studied associations between a phosphatriptycene derivative (**1a-g**) and tris(pentafluorophenyl)borane (**60**) to form a Lewis adduct or a FLP.*

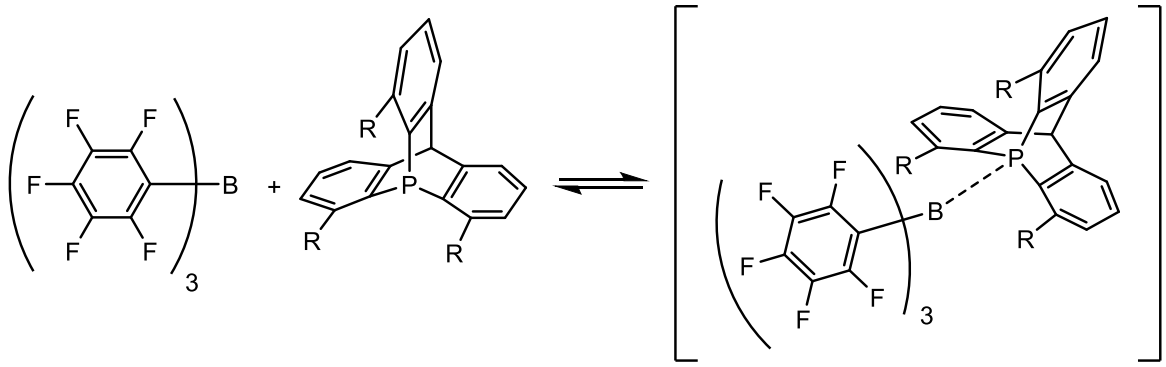

60 **1a-1g** **61a-61g**

Compounds 1 and 61	Substituents		
	R	**R**	**R**
a	H	H	H
b	Me	H	H
c	Me	Me	H
d	Me	Me	Me
e	*t*-Bu	H	H
f	*t*-Bu	*t*-Bu	H
g	*t*-Bu	*t*-Bu	*t*-Bu

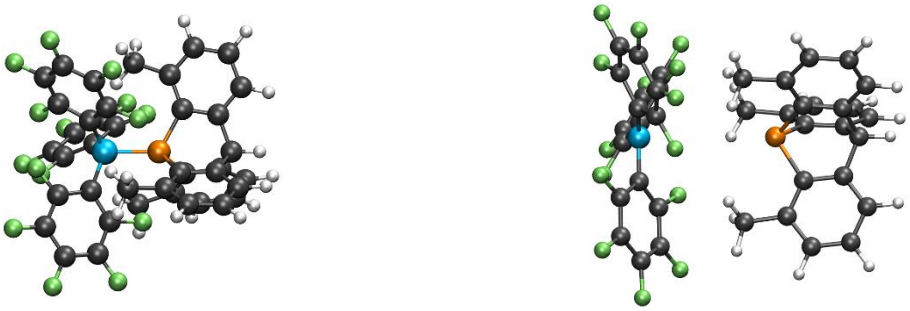

61d - S1 **61d - S2**

*Figure 21 - Representation of the two states of association between the Lewis acid and the Lewis base for complex **61d**. LEGEND: Orange = Phosphorus; Blue = Boron; Green = Fluorine; Grey = Carbon; White = Hydrogen.*

S2 compounds are characterised by longer distances between the boron and the phosphorus atoms, the molecules in the complex are more similar in geometry to the isolated ones and the formation of these complexes is mostly driven by the stabilisations due to van der Waals interactions between the two molecules.

These two stationary states are not observed for all studied complexes. In some cases, the difference of energy between the two states is so large that it does not correspond to a stationary

state anymore. It is the case for complex **61a** where the **S2** is not observed while the **S1** formation is very spontaneous (ΔG^0 of -37.9 kJ/mol). It is also the case for complexes **61f** and **61g** for which the adduct state **S1** would be so high in energy due to the steric hindrance caused by multiple *tert*-butyl groups that it is not formed at all. All other complexes are observed in two distinct states.

When both states are minima on the potential hypersurface, a transition state characterised by a barrier of activation should exist between them. This transition state was determined for complex **61b** (Figure 22). It displays a P-B distance intermediate (2.745 Å) between that of **S1** (2.107 Å) and **S2** (3.310 Å). At this distance, it is believed that the complex does not benefit fully from the stabilisation due to P-B bond formation, as **S1** complexes do, while it remains destabilised by steric hindrance, unlike **S2** complexes. Similar transition states are expected for all complexes that exhibit two states of association, although they were not determined. **S1** and **S2** states will now be studied and compared at the thermodynamic and structural levels.

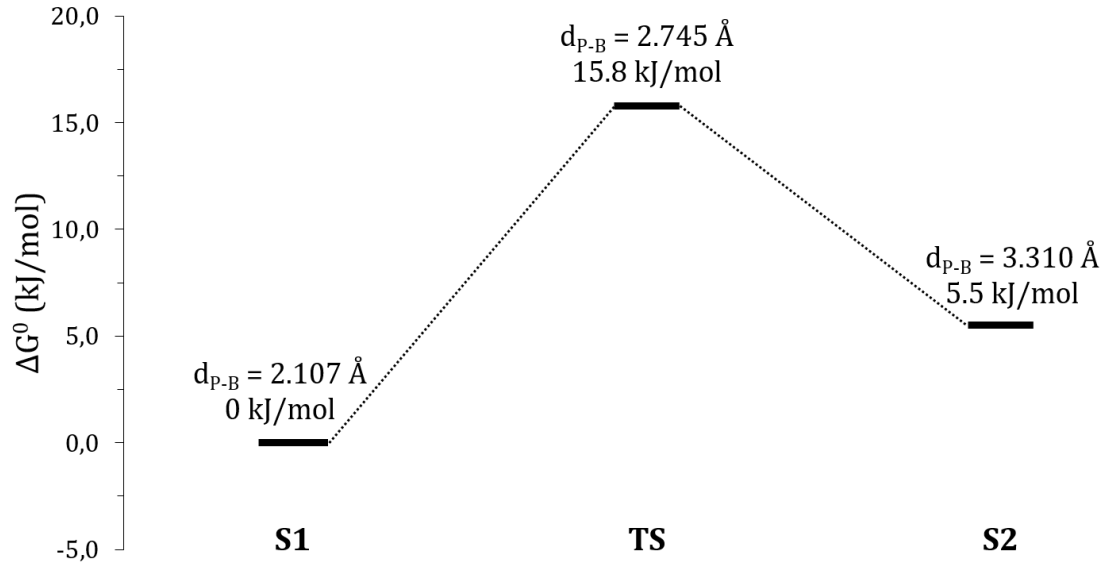

*Figure 22 - Gibbs free energy profile of complex **61b**. The Gibbs free enthalpy of **S1** complex was adopted as reference.*

3. Thermodynamics

*Table 6 - Electronic energy, enthalpy, entropy, and Gibbs enthalpy (at 298.15 K) for the reaction of formation of a Lewis adduct or for a Frustrated Lewis Pair between **60** and phosphatriptycenes having different substituents. The calculations were performed at the M06-2X/6-311G(d) level with the IEFPCM scheme to account for solvent (DCM) effects.*

Reaction	ΔE (kJ/mol)		ΔH⁰ (kJ/mol)		ΔS⁰ (J.mol⁻¹.K⁻¹)		ΔG⁰ (kJ/mol)		K_C	
	S1	**S2**	**S1**	**S2**	**S1**	**S2**	**S1**	**S2**	**S1**	**S2**
a	-104.0	/	-97.4	/	-199.6	/	**-37.9**	/	4.3E+06	/
b (1 Me)	-70.9	-59.6	-63.4	-52.8	-215.2	-198.1	**0.7**	**6.3**	7.4E-01	8.0E-02
c (2 Me)	-40.8	-51.7	-32.6	-44.6	-240.5	-191.3	**39.1**	**12.4**	1.4E-07	6.7E-03
d (3 Me)	-10.4	-42.6	-1.2	-35.8	-265.4	-187.2	**77.9**	**20.0**	2.2E-14	3.1E-04
e (1 *t*-Bu)	-4.4	-57.9	4.9	-51.5	-232.9	-197.7	**74.4**	**7.4**	9.4E-14	5.0E-02
f (2 *t*-Bu)	/	-40.9	/	-32.9	/	-208.7	/	**29.3**	/	7.4E-06
g (3 *t*-Bu)	/	-39.5	/	-37.0	/	-187.6	/	**19.0**	/	4.7E-04

As shown in Table 6, for **S1** complexes the Gibbs enthalpy of reaction ΔG⁰ increases almost linearly when successive methyl groups are added (Figure 23).

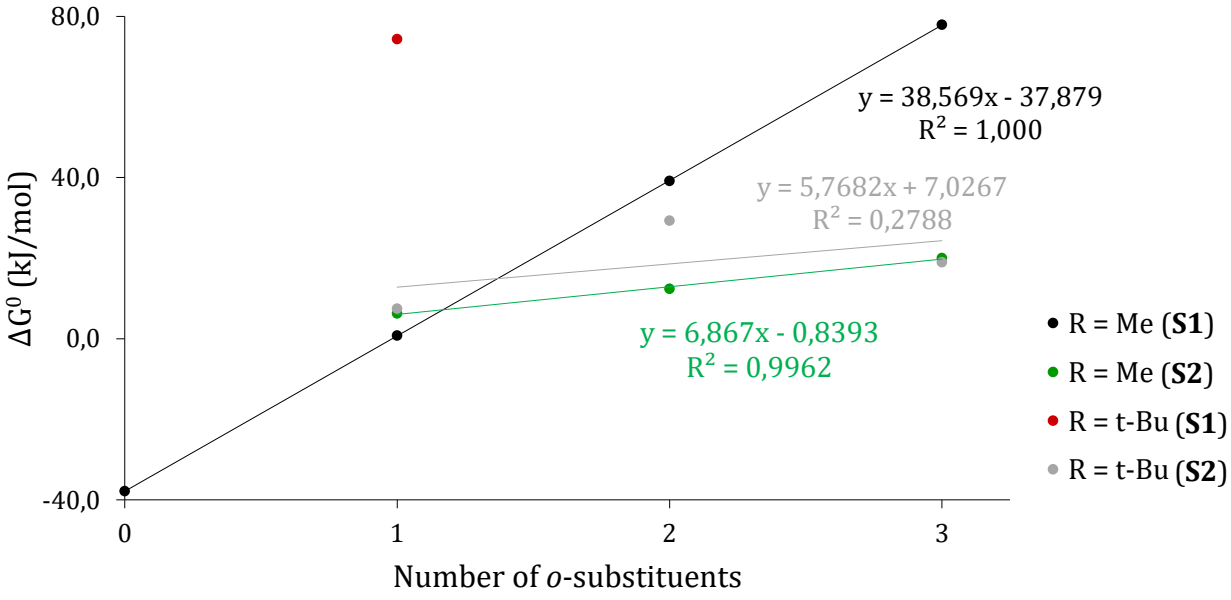

Figure 23 - Evolution of ΔG⁰ of the Lewis acid-base association as a function the number of substituents around the phosphorus atom.

The formation of the adduct in **S1** is preferred for the monomethylphosphatriptycene **1b** and even exclusive for phosphatriptycene **1a**, but as methyl groups are added and therefore as the steric hindrance increases for complexes **61c** and **61d**, **S2** gets preferred. As aforementioned, two main factors are opposed here: the stabilisation due to the bond formation between the boron and the

phosphorus, and the repulsion due to increasing steric hindrance between compound **62** and phosphatriptycenes **1a-g**. For complex **1a**, the stabilisation due to the bond formation is higher than the steric repulsions: the adduct is formed. For complexes **61c** and **61d** the steric hindrance is so important that the Lewis adduct is very high in energy, the complex will then preferentially adopt a more stable state that limits steric repulsions and maximises weak interactions: **S2**. In the case of complex **61b** in **S1**, one could assume that the stabilisation due to bond formation and the steric repulsions balance each other and the Gibbs free enthalpy of formation of the complex approaches 0 kJ/mol. In this situation, the **S2** is slightly less stable.

The adduct formation becomes even more difficult when *tert*-butyl groups are added, the adduct state **S1** is not even observed for complexes **61f** and **61g** and the ΔG^0 of formation is very high for complex **61e** (74.4 kJ/mol). The non-covalent state **S2** is favoured instead, with ΔG^0 values of 7.4, 29.3 and 19.0 kJ/mol with one, two and three *tert*-butyl groups respectively.

It should be noted that even though there is in some cases a strong stabilisation in going from **S1** to **S2** (up to -68 kJ/mol for complex **61e**), most of these complexes possess a positive ΔG^0 of formation, which means that this process is not spontaneous and that in solution, the reactants remain mostly isolated and only form the studied complexes in small quantity. If the formation of a **S1** complex may be detrimental for an eventual catalytic activity (as both Lewis acid and base are bonded to each other), the formation or lack of formation of a **S2** complex is not an indication of the quality of the complex as a FLP catalyst. Isolated in solution or involved in a **S2** complex, both the boron and the phosphorus atoms are free to act synergistically on a third molecule. To thoroughly assess the efficiency of a given complex as a FLP catalyst for a small molecule activation, one must simulate the said reaction and evaluate its thermodynamics.

A further analysis of Table 6 indicates that the process is strongly disfavoured entropically (only negative values), which was expected since two bulky compounds are associated. The entropic factor is however better for **S2** complexes because the two molecules are further apart in that situation than in a **S1** complex.

On the enthalpy level, the -97.4 kJ/mol value of complex **61a**, a strongly exothermic value, is due to the energy that is released upon the P-B bond formation. This factor decreases consistently with the addition of methyl groups, probably because the stabilisation due to bond formation is counter-balanced by steric repulsions. On the other hand, the corresponding values for **S2** complexes are mainly due to stabilising weak interactions between the methyl or *tert*-butyl groups of the phosphatriptycene and the perfluoroaryl groups of compound **60**. The lower values for **S2** complexes **61b**, **61c** and **61e** are probably explained by a partial overlap between the lone pair of the phosphorus and the empty p orbital of the boron (i.e. a partial bond formation). Indeed, the P-B distances in these complexes (3.310, 3.800 and 3.774 Å respectively, see section 4.

Structural aspects) could allow such an overlap. At longer distances however, like in **S2** complex **61d** (4.769 Å), such partial overlap is no longer possible, and the stabilisation is only due to weak interactions (Figure 24).

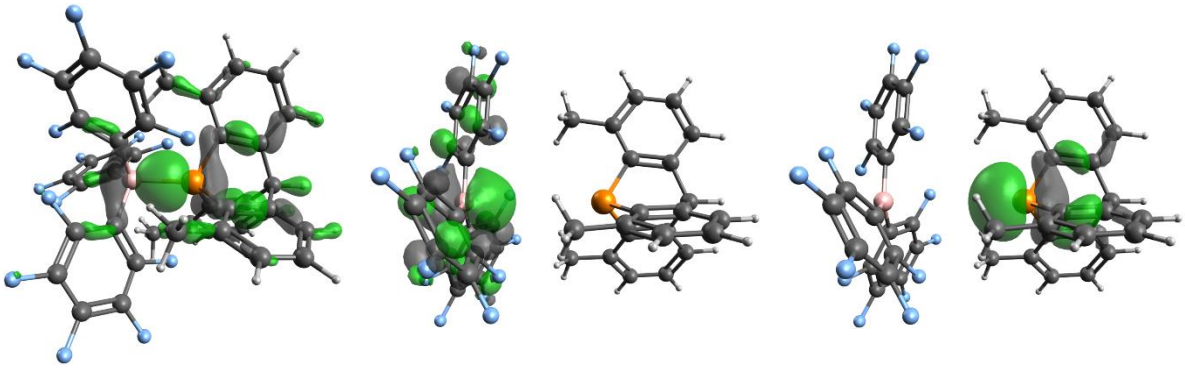

S1 – 61d
(σ-bonding orbital between P and B, HOMO-12)

S2 – 61d
(empty 2p orbital on B, LUMO)

S2 – 61d
(lone pair of P, HOMO-4)

*Figure 24 - Avogadro representation of the "atomic" and molecular orbitals involved in the formation of a bond between P and B atoms. Isovalue of 0.04500. The figure demonstrates the formation of a Lewis adduct in **S1** complex **61d** and the absence of overlap (for a same isovalue) between the empty 2p orbital of the B and the lone pair of the P in the corresponding **S2** complex.*

4. Structural aspects

In order to analyse the geometrical parameters (Table 7 and Table 8) of the optimised structures, a systematic atomic numbering was defined which will be employed for all compounds (Figure 25).

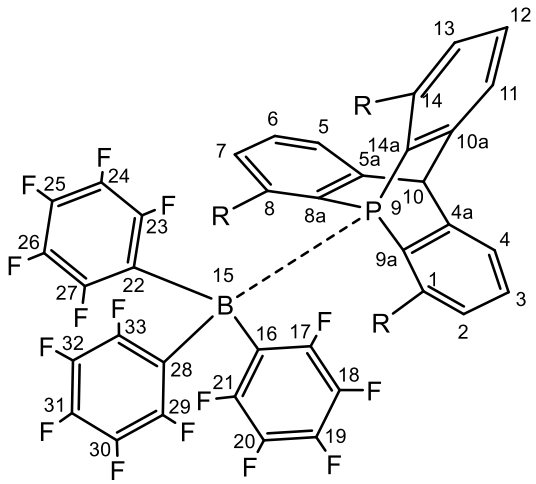

Figure 25 – Shared atomic numbering of all studied compounds.

The increase in the P-B distance due to steric hindrance can be observed when comparing the $d_{P\text{-}B}$ values shown in Table 7 to the reference 1.946 Å (M06-2X/6-311G(d)) B-P bong length in the $H_3B\text{-}PH_3$ Lewis adduct where there is no steric hindrance between the LA and the LB.

*Table 7 - M06-2X/6-311G(d) bond lengths (Å) of the **S1** and **S2** complexes and corresponding phosphatriptycene derivatives.*

REF	Substituents			S1 complexes with $B(C_6F_5)_3$					Isolated phosphatriptycene			
	R^1	R^8	R^{14}	$d_{P^9-B^{15}}$	$d_{P^9-C^{9a}}$	$d_{P^9-C^{8a}}$	$d_{P^9-C^{14a}}$	$d_{P^9-C^{10}}$	$d_{P^9-C^{9a}}$	$d_{P^9-C^{8a}}$	$d_{P^9-C^{14a}}$	$d_{P^9-C^{10}}$
a	H	H	H	2.103	1.842	1.841	1.841	2.832	1.852	1.852	1.852	2.928
b	Me	H	H	2.107	1.860	1.848	1.847	2.826	1.859	1.852	1.852	2.924
c	Me	Me	H	2.115	1.871	1.862	1.850	2.816	1.859	1.859	1.851	2.920
d	Me	Me	Me	2.097	1.870	1.870	1.870	2.797	1.858	1.858	1.858	2.916
e	*t*-Bu	H	H	2.255	1.915	1.869	1.847	2.843	1.878	1.848	1.848	2.910
REF	**Substituents**			**S2 complexes with $B(C_6F_5)_3$**					**Isolated phosphatriptycene**			
	R^1	R^8	R^{14}	$d_{P^9-B^{15}}$	$d_{P^9-C^{9a}}$	$d_{P^9-C^{8a}}$	$d_{P^9-C^{14a}}$	$d_{P^9-C^{10}}$	$d_{P^9-C^{9a}}$	$d_{P^9-C^{8a}}$	$d_{P^9-C^{14a}}$	$d_{P^9-C^{10}}$
b	Me	H	H	3.310	1.860	1.853	1.854	2.915	1.859	1.852	1.852	2.924
c	Me	Me	H	3.800	1.864	1.863	1.854	2.920	1.859	1.859	1.851	2.920
d	Me	Me	Me	4.769	1.860	1.860	1.859	2.917	1.858	1.858	1.858	2.916
e	*t*-Bu	H	H	3.774	1.883	1.849	1.851	2.909	1.878	1.848	1.848	2.910
f	*t*-Bu	*t*-Bu	H	4.486	1.890	1.875	1.857	2.894	1.882	1.875	1.847	2.891
g	*t*-Bu	*t*-Bu	*t*-Bu	5.801	1.877	1.870	1.880	2.873	1.878	1.877	1.877	2.870

*Table 8 - M06-2X/6-311G(d) angles (°) and pyramidalisation parameter (Pyr) of the **S1** and **S2** complexes and the corresponding phosphatriptycene derivatives. The value of the Pyr parameter in the isolated compound **60** is of 0.*

REF	Substituents			S1 complexes with $B(C_6F_5)_3$				Phosphatriptycene	
	R^1	R^8	R^{14}	C^{10}-P^9-B^{15} angle	Pyr_P	P^9-C^{9a}-C^1 angle	Pyr_B	P^9-C^{9a}-C^1 angle	Pyr_P
a	H	H	H	179.9	0.495	127.5	0.260	123.2	0.536
b	Me	H	H	174.2	0.493	129.9	0.297	123.2	0.534
c	Me	Me	H	171.9	0.490	130.6	0.303	123.2	0.533
d	Me	Me	Me	180.0	0.483	130.8	0.302	123.2	0.532
e	*t*-Bu	H	H	166.2	0.501	133.1	0.312	125.9	0.529
REF	**Substituents**			**S2 complexes with $B(C_6F_5)_3$**				**Phosphatriptycene**	
	R^1	R^8	R^{14}	C^{10}-P^9-B^{15} angle	Pyr_P	P^9-C^{9a}-C^1 angle	Pyr_B	P^9-C^{9a}-C^1 angle	Pyr_P
b	Me	H	H	162.4	0.531	124.1	0.027	123.2	0.536
c	Me	Me	H	162.3	0.533	123.8	0.011	123.2	0.534
d	Me	Me	Me	179.9	0.532	123.4	0.004	123.2	0.533
e	*t*-Bu	H	H	148.9	0.529	126.5	0.004	125.9	0.532
f	*t*-Bu	*t*-Bu	H	151.9	0.523	128.1	0.018	126.4	0.522
g	*t*-Bu	*t*-Bu	*t*-Bu	168.1	0.516	126.3	0.015	126.7	0.515

The P-B distance does not significantly vary for the five **S1** Lewis adducts, all bonds being of approximately 2.1 Å except complex **61e** with 2.255 Å due to the presence of the bulky *tert*-butyl group. **S1** complexes display geometrical parameters which are typical of covalently bonded Lewis adducts.

S2 complexes are structurally similar to typical intermolecular **FLPs** where there are no interactions between the Lewis acid and the Lewis base. The P-B distances are therefore much longer (varying from 3.310 Å in **61b**, where some small P-B interactions are still possible, to 5.801 Å in complex **61g**). These distances are long enough to insert small molecules such as hydrogen or methane.

The P^{9}-C^{8a}, P^{9}-C^{9a} and P^{9}-C^{14a} bond lengths account for the distortion of the triptycene when substituents are added and upon the approach of the $B(C_6F_5)_3$: bond lengths are stretched to insert compound **2** (Figure 26). The $d_{P^{9}-C^{10}}$ parameter is another factor of distortion: the bond length decreases as the phenyl rings are pushed back and draw the C^{10} more and more inward as schematised in Figure 26.

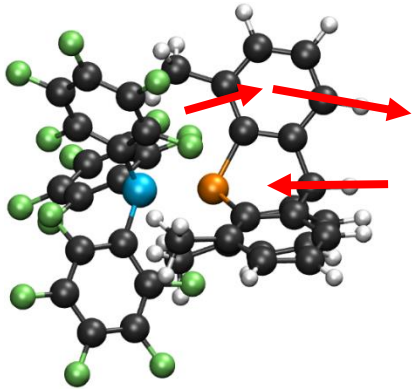

61d (**S1**)

*Figure 26 – Triptycene distortion with bigger substituents and upon approach of **60**.*

The C^{10}-P^{9}-B^{15} angle describes the angle of approach of compound **60** towards the phosphatriptycene. If the value deviates from 180°, the two molecules are no longer aligned (Figure 27). This mis-alignment may have a stabilising effect upon the approach of a small non-linear molecule such as methane.

The Pyr_P parameter describes the pyramidalisation of the phosphorus atom. As it is distorted when forming the adduct with **62** like in S1 complexes, this value decreases, the phosphorus becomes less pyramidal. When in a S2 complex, the values do not differ from the isolated molecules.

The P^{9}-C^{9a}-C^{1} angle further shows the distortion of the phosphatriptycene when forming the adduct in a **S1** complex. As the value increases, it indicates that the methyl or *tert*-butyl groups are pushed further apart from the phosphorus. Again, when in a **S2** complex, the values are similar to the ones of the isolated molecules.

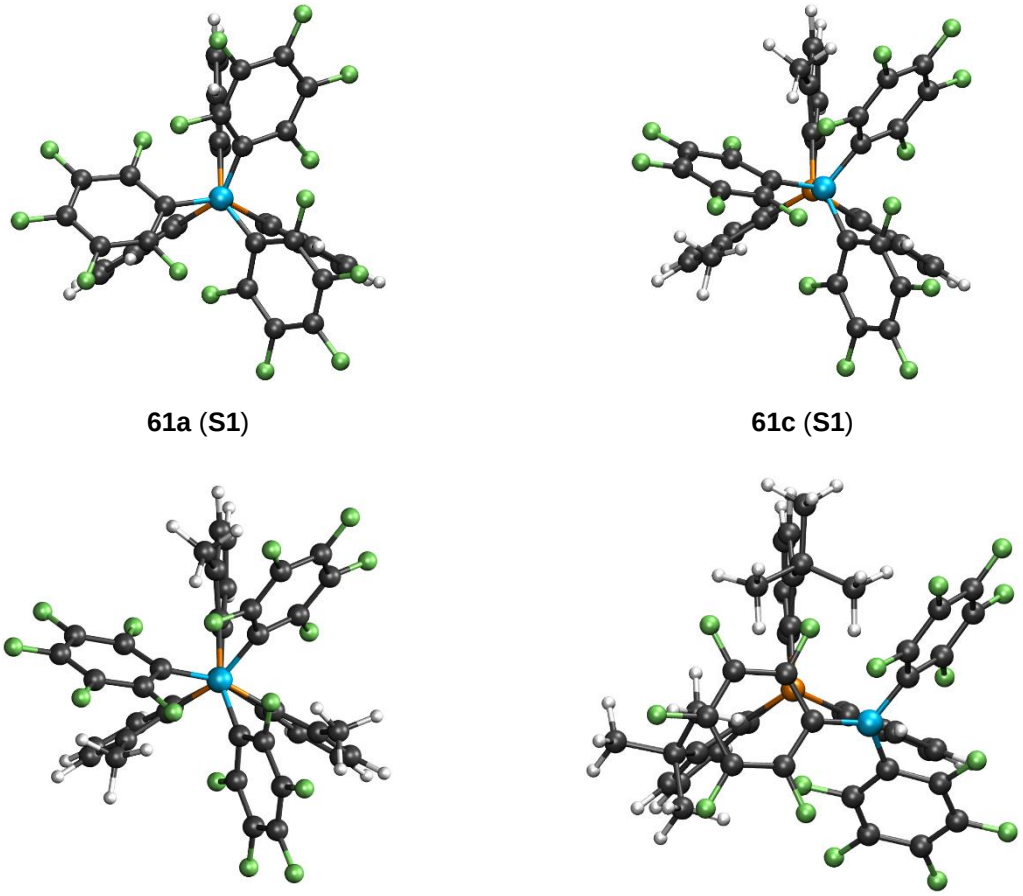

*Figure 27 - VMD representation of complexes a, c, d and f along the P^9-C^{10} axis. Phosphatriptycene in the background, tris(pentafluorophenyl)borane in the foreground. The boron atom in **61c** and **61f** is more and more displaced from the P^9-C^{10} axis with bigger substituents. The triptycene rings that bear a substituent are distorted. LEGEND: Orange = Phosphorus; Blue = Boron; Green = Fluorine; Grey = Carbon; White = Hydrogen.*

Finally, the Pyr_B parameter describes the pyramidalisation of the boron atom in compound **60**. The value of the isolated compound is 0 as the geometry of the boron is trigonal planar. When in a **S1** complex, the boron adopts a tetrahedral geometry, further demonstrating the formation of a Lewis adduct. In **S2** complexes, the boron remains mostly trigonal planar.

As a general rule, **S1** complexes are adopting a geometry reminiscent of a Lewis adduct whereas a **S2**-type complexes have geometry similar to that of the separated molecules. The two molecules then orient themselves towards the other in order to maximize weak interactions between methyl or *tert*-butyl groups and the perfluoroaryl groups of compounds **60** (Figure 28). **S2**-type complexes are most likely to be chemically active as a **FLP**.

The experimental P-B bond length is of 2.16 Å as determined by XRD, which is in good agreement with the calculations (2.10 Å).

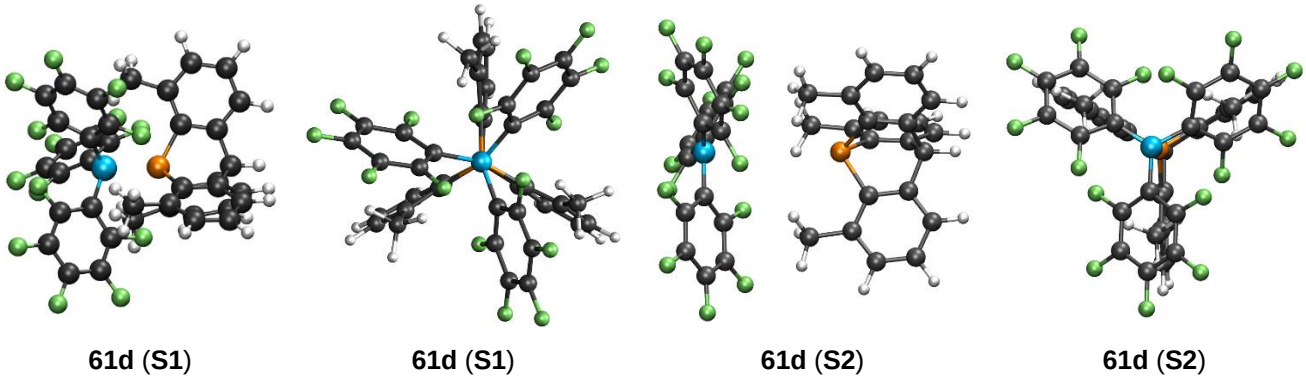

*Figure 28 - Comparison of the **S1** and **S2** geometries of complex **61d**. The methyl groups are intertwined between the aryl groups of **60** in **S1** and are pointing towards them in **S2**.*

5. Orientation study

It was shown in sections 3 and 4 that frustrated Lewis pairs are most likely formed with compounds **61c** to **61g**. It means that the Lewis basic phosphorus and Lewis acidic boron atoms do not interact with each other. In these frustrated Lewis pairs, both constituents can adopt in solution an infinite number of orientations towards the other. In fact, there is a statistical mixture of all orientations. The molecules will however preferentially adopt the most stable orientation, i.e. the one with the smallest energy. In this context, two limit structures of three complexes (complexes **61a**, **61d** and **61g**, without methyl groups, with three methyl groups or *t*-butyl groups on the phosphatriptycenes) will be compared: one with the phosphorus atom directly in front of the boron atom and one where they are pointing in the opposite direction[81] (Figure 29).

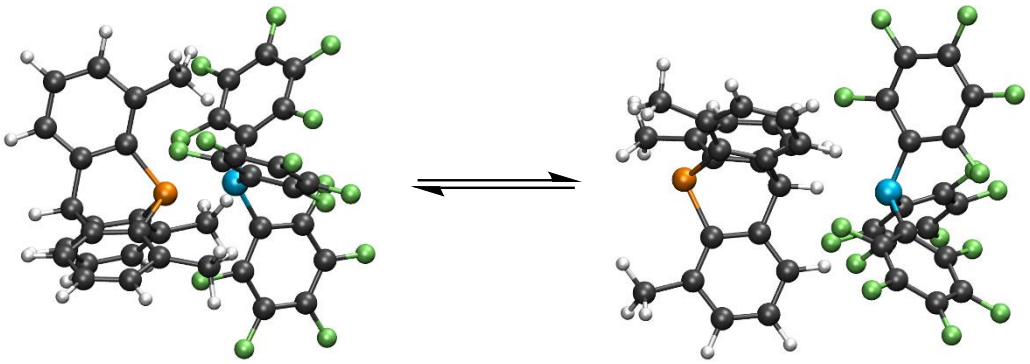

*Figure 29 - Compared orientations of complex **61d**. One with the phosphorus atom directly in front of the boron atom (left) and pointing in the opposite direction (right).*

Geometry optimisations and frequency calculations were performed (M06-2X/6-311G(d)) on complexes **61a**, **61d** and **61g** with the reverse orientation.

*Table 9 - M06-2X/6-311G(d) thermodynamic values of the formation of the reverse adduct and Δ(ΔG⁰) between the standard orientation and the reversed one. The optimisations of reversed complexes **61d** and **61g** gave structures with one imaginary frequency so far (-7.9 and -8.4 cm⁻¹ respectively) and are therefore not fully trustworthy but their values are indicated anyway, for information purpose.*

Reversed complex	ΔE (kJ/mol)	ΔH⁰ (kJ/mol)	ΔS⁰ (J.mol⁻¹.K⁻¹)	ΔG⁰ (kJ/mol)	Δ(ΔG⁰) (kJ/mol)
61a (S1)	-30.3	-24.9	-167.4	25.0	62.5
61d (S2)	-30.6	-27.9	-188.6	28.4	8.4
61g (S2)	-22.1	-19.6	-182.9	34.9	15.9

Results indicate that the standard orientation is preferred. In the case of complex **61a**, the Δ(ΔG⁰) between the standard and the reverse orientations is explained by the high stabilisation due to the formation of the P-B bond in S1 state. In the case of complex **61d**, the Δ(ΔG⁰) of 8.4 kJ/mol demonstrates the importance of the weak interactions between the methyl groups of the phosphatriptycene and the perfluorophenyl groups of **60**. A slightly bigger Δ(ΔG⁰) is observed for complex **61g** because more interactions seem possible with a *tert*-butyl group than with a methyl group.

6. NMR analysis

NMR calculations were performed on **1a-g**, **60** and **61a-g** at the B3LYP/6-311+G(2d,p) level of theory. The references used are the TMS (tetramethylsilane) for ^{1}H and ^{13}C NMR, phosphoric acid in water for ^{31}P NMR, and boron trifluoride diethyl etherate ($F_3B\text{-}OEt_2$) for ^{11}B NMR. The ^{31}P and ^{11}B NMR chemical shifts of the isolated compounds and corresponding complexes are given in Table 10.

When methyl groups are added on the phosphatriptycene, the chemical shift decreases regularly, from -40.3 ppm for no methyl group to -82.0 ppm for three methyl groups, demonstrating the electrodonating ability of this substituent. This tendency is less obvious when *t*-butyl groups are added. The chemical shift does decrease but in a weaker fashion to the methyl groups.

The NMR values of **S1** complexes indicate that these optimised compounds are Lewis adducts. Indeed, the decrease in shielding of the phosphorus is due to its σ-donation to the boron atom when the adduct is formed. On the other hand, the values of the chemical shift of the boron atom are typical of a four-coordinated boron centre, as in a Lewis adduct. These results are in concordance with the P-B bond lengths shown in Table 7. The values of **S2** complexes are similar to that of the isolated LA and LB, as generally for most FLPs since there are no covalent interactions between them.

*Table 10 - ^{31}P and ^{11}B chemical shifts of the isolated compounds (**1a-1g**, **2**) and the corresponding **S1** and **S2** complexes (**61a-61g**). The calculations were performed at the B3LYP/6-311+G(2d,p) level with the IEFPCM scheme to account for solvent (DCM) effects.*

Isolated phosphatriptycene		**Compound/ Complex**	**S1**		**S2**	
Compound	δ ^{31}P (ppm)		δ ^{31}P (ppm)	δ ^{11}B (ppm)	δ ^{31}P (ppm)	δ ^{11}B (ppm)
		60	/	51.0	/	51.0
1a	-40.3	**61a**	-18.0	-14.0	/	/
1b (1 Me)	-53.7	**61b** (1 Me)	-5.1	-13.2	-51.6	46.8
1c (2 Me)	-67.4	**61c** (2 Me)	6.4	-12.4	-62.5	50.7
1d (3 Me)	-82.0	**61d** (3 Me)	14.8	-12.7	-78.2	51.9
1e (1 *t*-Bu)	-45.2	**61e** (1 *t*-Bu)	-1.6	-2.6	-47.9	50.5
1f (2 *t*-Bu)	-46.6	**61f** (2 *t*-Bu)	/	/	-44.5	51.5
1g (3 *t*-Bu)	-52.2	**61g** (3 *t*-Bu)	/	/	-50.8	53.1

7. Analogy with triphenylphosphine

To compare the geometrical and thermodynamic results of the reactions shown in Table 5 to that of a more common phosphine like triphenylphosphine and methyl-substituted derivatives, similar calculations were performed with these last compounds (Table 11). This study will allow for the comparison of the LB ability of the phosphorus in the triptycene scaffold to that in a simple triphenyl configuration.

*Table 11 - Interaction between a phosphatriptycene derivative (**62a-d**) and tris(pentafluorophenyl)borane **60** to form a Lewis adduct or a FLP (**63a-63d**).*

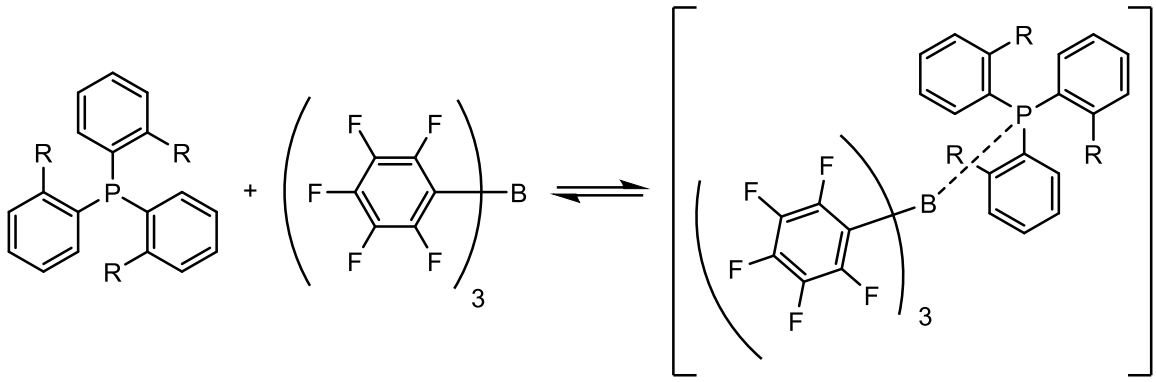

62a-d **60** **63a-d**

Reactions	Substituents		
	R	**R**	**R**
a	H	H	H
b	Me	H	H
c	Me	Me	H
d	Me	Me	Me

*Table 12 - Thermodynamic values of the formation of complexes **63a-d**.*

Reaction	ΔE (kJ/mol)	ΔH⁰ (kJ/mol)	ΔS⁰ (J.mol⁻¹.K⁻¹)	ΔG⁰ (kJ/mol)
a	-136.3	-128.9	-234.5	-59.0
b	-106.6	-98.7	-242.5	-26.3
c	-86.6	-79.9	-208.3	-17.8
d	-75.2	-66.8	-221.4	-0.8

*Table 13 - M06-2X/6-311G(d) bond lengths (Å) of complexes **63a-d** and corresponding phosphine derivatives.*

REF	Substituents			Complexes with $B(C_6F_5)_3$				Isolated phosphine		
	R	R	R^4	$d_{P^9-B^{15}}$	$d_{P^9-C^{9a}}$	$d_{P^9-C^{8a}}$	$d_{P^9-C^{14a}}$	$d_{P^9-C^{9a}}$	$d_{P^9-C^{8a}}$	$d_{P^9-C^{14a}}$
a	H	H	H	2.185	1.831	1.832	1.828	1.844	1.844	1.844
b	Me	H	H	2.262	1.859	1.836	1.829	1.848	1.842	1.845
c	Me	Me	H	3.328	1.849	1.853	1.840	1.844	1.847	1.846
d	Me	Me	Me	3.494	1.853	1.852	1.852	1.844	1.849	1.848

*Table 14 - M06-2X/6-311G(d) angles (°) of complexes **63a-d** and corresponding phosphine derivatives.*

REF	Substituents			Complexes with $B(C_6F_5)_3$			Isolated phosphine	
	R	R	R	Pyr_P	P^9-C^{9a}-C^1 angle	Pyr_B	Pyr_P	P^9-C^{9a}-C^1 angle
a	H	H	H	0.398	119.4	0.189	0.452	117.0
b	Me	H	H	0.408	123.9	0.241	0.450	118.1
c	Me	Me	H	0.433	119.8	0.018	0.423	118.2
d	Me	Me	Me	0.430	120.4	0.025	0.421	118.2

The values of the free enthalpy of reaction regularly increases as methyl groups are added on triphenylphosphine, indicating the adduct formation becomes less favourable. This observation is paralleled by the similarly increasing P-B distances. The negative values of free enthalpy of reaction show that their Lewis adduct is formed in majority in solution, except for the formation of complex **63d** where the adduct and the isolated molecules are roughly in equal quantity in solution. The steric hindrance is smaller in the case of triphenylphosphine derivatives as the methyl groups are not pointing towards compound **60** like phosphatriptycenes and this allows compounds **60** to approach closer to the phosphorus and facilitates the formation of a P-B bond (Figure 30).

63d **61d (S2)**

*Figure 30 - Tris(o-tolyl)phosphine **63d** and trimethylphosphatriptycene **61d** complexed with compound **60**. Contrary to complex **63d**, in the phosphatriptycene **61d** the methyl groups are pointing towards **60**, limiting its approach.*

The Pyr_P and Pyr_B parameters indicate that complexes **63a** and **63b** display the structure of a Lewis adduct as the boron is tetrahedral while complexes **63c** and **63c** are similar to **S2** complexes where the boron remains trigonal planar.

Furthermore, the intrinsic basicity of the phosphorus atom in the triphenylphosphine is stronger than the one of phosphatriptycene, making the adduct formation easier for **62**. As explained in *Part III*, section 3, the triptycene scaffold induces a strong s character in the lone pair of the phosphorus, lowering its energy and limiting the overlap with a p orbital such as the one of the boron atom.

8. Application in hydrogen activation

The theoretical calculations indicate that Frustrated Lewis pairs can be formed with one to three methyl groups on the triptycene. The weaker Lewis basicity of these compounds compared to classical triarylphosphines does not limit the applications in FLP catalysis. A weak Lewis basicity means that the conjugate acid is strong, making the proton in the P^+-H bond resulting from hydrogen splitting much more acidic than in classical phosphonium salts. It expands the scope of possible substrates for hydrogenation reactions. For examples, alkene hydrogenations require a weak Lewis base to proceed. Reported examples include the use of electrodeficient phosphine $(C_6F_5)Ph_2P$[82]. Such applications can be considered in the case of phosphatriptycenes and will be further discussed in the perspectives of this work (see *Part V*, section 2).

PART V – Conclusions and perspectives

1. Conclusions

Phosphines are among the most common Lewis bases in chemistry. Their applications span from ligands in organometallic catalysis to organocatalysts for asymmetric synthesis. More recently, sterically hindered phosphines have become Lewis bases of choice in the emerging field of frustrated Lewis pair (FLP) chemistry. In this context, the development of new bulky Lewis bases is of great importance. 9-phosphatriptycene **1a** and its derivatives have been put forward as interesting candidates for this purpose. This family of caged tricyclic phosphines has been nearly unexplored for catalyst design since their first synthesis in 1974. They are rigid, robust structures with many functionalizable positions and singular three-dimensional properties. In this work, we aimed at developing a new straightforward synthesis of 9-phosphatriptycene and adding methyl substituents in *ortho* position relative to the phosphorus (**1b-d**) in order to increase its steric hindrance. This would represent the first example of *ortho*-substituted phosphatriptycenes. In addition, a computational study of the FLP behaviour of phosphatriptycene derivatives when combined with the very strong tris(pentafluorophenyl)borane **60** was carried out.

Phosphatriptycene **1a** was synthesised in 55% yield over four steps from a commercially available aromatic compound **12** (Scheme 38). This novel synthesis relies on the formation of the precursor using a lithium or magnesium intermediate, which undergoes a triple cyclization on phenyl chloroformate followed by a Barton-McCombie deoxygenation. A second synthesis, however less practical, could be achieved using a trihalogenated triphenylmethane precursor **22** in 24% yield over six steps.

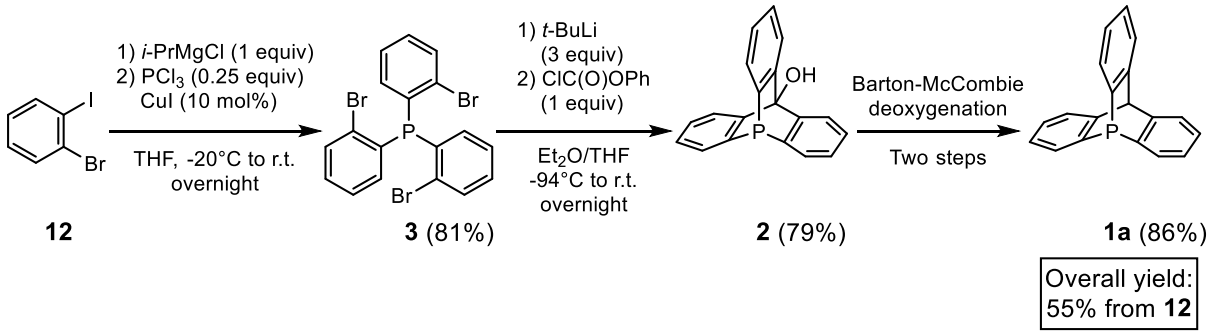

*Scheme 38 - Developed synthesis of phosphatriptycene **1a**.*

The functionalisation of the *ortho* position to the phosphorus by alkyl groups proved more challenging. The direct adaptation of the above synthesis with a methylated tribromoarylphosphine was unsuccessful. Several alternative strategies have been considered. Adding chlorine atoms instead of methyl groups increases the stability of the organometallic intermediate, which was added on an *ortho*-substituted phosphine **15** that we synthesised for the first time (Scheme 39).

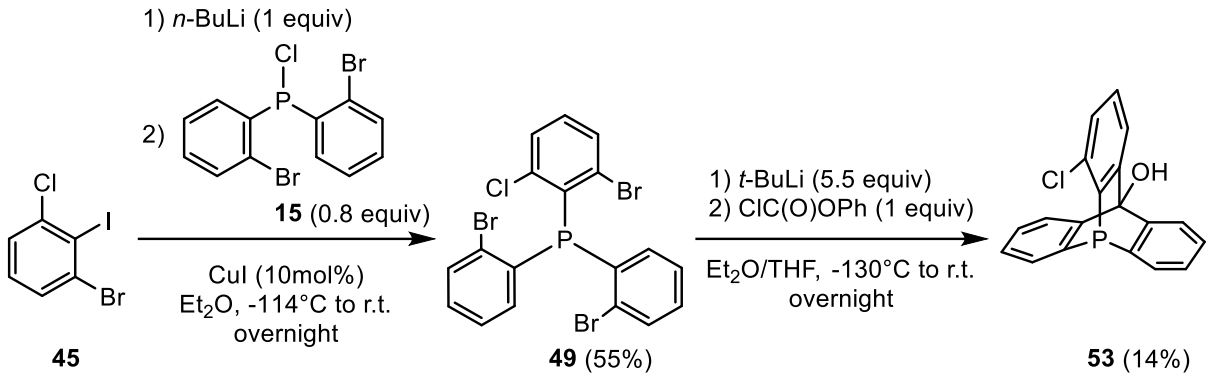

*Scheme 39 – Non-optimised synthesis of monochlorinated phosphatriptycene **53**.*

Furthermore, chloro-substituted phosphatriptycene **47** derived from **53** could be converted in methyl phosphatriptycene **1b** or any other substituents. This method has the advantage of widening the possible applications of *ortho*-substituted phosphatriptycenes.

Finally, a DFT investigation of the association between the studied compounds **1a-d** and tris(pentafluorophenyl)borane **60** showed that FLPs could be obtained from adding at least one methyl group on the triptycene. Two distinct states of association between the LA and LB were recognised, the first one (**S1**) favouring formation of covalent bonds (similar to a Lewis adduct), the second one (**S2**) favouring weak interactions between the two components. A good correlation was observed between the thermodynamic parameters of associations (ΔG^0), structural parameters and predicted NMR chemical shifts of the studied complexes.

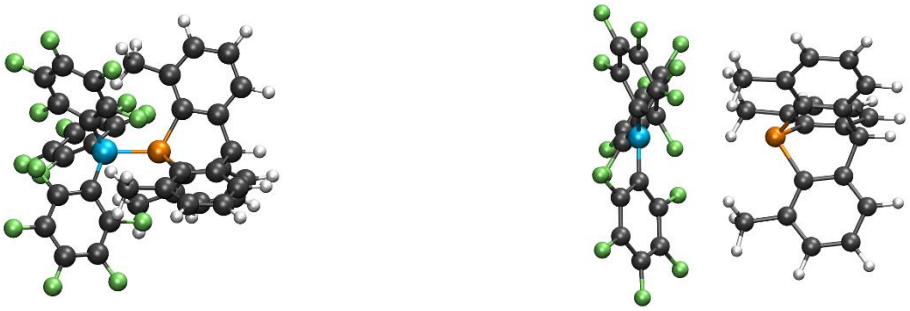

61d - S1 **61d - S2**

*Figure 31 - Representation of the two states of association between the Lewis acid and the Lewis base for complex **61d**. LEGEND: Orange = Phosphorus; Blue = Boron; Green = Fluorine; Grey = Carbon; White = Hydrogen.*

Comparison of Lewis basicity with triphenylphosphine derivatives as well as observations in crystal structures indicate that phosphatriptycenes are weak Lewis bases because of their strong pyramidal character that affects their lone pair. This thus opens a large range of potential reactions in frustrated Lewis pair catalysis since their phosphonium conjugated acid is stronger than classical phosphonium salts. This may be promising for expanding FLP-catalyzed hydrogenation to new substrates, such as alkenes, that are unreactive with known FLPs.

2. Perspectives

Several perspectives have been put forward. First, the method developed to synthesize the monochlorinated phosphatriptycene **53** can be extended to the synthesis of dichlorophosphatriptycene and subsequently to dimethylphosphatriptycene **1c**. In order to obtain a trisubstituted phosphatriptycene, an Ullmann coupling between **32** or **64** and an aryl chloride iodide could be employed [83, 84] (Scheme 40). A long-term objective of this work could be reached by performing the lithiation and cyclisation of **24** to obtain **1c**.

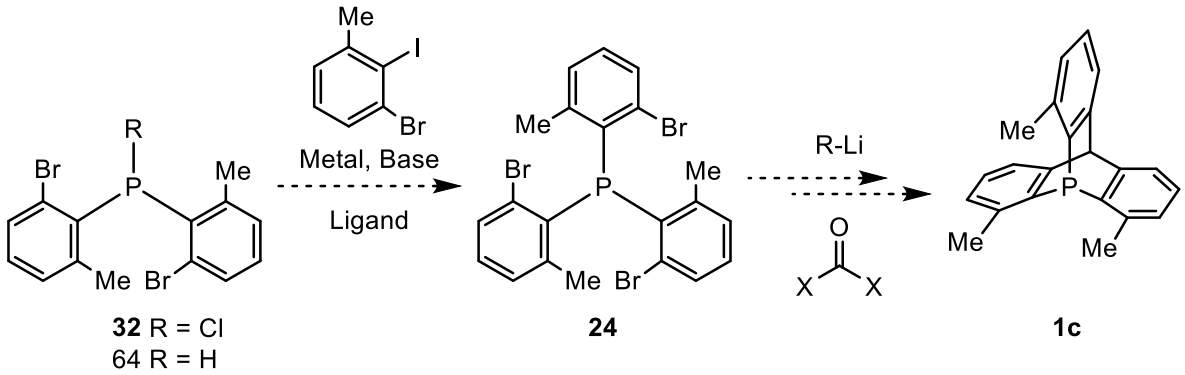

*Scheme 40 - Synthesis of trimethylated phosphine precursor **24** through an Ullmann coupling. Metal: Ni (R = Cl), CuI (R = H)[84].*

While most of our goals have been reached during this work, in particular the first synthetic route towards *ortho*-substituted phosphatriptycenes, and the detailed theoretical investigations of their stereoelectronic parameters, several long-term objectives are in progress in the group.

Using the monochlorinated phosphatriptycene **47**, an intramolecular FLP could be prepared by adding a Lewis acid in the *ortho* position. Such a compound would represent a new intramolecular FLP scaffold (Scheme 41).

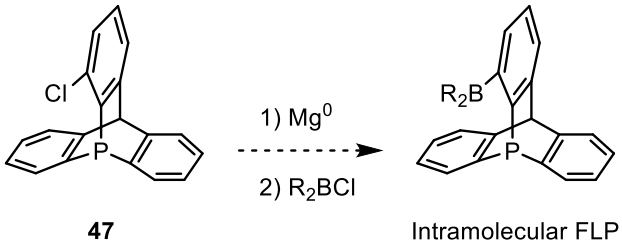

Scheme 41 - Formation of an intramolecular FLP.

By extending our developed synthesis of phosphatriptycene to a naphthyl-based starting material, a new propeller type of phosphatriptycene could be prepared (Scheme 42). This compound **67** would form a cavity around the phosphorus that should prevent the approach of bulky molecules while allowing smaller molecules inside. Further functionalisation of this cavity would expand the

scope of applications to asymmetric catalysis and to the area of P-chirogenic phosphorus catalysts and ligands.

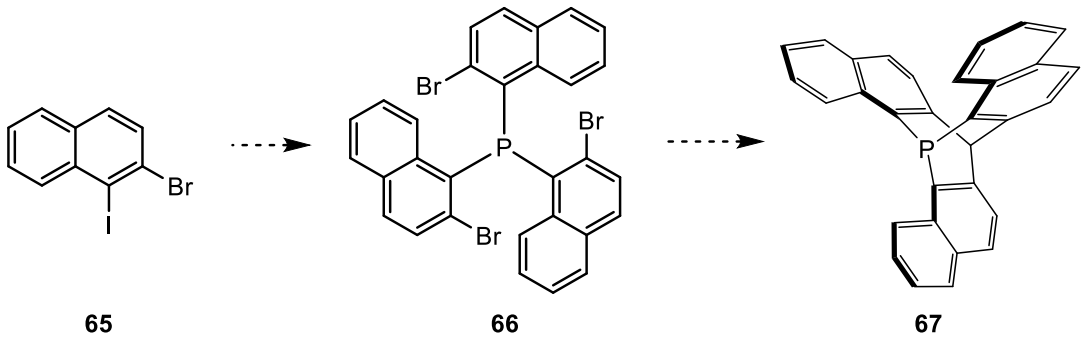

*Scheme 42 - Synthesis of naphthyl derivative of phosphatriptycene **68**.*

Indeed, phosphatriptycenes have the potential to become configurationally stable P-chirogenic catalysts. Three different substituents would lead to a chiral phosphorus in which inversion of the chiral centre leading to a racemisation of the compound is impossible due to the rigid triptycene scaffold. Starting from dichlorophosphatriptycene **68**, a chiral compound could be obtained in one step. This scaffold has the advantage of leading to the synthesis of diastereoisomers, which are separable via chiral resolution by crystallisation or chiral HPLC (Scheme 43).

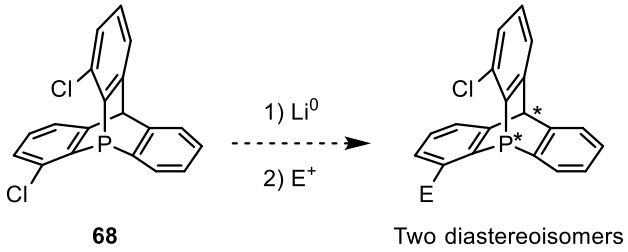

Scheme 43 - Synthesis of a chiral phosphatriptycene.

Since phosphatriptycenes display the weak Lewis basicity required in hydrogenations of alkenes, a possible application of the above compound that must be attempted is an enantioselective metal-free reduction.

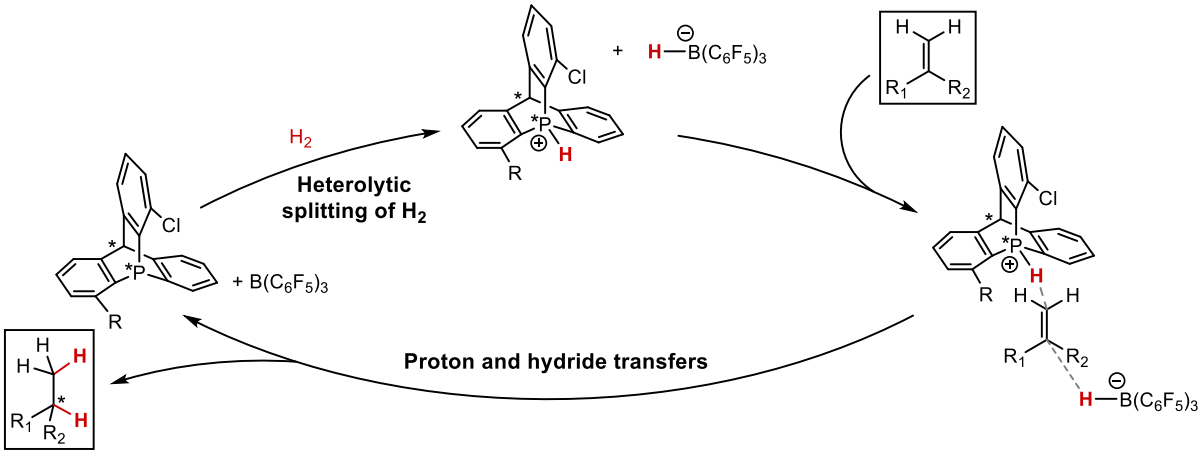

Scheme 44 - Plausible catalytic cycle of enantioselective hydrogenation of alkenes.

Part VI – Bibliography

[1] G. N. Lewis, *Valence and the Structure of Atoms and Molecules*, **1923**.

[2] S. E. Denmark and G. L. Beutner, "Lewis Base Catalysis in Organic Synthesis", *Angew. Chem. Int. Ed.* **2008**, *47*, 1560-1638.

[3] F. Hewitt and A. K. Holliday, "The Reaction of Diborane with the Alkyl Derivatives of Some Group V_B Elements", *J. Chem. Soc.* **1953**, 530-534.

[4] J. J. Li, *Name Reactions*, 3rd ed., New-York: Springer, **2006**.

[5] R. G. Pearson and J. Songstad, "Application of the Principle of Hard and Soft Acids and Bases to Organic Chemistry", *J. Am. Chem. Soc.* **1967**, *89*, 1827-1836.

[6] A. Rauk, L. C. Allen and K. Mislow, "Pyramidal Inversion", *Angew. Chem. Int. Ed.* **1970**, *9*, 6, 400-414.

[7] D. H. Valentine and J. H. Hillhouse, "Electron-Rich Phosphines in Organic Synthesis II. Catalytic Applications", *Synthesis* **2003**, *16*, 2437-2460.

[8] J. L. Methot and W. R. Roush, "Nucleophilic Phosphine Organocatalysis", *Adv. Synth. Catal.* **2004**, *346*, 1035-1050.

[9] C. A. Tolman, "Phosphorus Ligand Exchange Equilibria on Zerovalent Nickel. A dominant role for steric effects", *J. Am. Chem. Soc.* **1970**, *92*, 10, 2956-2965.

[10] P. C. Kamer and P. W. N. M. Van Leeuwen (Eds.), *Phosphorus(III) Ligands in Homogeneous Catalysis: Design and Synthesis,* Chichester: Wiley, **2012**.

[11] Z. L. Niemeyer, A. Milo, D. P. Hickey and M. S. Sigman, "Parameterization of phosphine ligands reveals mechanistic pathways and predicts reaction outcomes", *Nature Chem.* **2016**.

[12] C. Lindner, R. Tandon, B. Maryasin, E. Larionov and H. Zipse, "Cation affinity numbers of Lewis bases", *Beilstein J. Org. Chem.* **2012**, *8*, 1406-1442.

[13] K. D. Ashtekar, N. S. Marzijarani, A. Jaganathan, D. Holmes, J. E. Jackson and B. Borhan, "A New Tool To Guide Halofunctionalization Reactions: The Halenium Affinity (HalA) Scale", *J. Am. Chem. Soc.* **2014**, *136*, 13355-13362.

[14] H. Mayr, J. Ammer, M. Baidya, B. Maji, T. A. Nigst, A. R. Ofial and T. Singer, "Scales of Lewis Basicities toward C-Centered Lewis Acids (Carbocations)", *J. Am. Chem. Soc.* **2015**, *137*, 2580-2599.

[15] C. Laurence and J.-F. Gal, *Lewis Basicity and Affinity Scales: Data and Measurement*, Chichester: Wiley, **2010**.

[16] R. H. Crabtree, *The Organometallic Chemistry of the Transition Metals*, 6th ed., Hebeton, NJ: Wiley, **2014**.

[17] J. E. Huheey, E. A. Keiter et R. L. Keiter, *Inorganic Chemistry: Principles of Structures and Reactivity*, 4th ed., New-York: HarpensCollins College Publishers, **1994**.

[18] A. S. Guram, R. A. Rennels and S. L. Buchwald, "A Simple Catalytic Method for the Conversion of Aryl Bromides to Arylamines", *Angew. Chem. Int. Ed. Engl.* **1995**, 34, 12, 1348-1350.

[19] J. Louie and J. F. Hartwig, "Palladium-Catalyzed Synthesis of Arylamines from Aryl Halides. Mechanistic Studies Lead to Coupling in the Absence of Tin Reagents", *Tetrahedron Lett.* **1995**, *36*, 21, 3609-3612.

[20] J. P. Wolfe, H. Tomori, J. P. Sadighi, J. Yin and S. L. Buchwald, "Simple, Efficient Catalyst System for the Palladium-Catalyzed Amination of Aryl Chlorides, Bromides, and Triflates", *J. Org. Chem.* **2000***, 65*, 1158-1174.

[21] A. Aranyos, D. W. Old, A. Kiyomori, J. P. Wolfe, J. P. Sadighi and S. L. Buchwald, "Novel Electron-Rich Bulky Phosphine Ligands Facilitate the Palladium-Catalyzed Preparation of Diaryl Ethers", *J. Am. Chem. Soc.* **1999***, 121*, 4369-4378.

[22] T. E. Barder, S. D. Walker, J. R. Martinelli and S. L. Buchwald, "Catalysts for Suzuki-Miyaura Coupling Processes: Scope and Studies of the Effect of Ligand Structure", *J. Am. Chem. Soc.* **2005***, 127*, 4685-4696.

[23] R. Martin and S. L. Buchwald, "Palladium-Catalyzed Suzuki-Miyaura Cross-Coupling Reactions Employing Dialkylbiaryl Phosphine Ligands", *Acc. Chem. Res.* **2008***, 41*, 11, 1461-1473.

[24] T. P. Dang and H. B. Kagan, "The Asymmetric Synthesis of Hydratropic Acid and Amino-acids by Homogeneous Catalytic Hydrogenation", *J. Chem. Soc. Chem Commun.* **1971***,* 48.

[25] T. P. Yoon and E. N. Jacobsen, "Privileged Chiral Catalysts", *Science, 299*, 1691-1694, **2003**.

[26] J. P. Wolfe, S. Wagaw and S. L. Buchwald, "An Improved Catalyst System for Aromatic Carbon-Nitrogen Bond Formation: The Possible Involvement of Bis(Phosphine) Palladium Complexes as Key Intermediates", *J. Am. Chem. Soc., 118*, 7215-7216, **1996**.

[27] T. M. Trnka and R. H. Grubbs, "The Development of $L_2X_2Ru=CHR$ Olefin Metathesis", *Acc. Chem. Res.* **2001**, *34*, 18-29.

[28] M. Schlosser, (Ed.), *Organometallics in Synthesis*, Chichester: Wiley, **1994**.

[29] S. Akutagawa, "Chap. 16", in *Chirality in Industry: The Commercial Manufacture and Applications of Optically Active Compounds*, A. N. Collins, G. N. Sheldrake and J. Crosby (Eds.), Chichester, Wiley, **1992**.

[30] J. F. Young, J. A. Osborn, F. H. Jardine and G. Wilkinson, "Hydride intermediates in homogeneous hydrogenation reactions of olefins and acetylenes using rhodium catalysts", *Chem. Commun.* **1965***, 7*, 131-132.

[31] H. Guo, Y. Chiao Fan, Z. Sun, Y. Wu and O. Kwon, "Phosphine Organocatalysis", *Chem. Rev.* **2018***, 118*, 20, 10049-10293.

[32] H. Ni, W.-L. Chan and Y. Lu, "Phosphine-Catalyzed Asymmetric Organic Reactions", *Chem. Rev.* **2018***, 118*, 9344-9411.

[33] K. Morita, Z. Suzuki and H. Hirose, "A Tertiary Phosphine-catalyzed Reaction of Acrylic Coumpounds with Aldehydes", *Bull. Chem. Soc. Jpn.* **1968***, 41*, 2815.

[34] A. B. Baylis and M. E. D. Hillman, "German patent". Patent 2,155,113, **1972**.

[35] D. Basavaiah, A. Jaganmohan and T. Satyanarayana, "Recent Advances in the Baylis-Hillman Reaction and Applications", *Chem. Rev.* **2003***, 103*, 811-891.

[36] G. Masson, C. Housseman and J. Zhu, "The Enantioselective Morita–Baylis–Hillman Reaction and Its Aza Counterpart", *Angew. Chem. Int. Ed.* **2007***, 46*, 4614-4628.

[37] Y. Wei and M. Shi, "Multifunctional Chiral Phosphine Organocatalysts in Catalytic Asymmetric Morita-Baylis-Hillman and Related Reactions", *Acc. Chem. Res.* **2010***, 43*, 7, 1005-1018.

[38] H. C. Brown, H. I. Schesinger and S. Z. Cardon, “Studies in Stereochemistry. I. Steric Strains as a Factor in the Relative Stability of Some Coördination Compounds of Boron”, *J. Am. Chem. Soc.* **1942***, 64*, 2, 325-329.

[39] D. W. Stephan, ““Frustrated Lewis pairs”: a concept for new reactivity and catalysis”, *Org. Biomol. Chem.* **2008***, 6*, 1535-1539.

[40] G. C. Welch, R. R. San Juan, J. D. Masuda and D. W. Stephan, “Reversible, Metal-Free Hydrogen Activation”, *Science* **2006***, 314*, 1124-1127.

[41] G. C. Welch and D. W. Stephan, “Facile Heterolytic Cleavage of Dihydrogen by Phosphines and Boranes”, *J. Am. Chem. Soc.* **2007***, 129*, 1880-1881.

[42] D. W. Stephan and G. Erker, “Frustrated Lewis Pairs: Metal-free Hydrogen Activation and More”, *Angew. Chem. Int. Ed.* **2010***, 49*, 46–76.

[43] D. W. Stephan, “The broadening reach of frustrated Lewis pair chemistry”, *Science* **2016***, 354*, aaf7229.

[44] T. A. Rokob and I. Pápai, “Hydrogen Activation by Frustrated Lewis Pairs: Insights from Computational Studies”, *Top. Curr. Chem.* **2013***, 332*, 157-212.

[45] L. L. Zeonjuk, N. Vankova, A. Mavrandonakis, T. Heine, G.-V. Röschenthaler and J. Eicher, “On the mechanism of Hydrogen Activation by Frustrated Lewis Pairs”, *Chem. Eur. J.* **2013***, 19*, 17413-17424.

[46] H. Li, L. Zhao, G. Lu, Y. Mo and Z.-X. Wang, “Insight into the relative reactivity of "Frustrated Lewis pairs" and stable carbenes in activating H2 and CH4: A comparative computatinal study”, *Phys. Chem. Chem. Phys.* **2010***, 12*, 5268-5275.

[47] S. Gao, W. Wu and Y. Mo, “Steric and Electronic Effects on the Heterolytic H_2-Splitting by Phosphine-Boranes R_3B/PR'_3 (R = C_6F_5, Ph; R' = $C_6H_2Me_3$, t-Bu, Ph, C_6F_5, Me, H): A Computational Study”, *Int. J. Quantum Chem.* **2011***, 111*, 14, 3761-3775.

[48] T. A. Rokob, A. Hamza, A. Stirling, T. Soós and I. Pápai, “Turning Frustration into Bond Activation: A Theoretical Mechanistic Study on Heterolytic Hydrogen Splitting by Frustrated Lewis Pairs”, *Angew. Chem. Int. Ed.* **2008***, 47*, 2435-2438.

[49] S. Frömel, C. G. Daniliuc, C. Bannwarth, S. Grimme, K. Bussman, G. Kehr and G. Erker, “Indirect synthesis of a pair of formal methane activation products at a phosphane/borane frustrated Lewis pair”, *Dalton Trans.* **2016***, 45*, 19230-19233.

[50] N. Villegas-Escobar, A. Toro-Labbé, M. Becerra, M. Real-Enriquez, J. R. Mora and L. Rincon, “A DFT study of hydrogen and methane activation by $B(C_6F_5)_3$/P(t-Bu)$_3$ and $Al(C_6F_5)_3$/P(t-Bu)$_3$ frustrated Lewis pairs”, *J. Mol. Model.* **2017***, 23*, 234.

[51] R. A. Periana, D. J. Taube, S. Gamble, H. Taube, T. Satoh and H. Fujii, “Platinum Catalysts for the High-Yield Oxidation of Methane to a Methanol Derivative”, *Science* **1998***, 280*, 560-564.

[52] A. K. Cook, S. D. Schimler, A. J. Matzger and M. S. Sanford, “Catalyst-controlled selectivity in the C–H borylation of methane and ethane”, *Science* **2016***, 351*, 6280, 1421-1424.

[53] K. T. Smith, S. Berritt, M. González-Moreiras, S. Ahn, M. R. Smith III, M.-H. Baik and D. J. Mindiola, “Catalytic borylation of methane”, *Science* **2016***, 351*, 6280, 1424-1427.

[54] L. Chen, P. Ren and B. P. Carrow, “Tri(1-adamantyl)phosphine: Expanding the Boundary of Electron-Releasing Character Available to Organophosphorus Compounds”, *J. Am. Chem. Soc.* **2016***, 138*, 20, 6392-6395.

[55] E. Follet, P. Mayer, D. S. Stephenson, A. R. Ofial and G. Berionni, "Reactivity-Tuning in Frustrated Lewis Pairs:Nucleophilicity and Lewis Basicity of Sterically Hindered Phosphines", *Chem. Eur. J.* **2017***, 23*, 7422-7427.

[56] L. R. Moore, E. C. Western, R. Craciun, J. M. Spruell, D. A. Dixon, K. P. O'Halloran and K. H. Shaughnessy, "Sterically Demanding, Sulfonated, Triarylphosphines: Application to Palladium-Catalyzed Cross-Coupling, Steric and Electronic Properties, and Coordination Chemistry", *Organometallics* **2008***, 27*, 576-593.

[57] C. Jongsma, J. P. de Kleijn and F. Bickelhaupt, "Phosphatriptycene", *Tetrahedron* **1974***, 30*, 18, 3465-3469.

[58] C.-F. Chen and Y.-X. Ma, *Iptycenes Chemistry: From Synthesis to Applications*, Berlin: Springer, **2013**.

[59] J. Kobayashi, T. Agou and T. Kawashima, "A Novel and Convenient Synthetic Route to a 9-Phosphatriptycene and Systematic Comparisons of 9-Phosphatriptycene Derivatives", *Chem. Lett.* **2003***, 32*, 12, 1144-1145.

[60] T. Agou, J. Kobayashi and T. Kawashima, "Synthesis, Structure, and Reactivity of a Symmetrically Substituted 9-Phosphatriptycene Oxide and Its Derivatives", *Heteroat. Chem.* **2004***, 15*, 6, 437-446.

[61] H. Tsuji, T. Inoue, Y. Kaneta, S. Sase, A. Kawachi and K. Tamao, "Synthesis, Structure, and Properties of 9-Phospha-10-silatriptycenes and their Derivatives", *Organometallics* **2006***, 25*, 6142-6148.

[62] Y. Uchiyama, J. Sugimoto, M. Shibata, G. Yamamoto and Y. Mazaki, "Bromine Adducts of 9,10-Diheteratriptycene Derivatives", *Bull. Chem. Soc. Jpn.* **2009***, 82*, 7, 819–828.

[63] S. Konishi, T. Iwai and M. Sawamura, "Synthesis, Properties, and Catalytic Application of a Triptycene-Type Borate-Phosphine Ligand", *Organometallics* **2018***, 37*, 1876-1883.

[64] H. Ube, Y. Yasuda, H. Sato and M. Shionoya, "Metal-centred azaphosphatriptycene gear with a photo- and thermally driven mechanical switching function based on coordination isomerism", *Nature comms.* **2017***, 8*, 14296, 1-6.

[65] T. Agou, J. Kobayashi and T. Kawashima, "Evaluation of sigma-Donating Ability of a 9-Phosphatriptycene and Its Application to Catalytic Reactions", *Chem. Lett.* **2004***, 33*, 8, 1028-1029.

[66] T. Iwai, S. Konishi, T. Miyazaki, S. Kawamorita, N. Yokokawa, H. Ohmiya and M. Sawamura, "Silica-supported Triptycene-type Phosphine. Synthesis, Characterization, and Application to Pd-Catalyzed Suzuki–Miyaura Cross-coupling of Chloroarenes", *ACS Catal.* **2015***, 5*, 7254-7264.

[67] S. Kawamorita, T. Miyazaki, H. Ohmiya, T. Iwai and M. Sawamura, "Rh-Catalyzed Ortho-Selective C-H Borylation of N-Functionalized Arenes with Silica-Supported Bridgehead Monophosphine Ligands", *J. Am. Chem. Soc.* **2011***, 133*, 19310-19313.

[68] G. Berionni, L. Hu, A. Ben Saida, A. Chardon, M. Gama, A. Osi, D. Mahaut and X. Antognini Silva, "Opening up new research lines in Lewis acid/base catalysis", *Chimie Nouvelle* **2018***, 128*, 13-16.

[69] K. C. Caster, C. G. Keck and R. D. Walls, "Synthesis of Benzonorbornadienes: Regioselective Benzyne Formation", *J. Org. Chem.* **2001***, 66*, 2932-2936.

[70] L. D. Quin, *A Guide to Organophosphorus Chemistry*, New-York: Wiley-Interscience, **2000**.

[71] W. F. Bailey and E. R. Punzalan, "Convenient General Method For the Preparation of Primary Alkyllithiums by Lithium-Iodine Exchange", *J. Org. Chem.* **1990**, *55*, 5404-5406.

[72] C. Waldmann, O. Schober, G. Haufe et K. Kopka, "A Closer Look at the Bromine-Lithium Exchange with tert-Butyllithium in an Aryl Sulfonamide Synthesis", *Org. Lett.* **2013**, *15*, 112, 2954-2957.

[73] T. Agou, J. Kobayashi et T. Kawashima, «Dibenzophosphaborin: A Hetero-π-conjugated Molecule with Fluorescent Properties Based on Intramolecular Charge Transfer between Phosphorus and Boron Atoms,» *Org. Lett.* **2005**, *7*, 120, 4373-4376.

[74] S. E. Creutz and J. C. Peters, "Catalytic Reduction of N_2 to NH_3 by an Fe–N_2 Complex Featuring a C-Atom Anchor", *J. Am. Chem. Soc.* **2014**, *136*, 3, 1105-1115.

[75] A. Jancarík, J. Rybácek, K. Cocq, J. V. Chocholousová, J. Vacek, R. Pohl, L. Bednárová, P. Fiedler, I. Císarová, I. Stará and I. Starý, "Rapid Access to Dibenzohelicenes and their Functionalized Derivatives", *Angew. Chem. Int. Ed.* **2013**, *52*, 38, 9970-9975.

[76] B. G. Janesko, H. C. Fisher, M. J. Bridle and J.-L. Montchamp, "P(=O)H to P−OH Tautomerism: A Theoretical and Experimental Study", *J. Org. Chem.* **2015**, *80*, 10025-10032.

[77] R. G. Hicks, (Ed.), *Stable Radicals: Fundamentals and Applied Aspects of Odd-Electron Compounds*, Chichester: Wiley, **2010**.

[78] Y. Nishiyama, S. Yoshida and T. Hosoya, "Synthesis of Unsymmetrical Tertiary Phosphine Oxides via Sequential Substitution Reaction of Phosphonic Acid Dithioesters with Grignard Reagents", *Org. Lett.* **2017**, *19*, 3899-3902.

[79] M. Yamamura and T. Nabeshima, "Relationship between the Bowl-Shaped Geometry of Phosphangulene and an Axial Group on the Phosphorus Atom", *Bull. Chem. Soc. Jpn.* **2016**, *89*, 42-49.

[80] M. J. Frisch *et al*., *Gaussian 16, Revision B.01,* Gaussian, Inc., Wallingford CT, **2016**.

[81] L. Rocchigliani, G. Ciancaleoni, C. Zuccaccia and A. Macchioni, "Probing the Association of Frustrated Phosphine−Borane Lewis Pairs in Solution by NMR Spectroscopy", *J. Am. Chem. Soc.* **2014**, *136*, 112-115.

[82] L. Greb, P. Oña-Burgos, B. Schirmer, S. Grimme, D. W. Stephan and J. Paradies, "Metal-free Catalytic Olefin Hydrogenation: Low-Temperature H_2 Activation by Frustrated Lewis Pairs", *Angew. Chem. Int. Ed.* **2012**, *12*, 10311-10315.

[83] D. Gelman, L. Jiang and S. L. Buchwald, "Copper-Catalyzed C-P Bond Construction via Direct Coupling of Secondary Phosphines and Phosphites with Aryl and Vinyl Halides", *Org. Lett.* **2003**, *5*, 13, 2315-2318.

[84] I. P. Beletskaya and A. V. Cheprakov, "Copper in cross-coupling reactions - The post-Ullmann chemistry", *Coord. Chem. Rev.* **2004**, *248*, 2337-2364.

[85] A. E. Ashley, A. L. Thompson and D. O'Hare, "Non-Metal-Mediated Homogeneous Hydrogenation of CO2 CH3OH", *Angew. Chem. Int. Ed.* **2009**, *48*, 9839-9843.

PART VII - Material and methods

1. Quantum chemistry

1.1 Density functional theory

1.1.1 Introduction and first proof of concept

This section introduces the density functional theory (DFT)[1,2,3]. This method has been employed for all quantum calculations undertaken in the present master thesis.

DFT is quantum mechanical method that replaces the N-electron wavefunction dependent on the spin-space coordinates $\Psi(x_1, x_2, \ldots, x_N)$ and the related Schrödinger equation by the electron density $\rho(r)$ dependent on the space coordinates, which is conceptually much simpler. Indeed, it has been shown that all the properties of the system can be expressed using only electron density as variable.

In order to recast the electronic energy of the system, the so-called one- ($\rho_1(x_1)$) and two-electron ($\rho_2(x_1, x_2)$) densities are necessary. Their generalised expressions are:

$$\rho_1(x_1; x_1') = N \int \Psi^*(x_1, x_2, \ldots, x_N)\Psi(x_1', x_2', \ldots, x_N')dx_2 \ldots dx_N \quad (1)$$

$$\rho_2(x_1, x_2; x_1', x_2') = N(N-1) \int \Psi^*(x_1, x_2, \ldots, x_N)\Psi(x_1', x_2', \ldots, x_N')dx_3 \ldots dx_N \quad (2)$$

These expressions define the probability of finding any electron in a spin-volume dx_1 around x_1 (for $\rho_1(x_1)$) or two electrons in volumes in dx_1 and dx_2 around x_1 and x_2 (for $\rho_2(x_1, x_2)$) and the other electrons anywhere else (the N and $N(N-1)$ factors account for the indiscernibility of the electrons, making sure that the electronic density is a measure of the presence of *any* electron in the spin-volume). A simplified form of the expression of the electronic energy of the system using one- and two-electron densities can be obtained, starting from the Hamiltonian and its expectation value

$$E = \langle \Psi | \hat{H} | \Psi \rangle = \int_{x_1'=x_1} h(1)\rho_1(x_1; x_1')dx_1 + \frac{1}{2} \int_{\substack{x_1'=x_1 \\ x_2'=x_2}} g(1,2)\rho_2(x_1, x_2; x_1', x_2')dx_1 dx_2 \quad (3)$$

where $h(1)$ and $g(1,2)$ result from the decomposition of the electronic Hamiltonian into one- and two-electron terms:

$$\hat{H} = \hat{H}^{elec} = \sum_i^N h(i) + \frac{1}{2}\sum_{i \neq j}^N g(i,j) \quad (4)$$

Expression (3) demonstrates that the energy, and subsequently the properties of any system, can be written using the one- and two-electron densities. Moreover, when wavefunctions are defined by a single determinant (which is often the case, Slater determinant is the most appropriate way to describe wavefunctions), the two-electron density can be written as a function of the one-electron density:

$$\rho_2(x_1, x_2; x_1', x_2') = \rho_1(x_1; x_1')\rho_1(x_2; x_2') - \rho_1(x_2; x_1')\rho_1(x_1; x_2') \quad (5)$$

This leads to the conclusion that the one-electron density is sufficient to describe the energies and properties of any system.

1.1.2 The Hohenberg and Kohn theorems

The Hohenberg and Kohn theorems[4] represent the theoretical basis upon which is founded the density functional theory. The aforementioned affirmation that all the properties of the system can be expressed using only electron density as variable arises from the first of these theorems. It states that the external potential $\hat{V}_{ext}(r)$ can be determined (within a constant) by the electronic density. Furthermore, since the electronic density, when integrated over the space, gives the number of electrons of the system ($N = \int \rho(r)\, dr$) and it therefore also determines the kinetic energy operator $\hat{T}$ and the electron repulsion operator $\hat{V}_{ee}$ as both only depend on the number of electrons. With the external potential and the kinetic energy operators known, we have access to the Hamiltonian of the system and, subsequently, to all its properties through the Schrödinger equation:

$$\hat{H} = \hat{T} + \hat{V} \quad \Rightarrow \quad \hat{H}\Psi = E\Psi \quad (6)$$

with $\hat{V} = \hat{V}_{ee}(r) + \hat{V}_{ext}(r)$ The expression of the energy as a functional of $\rho(r)$:

$$E_v[\rho(r)] = T[\rho(r)] + V_{ne}[\rho(r)] + V_{ee}[\rho(r)] \quad (7)$$

where V_{ne} is the electron-nuclei attraction term, which corresponds most of the time to the external potential. The above equation can be recast to split the V_{ee} terms into a coulomb $J[\rho(r)]$ and a non-classical term and further manipulation of the equation introduces the Hohenberg and Kohn functional ($F_{HK}[\rho(r)]$), which is a universal functional independent of the given system.

$$\begin{aligned} E_v[\rho(r)] &= T[\rho(r)] + V_{ne}[\rho(r)] + J[\rho(r)] + nonclassical\ term \\ &\searrow \\ E_v[\rho(r)] &= \int \rho(r)v(r)dr + F_{HK}[\rho(r)] \end{aligned} \quad (8)$$

The second Hohenberg-Kohn theorem gives insight into how to actually calculate the electron density of a given system. It states that the electron density of the ground state is the one that minimises the total energy of the system. However, using approximate densities, this energy will

always remain higher than the *real* energy of this ground state, it is the concept of the variation principle. Solutions can thus be obtained by minimizing the energy, using a Lagrange multiplier with the constraint that the integration of the electron density over space gives the number of electrons of the system, *N*:

$$\delta\left\{E_v[\rho(r)] - \mu\left[\int \rho(r)dr - N\right]\right\} = 0 \tag{9}$$

or,

$$\mu = \frac{\delta E_v[\rho(r)]}{\delta\rho(r)} = v(r) + \frac{\delta F_{HK}[\rho(r)]}{\delta\rho(r)} \tag{10}$$

where μ is the Lagrange multiplier. The resolution of this equation would provide the exact ground state energy but F_{HK} contains a non-classical part, called the exchange-correlation that is not known. In order to solve this equation, approximate Hohenberg-Kohn functionals must be employed.

1.1.3 The Kohn-Sham method

The Kohn-Sham method[5] is the modern way of using density functional theory. This method consists in substituting the real system of interacting electrons by a fictitious one. In the latter, the electrons are independent but have the overall same density as the real system. Kohn-Sham spin-orbitals ($\theta_i(x)$) are introduced. The squares of their norm sum up to give the aforementioned Kohn-Sham density:

$$\rho(r) = \sum_i^N \int |\theta_i(x)|^2 d\omega \tag{11}$$

The global wavefunction of the system is described by a Slater determinant:

$$\Psi = \frac{1}{\sqrt{N!}} det|\theta_1(x_1), \theta_2(x_2), \dots, \theta_N(x_N)| \tag{12}$$

The Hamiltonian of this fictitious system is said to be “independent” because it does not possess any two-electron term:

$$\hat{H}_S = \sum_i^N \frac{-1}{2}\nabla_i^2 + \sum_i^N v_{eff}(r_i) \tag{13}$$

It does however possess, in addition to the kinetic energy operator, an effective potential. In order to define this parameter, several steps are needed. Starting from the Kohn-Sham equivalent of equation (8) and using the variation principle, the Hohenberg-Kohn functional can be rewritten:

$$F[\rho(r)] = T_S[\rho(r)] + J[\rho(r)] + E_{XC}[\rho(r)] \quad (14)$$

which defines the exchange-correlation (XC) energy functional $E_{XC}[\rho(r)]$:

$$E_{XC}[\rho(r)] = T[\rho(r)] - T_S[\rho(r)] + V_{ee}[\rho(r)] - J[\rho(r)] \quad (15)$$

This functional is the one that must be selected at the beginning of each DFT calculation. It contains two terms, a positive (T-T_S, kinetic energy) and a negative one, containing the two-electron exchange energy, the correlation energy and the self-interaction correction.

The functional derivative of the energy functional $E_v[\rho(r)]$ with respect to the electron density defines the effective potential:

$$v_{eff}(r) = v(r) + \int \frac{\rho(r')}{|r - r'|} dr' + v_{xc}(r) \qquad \text{with} \qquad v_{xc}(r) = \frac{\delta E_{XC}[\rho(r)]}{\delta \rho(r)} \quad (16)$$

where $v_{xc}(r)$ is the exchange-correlation potential. The effective potential corresponds to the potential that surrounds all the electrons. It is a key part of the Kohn-Sham equation (shown below in its canonical form):

$$\left[\frac{-1}{2}\nabla^2 + v_{eff}(r)\right]\Theta_n(x) = \varepsilon_n \Theta_n(x) \quad (17)$$

Solving the Kohn-Sham equation provides the electronic density of the system. Since the effective potential depends on the electron density, the resolution starts from a guest density, and proceeds self-consistently. It is an iterative process, a SCF (Self-Consistent Field) cycle is carried out as follows: from the guess density, the effective potential is evaluated (16) and inserted in the Kohn-Sham equation (17) which is solved (the energy can be evaluated), a new density is proposed and the cycle starts again until convergence towards the minimum energy (variation principle).

In the effective potential, the exact expression of the exchange-correlation functional is not known. It is thus approximated, leading to approximate densities and energies. This term accounts for electron correlation effects. Many exchange-correlation functionals have been developed with several levels of approximation (see next section). If the exact XC functional was known, the Kohn-Sham method would be an exact method.

1.1.4 Exchange-correlation functionals

As abovementioned, many functionals have been designed over the years and they are sorted in different categories. Hereafter are cited several of these categories and their characteristic.

In the Local Density Approximation functionals (LDA), a uniform electron gas is applied on infinitesimal parts of the globally non-uniform system. The Generalised Gradient Approximation (GGA) includes a dependence on the gradient of the electron density to the local density approximation. The meta-GGA adds a dependence on the kinetic energy density. Hybrid functionals are obtained by adding a certain percentage (depending on the functional) of exact Hartree-Fock (HF) exchange. The long-range corrected or range-separated hybrid functionals split the exchange potential into short- and long-range terms with different HF exchange percentages. This allows to better describe charge-transfer effects due to a correct -1/r asymptotic dependence of the exchange potential while retaining more DFT exchange at short range to avoid results similar to a "classical" HF method. In double hybrids functionals, the correlation functional is partially described by MP2 while HF exchange is still added to the exchange functional. These latter functionals improve significantly the results but their computational cost is far higher than that of the other functionals. Empirical dispersion corrections can also be included to (better) describe the London dispersion forces.

Note that increasing the complexity of the functional does not ensure better results. Simpler functionals can be more suited for a given system. In this project, the M06-2X functional was used. It is a hybrid meta-GGA functional that is suited, according to its developers, to describe main-group thermochemistry, kinetics and noncovalent interactions[6]. NMR calculations were performed with the B3LYP functional since it has been demonstrated to predict NMR chemical shifts with satisfying accuracy[7,8].

1.2 Solvent effects and the polarizable continuum model

Since our compounds under investigation are in solution, an adequate description of the solvent effects is also crucial. A fundamental quantity that describes the interactions between the system and its surroundings is the enthalpy of solvation ΔG_S^0 that characterizes the energetic transition when going from gas phase to the solvent.

$$K_S = \frac{[X]_{Sol}}{[X]_{Gas}} = e^{-\Delta G_S^0(X)/RT} \tag{18}$$

where K_S is the equilibrium constant for going from gas phase to solution and $[X]_{Sol}$ and $[X]_{Gas}$ represent the concentration of the X compound in solution or in gas phase respectively.

The free enthalpy of solvation affects the studied system on all levels: structure, reactivity, responses to perturbation, etc. It is divided in several contributions. The electrostatic interactions between the solute and the solvent molecules, the cavitation energy which is the amount of energy needed to form the cavity in solution that will contain the solute without solute-solvent interactions, the dispersion forces (induced dipole/induced dipole interactions) that represents the major contribution, and finally the changes in the bulk solvent structure.

Solvents effects can be described using two models: the explicit and implicit models. The former simulates the solvent molecules, gives better, more precise results, but requires much higher computational costs while the latter does not simulate the solvent molecules explicitly and it is less time-and energy consuming.

The Polarizable Continuum Model (PCM) is an implicit solvation method[9]. In this model a cavity that contains the solvated molecule is drawn by circulating a probe sphere around the solute molecule. This sphere has a radius equal to the van der Waals radius of the solvent molecule. It defines two surfaces, the outer one is the solvent accessible surface and the inner is the solvent exclusion surface (Figure 32).

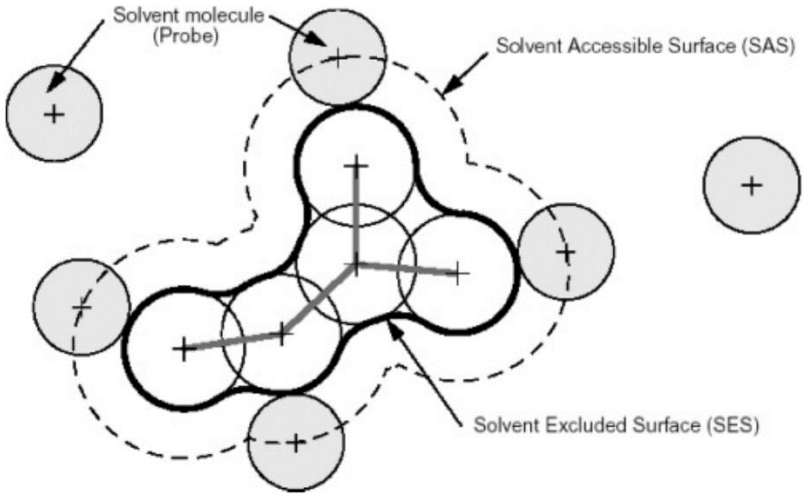

Figure 32 - Cavity formed by circulating a probe solvent molecule around the studied compound. Picture extracted from reference [9].

In this method, the explicit solute-solvent interactions are replaced by a continuum characterised by a dielectric constant ε that will apply on the solute an electric field, thus simulating the solvent effects. The mathematical development of the PCM model is now put in an integral equation formalism (IEF, in the IEFPCM approach). The subtlety in the PCM approach is that the charge distribution of the solute induces a polarisation of the dielectric continuum which in turn polarizes the solute charge distribution. It is thus a self-consistent model that must be solved in an iterative manner.

1.3 Responses to an external magnetic field and NMR chemical shifts

The response of the system to an external magnetic field is the principle of the NMR analysis. As a function of their electronic environment, nuclei having a non-zero magnetic moment will react differently to that perturbation so that their response will serve as an indication of their chemical environment. A component of the magnetic shielding tensor ($\overleftrightarrow{\sigma}$) of a nucleus is given by:

$$\sigma_{\zeta\eta} = -\frac{\delta B_\zeta}{\delta B_\eta^{ext}} \tag{19}$$

The chemical shift of a nucleus A is defined as the variation of the shielding tensor with respect to a given reference:

$$\delta_A = \sigma_{ref} - \sigma_A \quad where \quad \sigma = \frac{1}{3}\left(\sigma_{xx} + \sigma_{yy} + \sigma_{zz}\right) \tag{20}$$

In order to determine these quantities, the response of the system to the external magnetic field must be quantified. The Hamiltonian of the system is thus modified to include contribution from the interactions with the external magnetic field. A direct modification of the Hamiltonian is however problematic as its perturbed expression is dependent on the choice of the origin of the system. It does not have any consequences when exact wavefunctions and complete atomic basis sets are used but it is no longer the case for approximate situations. An elegant approach that solves this problem is the use of London atomic orbitals χ^{London}, that are themselves dependent on the origin and on the magnetic field, the expression for a *p* orbital is:

$$\chi_p{}^{London}(\vec{r}, \vec{G}, \vec{B}) = \chi_p(\vec{r}) e^{\frac{-i}{2}(\vec{B}\times\vec{G}).\vec{r}} \tag{21}$$

where $\vec{G}$ is the origin of the atomic orbital. The resulting $\overleftrightarrow{\sigma}$ values become thereafter independent of the choice of the origin. It is the GIAO (Gauge Including Atomic Orbitals) scheme. It was employed for the determination of NMR chemical shifts in the master thesis, using the Coupled-Perturbed Kohn-Sham iterative method.

1.4 Atomic basis sets

Any SCF-LCAO-MO calculation needs an atomic basis set[10]. It is at the heart of the calculation as it defines the atomic orbitals that will in turn describe the molecular orbitals (in the LCAO scheme), necessary to obtain the electronic density and wavefunction of the system. These basis sets are defined as contractions of gaussian functions. These functions aim to best simulate the exact atomic orbitals, solutions of the Schrödinger equation. The basis sets have been divided in several categories with respect to their composition.

The minimal basis sets or simple ζ comprise a single basis function for each atomic orbital occupied in the ground state of that atom (for shells and subshells that are at least partially occupied). One of these basis sets is STO-3G (Slater Type Orbital) where each basis function is a contraction of three gaussian primitive functions.

Double or Triple ζ include two or three basis functions, respectively, for each orbital occupied in the atom ground state. The split valence basis sets split the number of basis functions between the core orbitals (usually described with simple ζ) and the valence orbitals (with double or triple ζ). This method comes form the understanding that most of the chemistry of an atom is performed by the valence orbitals, so they should be more flexible than the core ones. Basis sets with two or three valence atomic orbitals are called valence double- and triple-ζ basis sets, respectively. The addition of polarisation functions to these basis sets can account for environment effects on the atom. p functions can be implemented on hydrogen or d and f functions can be added on atoms from the second and third periods. For example, a hydrogen atom involved in a covalent bond will no longer possess a perfectly spherical 1s orbital. The addition of a set of p functions can correct this imprecision. Furthermore, diffuse functions can also be added to the basis sets. They allow a better description of the outer part of the orbitals and the electronic density. s and p functions are added on atoms from the second and third period while only s functions are applicable on hydrogen atoms.

J. A. Pople developed a series of basis sets such as STO-3G, 6-31G, 6-311G(d,p), 6-311++G(3df,3pd), etc, mainly valence double or triple ζ. During this master thesis, the 6-311G(d) basis sets was mainly used. It is a Pople valence triple ζ basis set. It possesses a single basis function, contraction of six gaussians, for the core orbitals while the valence orbitals are described by three basis functions, one is a contraction of 3 gaussians and the two other consist in a single gaussian function. A set of five polarisation functions are added: d orbitals for the atoms of the second and third period. NMR calculations will be performed using the 6-311+G(2d,p) basis set. It contains a set of s and p diffuse functions on the second and third period atoms and one set of s diffuse functions on the hydrogens. Two sets of d polarisation functions on second and third

period atoms and a set of s functions on hydrogens are also included. Such a larger basis set is needed to describe the shielding tensor.

1.5 Thermochemistry and equilibrium constants

The thermochemistry is the study of the thermodynamic functions of a given chemical system[11]. Those are macroscopic values, resulting from the state and the energy of the matter at the molecular level. Statistical thermodynamics make the bridge between the molecular and macroscopic chemistry. The partition function (Ω) is of paramount importance in this field as it contains all the information of the system. It is defined as follows:

$$\Omega = \sum_i g_i e^{\frac{-\varepsilon_i}{kT}} \tag{22}$$

$$\Omega = \Omega_{trans}\, \Omega_{vib}\, \Omega_{rot}\, \Omega_{el} \tag{23}$$

where g_i is the degeneracy of the i level of energy, ε_i, k, is the Boltzmann constant and T, the temperature. Equation (23) highlights that the partition function is the product of several contributions (trans = translation; vib= vibrations; rot = rotation; el = electronic). Each state function of the system (internal energy, free Gibbs enthalpy, entropy, enthalpy, …) can be expressed as a function of the partition function.

For the thermochemical study of the present work, vibrational frequency calculations were performed. From these calculations as well as the mass and the rotation constants, one determines the partition function and subsequently the various state functions of the system.

Equilibrium constants are also determined in this work. The calculated values are K_C: equilibrium constant expressed as a function of the concentrations in solution. K_C and K_P (K_P: equilibrium constant in terms of the pressure of the constituents of the system, rapported to the standard 1bar pressure) are related in the case of complex formation by the following expression:

$$K_P = \frac{K_C P^{\ominus}}{C^{\ominus} RT} \tag{24}$$

where $C^{\ominus}$ is the standard concentration of 1M and $P^{\ominus}$ is the standard 1 bar pressure.

1.6 Bibliography

[1] R. G. Parr and W. Yang, *Density-Functional Theory of Atoms and Molecules*, New York: Oxford University Press, **1989**.

[2] W. Koch and M. C. Holtausen, *A Chemist's Guide to Density Functional Theory*, 2nd ed., Weinheim: Wiley-VCH, **2001**.

[3] P. Geerlings, F. De Proft and W. Langenaeker, "Conceptual Density Functional Theory", *Chem. Rev.* **2003**, *103*, 1793-1873.

[4] A. Hohenberg and W. Kohn, "Inhomogeneous Electron Gas", *Phys. Rev.* **1964**, *136*, B864.

[5] W. Kohn and L. J. Sham, "Self-Consistent Equations Including Exchange and Correlation Effects", *Phys. Rev.* **1965**, *140*, A1133.

[6] Y. Zhao and D. G. Truhlar, "The M06 suite of density functionals for main group thermochemistry, thermochemical kinetics, noncovalent interactions, excited states, and transition elements: two new functionals and systematic testing of four M06-class functionals and 12 other functionals", *Theor. Chem. Account* **2008**, *120*, 215-241.

[7] J. R. Cheeseman, G. W. Trucks, T. A. Keith and M. J. Frisch, "A comparison of models for calculating nuclear magnetic resonance shielding tensors", *J. Chem. Phys.* **1996**, *104*, 14, 5497-5509.

[8] P. R. Rablen, S. A. Pearlman and J. Finkbiner, "A Comparison of Density Functional Methods for the Estimation of Proton Chemical Shifts with Chemical Accuracy", *J. Chem. Phys.* **1999**, 103, 7357-7363.

[9] J. Tomasi, B. Mennucci and R. Cammi, "Quantum Mechanical Continuum Solvation Models", *Chem. Rev.* **2005**, *105*, 2999-3093.

[10] A. Szabo and N. S. Ostlund, *Modern Quantum Chemistry: Introduction to Advanced Electronic Structure Theory*, New-York: Dover Publications, **1996**.

[11] P. Atkins et J. De Paula, *Atkins' Physical Chemistry*, 10th ed., Oxford: Oxford University Press, **2014**.

2. Experimental section

2.1 Synthetic procedures and characterisation

2.1.1 General laboratory procedure

All moisture-sensitive reactions were performed under an atmosphere of argon in flame-dried schlenck flasks.

2.1.2 Analytical methods

^{1}H, ^{13}C, and ^{31}P NMR spectra were recorded on a Jeol 400 MHz NMR spectrometer and the observed signals are reported in parts per million (ppm) relative to the residual signal of the non-deuterated solvent. The following abbreviations are used to describe multiplicities s = singlet, d = doublet, t = triplet, q = quartet, quin = quintuplet, br = broad, m = multiplet.

2.1.3 Material

All anhydrous solvents were dried with a solvent purification system. Solvents, reagents and chemicals were purchased from Sigma-Aldrich, Carbosynth, FluoroChem and TCI and used without further purification.

9-phosphatriptycene (1a)

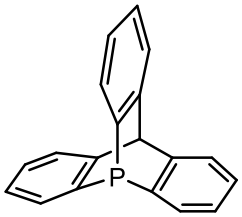

Chemical formula: $C_{19}H_{13}P$
Molecular weight: 272.07 g/mol
Physical State: White solid

Under an argon atmosphere, AIBN (230 mg, 1.38 mmol, 1.0 equiv) followed by *n*-Bu_3SnH (1.6 g, 5.52 mmol, 4.0 equiv) were added to a solution of 9-phospatriptycene-10-phenyl thiocarbonate **19** (565 mg, 1.38 mmol, 1.0 equiv) in toluene (20 mL) at room temperature. After 1h of stirring at room temperature, 40 mL of a saturated solution of NH_4Cl was added. The reaction mixture was heated at 75°C overnight. After cooling at room temperature, the resulting mixture was washed first with a saturated solution of KF (3x25 mL) and the aqueous layer was extracted with CH_2Cl_2 (3x50 mL). Combined organic layers were then washed with brine, dried over $MgSO_4$, filtered and concentrated under reduced pressure.

Purification by silica gel column chromatography using hexane:CH_2Cl_2 15:1 as eluent afforded 9-phosphatriptycene (367 mg, 1.33 mmol, 97%) as a white solid.

Crystals suitable for X-ray structure analysis were obtained by slow evaporation of a saturated solution of 9-phosphatriptycene in *n*-pentane.

^{1}H NMR (400 MHz, CD_2Cl_2): δ_H = 7.83-7.71 (m, 3 H), 7.54 (d, *J* = 7.4 Hz, 3H), 7.22-7.12 (m, 3 H), 7.12-7.02 (m, 3 H), 5.62 (s, 1H).

^{13}C NMR (102 MHz, CD_2Cl_2): δ_C = 149.3 (d, *J* = 3.3 Hz), 140.9 (d, *J* = 9.1 Hz), 132.4 (d, *J* = 36.6 Hz), 128.5, 125.6, 125.3 (d, *J* = 12.4 Hz), 59.6.

^{31}P NMR (162 MHz, CD_2Cl_2): δ_p = -64.6.

9-phospha-10-hydroxytriptycene (2)

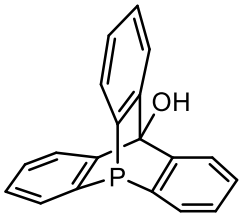

Chemical formula: $C_{19}H_{13}OP$
Molecular weight: 288.27 g/mol
Physical State: White solid

Under an argon atmosphere, *t*-BuLi (7.5 mL, 13 mmol, 3.0 equiv) was added dropwise to a solution of tris(2-bromophenyl)phosphine (2.12 g, 4.25 mmol, 1.0 equiv) in a mixture of Et_2O:THF (1:1) (100 mL) at -94°C. After 2h at –94°C, phenylchloroformate (0.530 mL, 4.2 mmol, 1.0 equiv) was added dropwise to the above solution at -94 °C under Ar. After 1h at –94°C, the mixture was allowed to warm up to room temperature and stirred overnight. After overnight, 40 mL of a saturated solution of NH_4Cl was added. The aqueous layer was extracted with EtOAc (3x60 mL), the combined organic layers were washed with brine, dried over $MgSO_4$ and concentrated under reduced pressure.

Purification by silica gel column chromatography using cyclohexane:EtOAc 13.1/1 as eluent afforded 9-phospha-10-hydroxytriptycene (967 mg, 3.35 mmol, 79%) as a white solid.

Crystals suitable for X-ray structure analysis were obtained by slow evaporation of a saturated solution of -phospha-10-hydroxytriptycene in EtOAc.

^{1}H NMR (400 MHz, $CDCl_3$): δ_H = 7.81-7.74 (m, 6 H), 7.31-7.23 (m, 3 H), 7.16-7.06 (m, 3 H), 3.45 (s, 1 H).

^{13}C NMR (101 MHz, $CDCl_3$): δ_C = 149.9 (d, *J* = 3.3 Hz), 139.6 (d, *J* = 7.8 Hz), 132.4 (d, *J* = 36.4 Hz), 128.49 (d, *J* = 1.6 Hz), 125.6 (d, *J* = 12.5 Hz), 120.9.

^{31}P NMR (161 MHz, $CDCl_3$): δ_p = -71.9

Tris(2-bromophenyl)phosphine (3)

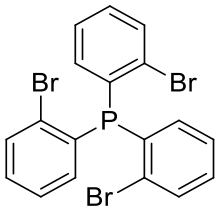

Chemical formula: $C_{18}H_{12}Br_3P$

Molecular weight: 498.97 g/mol

Physical State: White solid

Prepared according to the literature[1]. Under an argon atmosphere, *i*-PrMgCl (2M in THF, 20 mL, 40.0 mmol, 1 equiv) was added over 20 min to a solution of 1-bromo-2-iodobenzene (5.2 g, 41.0 mmol, 1 equiv) in THF (41 mL) at – 20 °C. After 2h at –41°C, PCl_3 (0.9 mL, 10.3 mmol, 0.26 equiv) was added dropwise to the above solution, followed by CuI (190 mg, 1.0 mmol, 0.1 equiv) as a solid under a vigorous flow of argon. The resulting solution was stirred at –20 °C for 30 min and then allowed to warm up at room temperature overnight. After 16h at room temperature, 35 mL of a saturated solution of NH_4Cl was added. The aqueous layer was extracted with EtOAc (3x30 mL), the combined organic layers were dried over $MgSO_4$, filtered and concentrated under reduced pressure.

The resulting solid was solubilised in a mixture of toluene/MeOH 1:1 (18 mL), filtration following by washing with cold MeOH afforded tris(2-bromophenyl)phosphine **3** (4.16 g, 8.33 mmol, 81%) as a white solid.

Crystal suitable for X-ray structure analysis were obtained by slow evaporation of a saturated solution of the title compound in EtOAc.

^1H and ^{31}P NMR data are in good agreement with the literature values.

^1H NMR (400 MHZ, $CDCl_3$): δ_H = 7.66-7.58 (m, 3 H), 7.29-7.19 (m, 6 H), 6.76-6.70 (m, 3 H).

^{31}P NMR (162 MHz, $CDCl_3$): δ_p = -2.9.

[1] S. Konishi, T. Iwai and M. Sawamura, "Synthesis, Properties, and Catalytic Application of a Triptycene-Type Borate-Phosphine Ligand", *Organometallics* **2018**, *37*, 12, 1876-1883.

Bis(2-bromophenyl)chlorophosphine (15)

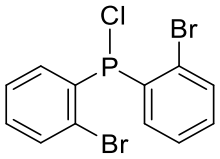

Chemical formula: $C_{12}H_8Br_2ClP$
Molecular weight: 378.42 g/mol
Physical state: Very light yellow solid

Under an argon atmosphere, *i*-PrMgCl (2M in THF, 36 mL, 72 mmol, 1.0 equiv) was added dropwise to a solution of 1-bromo-2-iodobenzene (20 g, 71 mmol, 1.0 equiv) in THF (75 mL) at –41 °C. After 2h at –41°C, PCl_3 (3.1 mL, 36 mmol, 0.5 equiv) was added dropwise to the above solution. After 1h at – 40°C, the solution was warmed up at room temperature and stirred overnight. Filtration of the resulting suspension over a plug of silica gel using THF as eluent afforded a white solid which was redissolved in Et_2O and filtered. Concentration under vacuum afforded bis(2-bromophenyl)chlorophosphine (8.4 g, 22 mmol, 61%) as a very light yellow solid with a purity >90%.

^{1}H NMR (400 MHZ, CD_2Cl_2): δ_H = 7.63-7.56 (m, 2 H), 7.47 (tdd, *J* = 10.4, 5.4, 4.5 Hz, 2 H), 7.42-7.35 (m, 2 H), 7.35-7.28 (m, 2 H)

^{31}P NMR (162 MHz, CD_2Cl_2): δ_p = 71.1.

9-phospatriptycene-10-phenyl thiocarbonate (19)

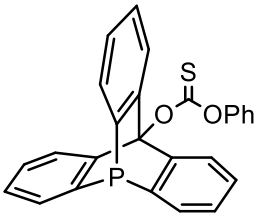

Chemical formula: $C_{26}H_{17}O_2PS$
Molecular weight: 424.06 g/mol
Physical State: Yellow solid

Under an argon atmosphere NaH (60% w., 483 mg, 12.08 mmol, 1.2 equiv) was added portionwise to a solution of 9-phospha-10-hydroxytriptycene (2.9 g, 10.07 mmol, 1.0 equiv) in THF (100 mL) at room temperature. After 1h at room temperature phenylchlorothiocarbonate (1.91 g, 12.08 mmol, 1.2 equiv) was added dropwise under Ar. After 30 min at room temperature, 40 mL of a saturated solution of NH_4Cl was added. The aqueous layer was extracted with CH_2Cl_2 (3x100 mL), washed with brine, dried over $MgSO_4$, filtered and concentrated under reduced pressure.

Purification by silica gel column chromatography using hexane:EtOAc 50/1 as eluent afforded 9-phospatriptycene-10-phenyl thiocarbonate (4.11 g, 9.16 mmol, 91%) as a yellow solid.

^{1}H NMR (400 MHZ, DMSO-d_6): δ_H =7.82 (dd, *J* = 18.1, 8.1 Hz, 6H), 7.45-7.21 (m, 5H), 7.20–7.06 (m, 6H).

^{13}C NMR (102 MHz, DMSO-d_6): δ_C = 190.9, 153.4, 146.3 (d, *J* = 3.5 Hz), 138.81 (d, *J* = 8.6 Hz), 132.5 (d, *J* = 37.0 Hz), 129.8, 128.1 (d, *J* = 1.43 Hz), 127.1, 126.1 (d, *J* = 12.51 Hz), 123.2, 121.5, 93.9 (d, *J* = 1.84 Hz).

^{31}P NMR (162 MHz, CD_2Cl_2): δ_p = -71.9.

1-bromo-2-iodo-3-methylbenzene (25)

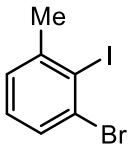

Chemical formula: C_7H_6BrI
Molecular weight: 296.93 g/mol
Physical State: White solid

Prepared according to the literature[2]. In a 1L flask, HCl (25 mL, 37%w.) and 2-bromo-6-methylaniline (4.96 g, 26.7 mmol, 1.0 equiv.) are added. 2-bromo-6-methylaniline is added as a powder. As the compound becomes easily liquid at room temperature, it is put in an ice cold Becher to be grinded and obtain a fine powder. The resulting milky white heterogeneous solution is stirred at room temperature for 25 min. Ice (60 g) is added in the flask and the mixture is put at 0°C. Sodium nitrite $NaNO_2$ (4.07 g , 59.0 mmol, 2.2 equiv.) is added slowly and the solution is stirred at this temperature for 30 minutes. An orange gas (nitrogen dioxide, NO_2) appears in the flask. Potassium iodide (17.78 g, 107.1 mmol, 4.0 equiv.) is added in one pot at 0°C, a dark grey and orange moss appears instantly and fills half of the flask. Flask put out of the ice batch a few minutes after addition and the solution is stirred at room temperature for 20 minutes before being heated at 60°C for 45 minutes and allowed to cool down to room temperature and stirred overnight. The solution becomes metallic pink with grey metallic deposits on the flask. Quenching with an aqueous solution of $Na_2S_2O_5$ (60 g in 100 mL of water), solution left stirring for 1 h. Extraction with pentane (3x100 mL) and solvents evaporated.

Purification by a pad of silica gel (eluent: pentane) and solvents evaporated to afford 1-bromo-2-iodo-3-methylbenzene (m = 6,94 g, yield = 87 %) as a white crystalline solid.

^{1}H NMR (400 MHZ, DMSO-d_6): δ_H = 7.45 (ddd, *J* = 7.7, 1.8, 0.6 Hz, 1H), 7.15 (ddd, *J* = 7.5, 1.8, 0.6 Hz, 1H), 7.10 (t, *J* = 7.6 Hz, 1H), 2.55 (s, 3H).

^{13}C NMR (102 MHz, DMSO-d_6): δ_C = 145.0, 130.7, 130.0, 129.0, 108.1, 31.2.

[2] A. Jancarík, J. Rybácek, K. Cocq, J. V. Chocholousová, J. Vacek, R. Pohl, L. Bednárová, P. Fiedler, I. Císarová, I. Stará and I. Starý, "Rapid Access to Dibenzohelicenes and their Functionalized Derivatives", *Angew. Chem. Int. Ed.* **2013**, *52*, 38, 9970-9975.

Tris(*p*-tolylsulfanyl)phosphine oxide (39)

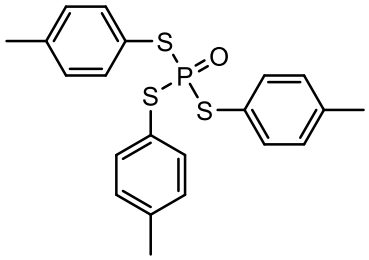

Chemical formula: $C_{21}H_{21}OPS_3$
Molecular weight: 416.55 g/mol
Physical State: Yellow solid

Prepared with a procedure adapted from the literature[3]. Under an argon atmosphere, NEt_3 (8.4 mL, 60 mmol, 3.8 equiv) was added to a solution of 4-methylbenzenethiol (5.01 g, 40.3 mmol, 5.0 equiv) in THF (140 mL) at 0°C. Phosphorus oxychloride (1.5 mL, 16 mmol, 1.0 equiv) was then added dropwise to the above solution at 0°C under Ar. After 2h at 0°C, 140 mL of a saturated solution of NH_4Cl was added. The organic layer was extracted with EtOAc (3x100 mL), the combined organic layers were washed with brine, dried over $MgSO_4$, filtered and concentrated under vacuum.

Purification by silica gel column chromatography using cyclohexane:EtOAc 84/16 as eluent afforded tris(*p*-tolylsulfanyl)phosphine oxide **39** (2.26 g, 5.4 mmol, 34%) as a yellow solid.

^{1}H NMR (400 MHZ, $CDCl_3$): δ_H = 7.46-7.40 (m, 6 H), 7.20-7.14 (m, 6 H), 2.36 (d, *J* = 2.4 Hz, 9H).

^{13}C NMR (102 MHz, $CDCl_3$): δ_C = 140.1 (d, *J* = 3.7 Hz), 135.7 (d, *J* = 4.6 Hz), 130.2 (d, *J* = 2.8 Hz), 123.3 (d, *J* = 7.1 Hz), 21.43 (d, *J* = 1.3 Hz).

^{31}P NMR (162 MHz, $CDCl_3$): δ_p = 57.3.

[3] Y. Nishiyama, S. Yoshida and T. Hosoya, "Synthesis of Unsymmetrical Tertiary Phosphine Oxides via Sequential Substitution Reaction of Phosphonic Acid Dithioesters with Grignard Reagents", *Org. Lett.* **2017**, *19*, 3899-3902.

(2-bromo-6-chlorophenyl)bis(2-bromophenyl)phosphine (49)

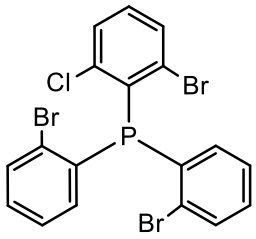

Chemical formula: $C_{18}H_{11}Br_3ClP$
Molecular weight: 533.41 g/mol
Physical State: Off-white powder

Under an argon atmosphere, *n*-BuLi (2.5 M in hexane, 6.6 mL, 16.51 mmol, 1.0 equiv) was added dropwise to a solution of 2-bromo-6-chlorobromobenzene (5.24 g, 16.52 mmol, 1.0 equiv) in Et_2O (82 mL) at –114°C. After 1h30 at –114°C, a solution of phosphorus-bis-(2-bromophenyl)-chloride **15** (5.01 g, 13.2 mmol, 0.8 equiv) in 8 mL of THF was added dropwise to the above solution, following by CuI (251 mg, 1.32 mmol, 0.1 equiv) as a solid under a vigorous flow of argon. After maintaining the temperature at -114°C for 30 min, the bath was removed and the resulting solution was allowed to warm up to room temperature and stirred overnight. After overnight, 80 mL of a saturated solution of NH_4Cl was added. The aqueous layer was extracted with EtOAc (3x80 mL), the gathered organic layers were washed with brine, dried over $MgSO_4$ and concentrated under vacuum.

Trituration of the resulting solid with a mixture of toluene:MeOH 1:1 (20 mL) following by filtration and washing with cold MeOH (25 mL) afforded (2-bromo-6-chlorophenyl)bis(2-bromophenyl)phosphine (3.90 g, 7.31 mmol, 55%) as an off-white powder.

Crystal suitable for X-ray structure analysis were obtained by slow evaporation of a saturated solution of (2-bromo-6-chlorophenyl)bis(2-bromophenyl)phosphine in EtOAc.

^{1}H NMR (400 MHZ, CD_2Cl_2): δ_H = 7.65-7.55 (m, 3 H), 7.39-7.34 (m, 1 H), 7.27-7.19 (m, 5 H), 7.11-7.05 (m, 2 H).

^{13}C NMR (102 MHz, CD_2Cl_2): δ_C = 142.3 (d, *J* = 7.9 Hz), 135.5 (d, *J* = 2.3 Hz), 134.0, 133.5, 133.4 (d, *J* = 3.0 Hz), 132.7, 131.2, 129.1 (d, *J* = 81.5 Hz), 127.9.

^{31}P NMR (162 MHz, CD_2Cl_2): δ_p = 8.2.

bis(2-bromo-6-chlorophenyl)chlorophosphine (50)

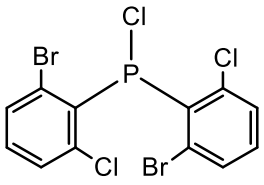

Chemical formula: $C_{12}H_6Br_2Cl_3P$
Molecular weight: 447.31 g/mol
Physical State: Light-yellow solid

Under an argon atmosphere, *i*-PrMgCl (2M in THF, 2.4 mL, 4.7 mmol, 1 equiv) was added dropwise to a solution of 2-bromo-6-chloroiodobenzene (1.502 g, 4.73 mmol, 1 equiv) in THF (4.8 mL) at –41°C. After 1h at –41°C, PCl_3 (0.210 mL, 2.4 mmol, 0.5 equiv) was added dropwise to the above solution under argon. After 3h30 at –41°C the solution was allowed to warm up to room temperature and stirred overnight. Filtration over a plug of silica gel using THF as eluent afforded a white gel which was redissolved in Et_2O and filtered. Concentration under vacuum afforded bis(2-bromo-6-chlorophenyl)(2-bromophenyl)phosphine (826 mg, 1.84 mmol, 77%) as a light-yellow solid with a purity >90%.

^{1}H NMR (400 MHZ, $CDCl_3$): δ_H = 7.53-7.46 (m, 2 H), 7.36-7.31 (m, 2 H), 7.18-7.11 (m, 2 H).

^{31}P NMR (162 MHz, $CDCl_3$): δ_p = 82.0.

1-chloro-9-phospha-10-hydroxytriptycene (53)

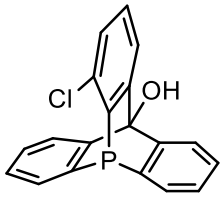

Chemical formula: $C_{19}H_{12}ClOP$
Molecular weight: 322.72 g/mol
Physical State: White powder

Under an argon atmosphere, *t*-BuLi (1.9M in pentane, 2.7 mL, 5.2 mmol, 5.5 equiv) was added dropwise to a solution of (2-bromo-6-chlorophenyl)bis(2-bromophenyl)phosphine (500 mg, 0.940 mmol, 1 equiv) in a mixture of THF:Et_2O 1:1 (30 mL) at –130°C. After 4h at –130°C, phenylchloroformate (0.120 mL, 0.94 mmol, 1 equiv) was added dropwise under argon at –130°C. The resulting solution was stirred at this temperature for 2h and allowed to warm up to room temperature and stirred overnight. After overnight, 20 mL of a saturated solution of NH_4Cl was added. The aqueous layer was extracted with EtOAc (3x10 mL), the organic layers were washed with brine, dried over $MgSO_4$ and concentrated under vacuum.

Purification by silica gel column chromatography using cyclohexane:EtOAc 30/1 as eluent, afforded 1-chloro-9-phospha-10-hydroxytriptycene **53** (42.5 mg, 0.131 mmol, 14%) as a white powder.

^{1}H NMR (400 MHZ, $CDCl_3$): δ_H = 7.94-7.79 (m, 2 H), 7.79-7.76 (m, 2 H), 7.71-7.69 (m, 1 H), 7.29-7.25 (m, 2 H), 7.16-7.09 (m, 4 H).

^{31}P NMR (162 MHz, $CDCl_3$): δ_p = -80.98.

2.1 Crystallographic data

Single-crystal diffraction data of all molecules were collected on an Oxford Diffraction Gemini Ultra R system (4-circle kappa platform, Ruby CCD detector) using Mo K_α radiation (λ = 0.71073 Å). The structures were solved by SHELXT and then refined by full-matrix least-squares refinement of |F| using SHELXL-2016.

*Table 15 - Crystal data for compounds **1a**, **2**, **3**, **16**, **49** and **59**.*

Compound	1a	2	3	16	49	59
Formula	$C_{19}H_{13}OP$	$C_{19}H_{13}OP$	$C_{18}H_{12}Br_3P$	$C_{25}H_{17}Br_2O_2P$	$C_{18}H_{11}Br_3ClP$	$C_{18}H_{13}OPSi$
Crystal system	Monoclinic	Triclinic	Monoclinic	Monoclinic	Monoclinic	Monoclinic
Space group	C c	P $\bar{1}$	P 2_1/c	P 2_1/n	P 2_1/c	I 2/a
a (Å)	15.074(2)	7.2966(4)	7.4449(15)	10.0619(5)	7.8463(3)	27.00733(17)
b (Å)	8.210(1)	8.2064(4)	7.932(2)	4.0814(7)	16.1174(5)	9.24690(7)
c (Å)	13.207(2)	13.0501(7)	30.540(7)	15.5759(8)	14.7534(4)	27.49100(18)
α (°)	90	82.694(4)	90	90	90	90
β (°)	120.53(2)	80.962(4)	92.54(2)	92.119(4)	104.946(3)	100.0424(6)
γ (°)	90	69.948(5)	90	90	90	90
Volume (Å^3)	1407.87	722.675	1801.71	2205.37	1802.62	6760.25
Z	4	2	4	4	4	16
R factor (%)	n.a.	3.65	25.17	4.59	3.09	6.35
T (K)	Room Temp (283-303)	Room Temp (283-303)	Room Temp (283-303)	Room Temp (283-303)	Room Temp (283-303)	Room Temp (283-303)

X-ray structure of tris(2-bromophenyl)phosphine (1a)

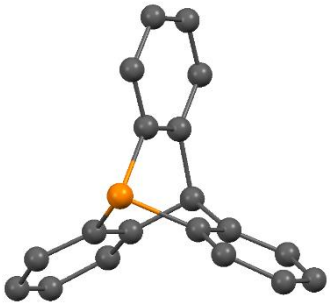

*Figure 33 – X-ray structure of compound **3**. Ellipsoids could not be displayed because of lack of data in the .cif file.*

*Table 16 - Orthographic coordinates of compound **1a**. Values given in Å.*

Atom	X	Y	Z
P	0.000	1.984	0.000
C	-0.098	1.175	-1.664
C	0.957	1.217	-2.546
C	0.894	0.607	-3.780
C	-0.308	-0.054	-4.112
C	-1.410	-0.080	-3.266
C	-1.278	0.539	-1.982
C	1.629	1.203	0.284
C	2.665	1.225	-0.646
C	3.876	0.557	-0.391
C	4.005	-0.111	0.779
C	3.050	-0.095	1.722
C	1.866	0.559	1.490
C	0.806	3.497	-0.702
C	1.822	3.415	-1.626
C	2.414	4.588	-2.086
C	1.857	5.820	-1.664
C	0.853	5.855	-0.784
C	0.333	4.718	-0.250
C	2.192	1.970	-1.976

X-ray structure of 9-phospha-10-hydroxytriptycene (2)

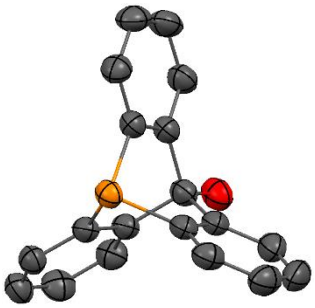

*Figure 34 – X-ray structure of compound **2**.*

*Table 17 - Orthographic coordinates of compound **2**. Values given in Å.*

Atom	X	Y	Z
P	5.108	0.646	9.975
O	0.947	1.327	9.105
H	0.484	0.957	9.636
C	3.146	1.649	8.297
C	4.526	1.481	8.444
C	5.392	1.973	7.481
H	6.309	1.848	7.570
C	4.886	2.653	6.384
H	5.465	2.997	5.743
C	3.527	2.820	6.243
H	3.194	3.275	5.504
C	2.645	2.315	7.193
H	1.727	2.424	7.086
C	2.703	1.769	10.726
C	4.044	1.647	11.088
C	4.522	2.287	12.221
H	5.420	2.217	12.451
C	3.659	3.031	13.009
H	3.978	3.459	13.770
C	2.335	3.136	12.667
H	1.758	3.628	13.205
C	1.850	2.516	11.529
H	0.952	2.599	11.301
C	2.596	-0.415	9.539
C	3.917	-0.748	9.856
C	4.277	-2.075	10.004
H	5.152	-2.298	10.226
C	3.330	-3.071	9.822
H	3.569	-3.963	9.930
C	2.044	-2.747	9.484
H	1.418	-3.421	9.350
C	1.665	-1.422	9.339
H	0.790	-1.210	9.107
C	2.265	1.081	9.423

X-ray structure of tris(2-bromophenyl)phosphine (3)

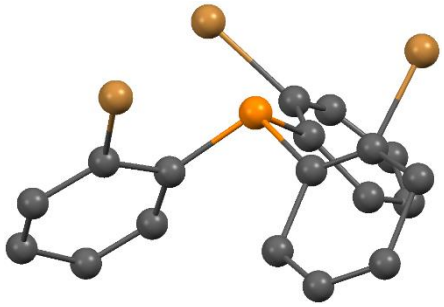

*Figure 35 – X-ray structure of compound **3**. Ellipsoids could not be displayed because of lack of data in the .cif file.*

*Table 18 - Orthographic coordinates of compound **3**. Values given in Å.*

Atom	X	Y	Z
Br	1.251	8.674	9.769
Br	0.692	6.768	14.718
Br	-1.630	4.232	10.474
P	0.924	5.997	11.566
C	1.499	2.768	14.877
H	1.497	2.105	15.529
C	0.999	5.005	10.041
C	1.709	2.451	13.492
H	1.899	1.570	13.273
C	0.059	4.363	9.583
C	2.322	5.021	9.245
H	3.098	5.426	9.558
C	3.848	8.812	10.770
H	3.939	9.526	10.170
C	1.664	3.339	12.497
H	1.914	3.092	11.635
C	2.524	6.806	11.575
C	2.668	8.059	10.859
C	1.299	4.045	15.182
H	1.274	4.354	16.058
C	1.120	4.934	14.035
C	-0.160	3.704	8.299
H	-0.967	3.367	7.997
C	2.242	4.378	8.036
H	2.985	4.462	7.485
C	1.213	4.704	12.771
C	1.250	3.665	7.566
H	1.370	3.148	6.791
C	4.882	8.408	11.624
H	5.611	8.964	11.779
C	4.822	7.139	12.308
H	5.551	6.798	12.773
C	3.664	6.480	12.235
H	3.631	5.675	12.702

Bis(2-bromophenyl)(2-(phenyl acetate))phosphine (16)

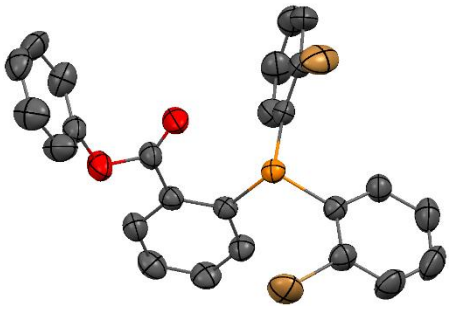

*Figure 36 – X-ray structure of compound **16**.*

*Table 19 - Orthographic coordinates of compound **16**. Values given in Å.*

Atom	X	Y	Z	Atom	X	Y	Z
Br	6.139	7.527	12.765	C	4.714	10.737	9.071
Br	0.339	7.504	13.399	H	4.581	10.697	8.152
P	3.185	8.841	12.412	C	-0.679	10.125	13.098
O	3.216	8.727	8.031	H	-1.490	9.723	13.309
O	2.005	8.567	9.888	C	1.079	8.318	6.989
C	4.058	9.049	14.018	H	0.775	9.150	7.274
C	1.703	9.909	12.665	C	2.796	6.669	6.928
C	5.285	8.400	14.219	H	3.644	6.381	7.181
C	4.153	9.946	11.292	C	3.957	9.915	9.914
C	0.491	9.357	13.011	C	0.577	12.064	12.556
C	5.144	10.802	11.780	H	0.617	12.982	12.415
H	5.318	10.823	12.693	C	5.347	9.008	16.509
C	3.512	9.671	15.125	H	5.773	8.996	17.335
H	2.702	10.118	15.039	C	5.921	8.384	15.433
C	2.909	9.009	9.311	H	6.739	7.952	15.526
C	2.322	7.888	7.323	C	5.869	11.614	10.938
C	-0.615	11.465	12.868	H	6.517	12.180	11.291
H	-1.388	11.980	12.923	C	4.148	9.646	16.365
C	5.648	11.597	9.579	H	3.754	10.064	17.097
H	6.125	12.163	9.016	C	0.264	7.500	6.214
C	1.721	11.292	12.452	H	-0.595	7.772	5.988
H	2.525	11.706	12.235	C	1.976	5.878	6.144
C	0.740	6.285	5.787	H	2.283	5.048	5.856
H	0.209	5.742	5.250				

X-ray structure of Bis(2-bromophenyl)(2-bromo-6-chlorophenyl)phosphine (49)

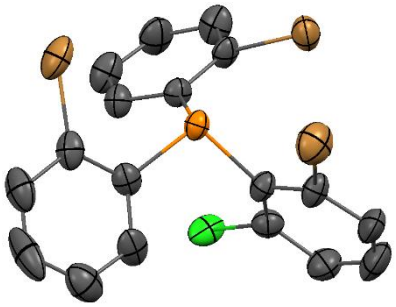

*Figure 37 – X-ray structure of compound **49**.*

*Table 20 - Orthographic coordinates of compound **49**. Values given in Å.*

Atom	X	Y	Z
Br	-2.157	11.704	6.345
Br	-0.372	9.441	1.584
Br	-0.033	8.198	7.092
Cl	2.240	13.114	5.422
P	0.223	10.316	4.685
C	-0.323	11.950	4.139
C	2.959	9.801	4.061
H	3.189	10.147	4.893
C	0.884	9.796	7.350
C	-1.365	12.592	4.864
C	1.081	10.732	6.298
C	1.287	10.071	8.648
H	1.088	9.478	9.335
C	-0.340	13.865	2.630
H	-0.038	14.273	1.853
C	1.380	9.409	2.329
C	0.158	12.641	3.011
H	0.838	12.256	2.505
C	1.654	9.905	3.591
C	3.908	9.190	3.295
H	4.764	9.076	3.644
C	1.785	11.861	6.594
C	-1.850	13.871	4.527
H	-2.513	14.281	5.037
C	2.291	12.050	7.920
H	2.847	12.772	8.099
C	-1.318	14.496	3.416
H	-1.605	15.350	3.188
C	2.417	8.812	1.559
H	2.229	8.469	0.715
C	1.966	11.202	8.907
H	2.217	11.397	9.782
C	3.649	8.739	2.031
H	4.331	8.385	1.510

X-ray structure of 9-phosphatriptycene-10-silanol (59)

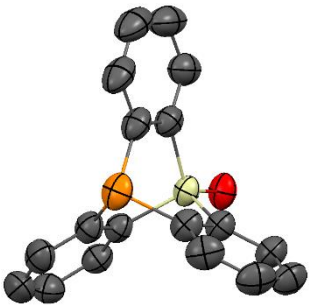

*Figure 38 – X-ray structure of compound **59**. It was synthesised by Lei Hu in the context of his PhD and was used in this Master thesis.*

*Table 21 - Orthographic coordinates of compound **59**. Values given in Å.*

Atom	X	Y	Z
Si	20.397	5.737	16.005
P	22.381	4.796	18.175
O	19.326	6.224	14.862
C	21.207	7.094	16.984
C	19.684	4.592	17.287
C	22.072	6.609	17.978
C	22.129	4.396	14.067
H	21.571	4.678	13.378
C	18.414	4.033	17.336
H	17.771	4.300	16.718
C	22.711	4.353	16.403
C	21.849	4.769	15.373
C	23.235	3.606	13.775
H	23.415	3.360	12.897
C	20.636	4.183	18.244
C	18.091	3.084	18.294
H	17.242	2.703	18.303
C	23.812	3.551	16.095
H	24.377	3.260	16.774
C	21.058	8.478	16.836
H	20.495	8.817	16.178
C	19.029	2.702	19.235
H	18.810	2.074	19.885
C	24.063	3.190	14.793
H	24.801	2.658	14.598
C	20.293	3.257	19.205
H	20.921	3.002	19.843
C	22.738	7.511	18.815
H	23.307	7.191	19.477
C	21.755	9.346	17.673
H	21.673	10.265	17.557
C	22.559	8.853	18.667
H	22.987	9.441	19.246